Article

OR7A10 GPCR engineering boosts CAR-NK therapy against solid tumours

https://doi.org/10.1038/s41586-026-10149-8

Received: 27 April 2025

Accepted: 15 January 2026

Published online: 25 February 2026

Check for updates

Luojia Yang[1,2,3,4,5,13], Paul A. Renauer[1,2,3,13], Kaiyuan Tang[1,2,3,4,5], Josh Saskin[1,2,3,4,5,6], Liqun Zhou[1,2,3,4,7], Charles Zou[1,2,3,4,5], Seok-Hoon Lee[1,2,3], Madison Fox[1,2,3,4,7], Samuel Johnson-Noya[1,2], Benedict Weiss[1,2], Stephanie Deng[1,2,3,6], Paris Fang[1,2], Binfan Chen[1,2,3], Giacomo Sferruzza[1,2,3], Saba Fooladi[1,2,3], Kai Zhao[1,2,3], Daniel Park[1,2], Feifei Zhang[1,2,3], Jiayi Tu[8], Jing Chen[8], Jennifer Moliterno[9], Murat Gunel[9], Lei Peng[1,2,3,9,14] ✉ & Sidi Chen[1,2,3,4,5,6,7,9,10,11,12,14] ✉

Chimeric antigen receptor (CAR)-natural killer (NK) cell therapies hold promise for solid tumours but remain limited because of poor tumour infiltration, persistence and resistance in the tumour microenvironment[1–4]. Here, to identify gain-of-function targets that enhance CAR-NK cell efficacy, we performed an unbiased in vivo CRISPR activation screen followed by a barcoded targeted in vivo open reading frame screen in primary human CAR-NK cells. We identified and comprehensively validated OR7A10, a G protein-coupled receptor (GPCR), as the top candidate. Engineering CAR-NK cells with *OR7A10* cDNA (a CRISPR-independent method with a simple manufacturing strategy) enhanced their proliferation, activation, degranulation, cytokine production, death ligand expression, chemokine receptor expression, cytotoxicity, persistence, metabolic fitness and tumour microenvironment resistance. Moreover, exhaustion in primary human NK cells derived from multiple peripheral blood and cord blood donors was reduced. *OR7A10* gain-of-function CAR-NK cells displayed strong in vivo efficacy across multiple solid tumour models. For example, 100% complete response with long-term tumour control and survival benefit in an orthotopic breast cancer mouse model were achieved. These findings establish *OR7A10*-engineered CAR-NK cells as a highly potent and scalable off-the-shelf therapeutic for solid tumours.

NK cells are cytotoxic lymphocytes with a potent ability to eliminate tumours and virally infected cells, and can bypass major histocompatibility complex restriction and previous sensitization[1–4]. By recognizing germline-encoded ligands associated with oncogenic transformation[5–7], NK cells can target cancer cells that have a low mutational burden or lack neoantigen presentation[8–10]. Adoptive CAR-NK cell therapy is relatively safe, carries minimal risk of graft-versus-host disease (GVHD) or cytokine release syndrome and is amenable to off-the-shelf manufacturing[11–13]. These advantages have fuelled growing interest in developing NK cell-based therapies for solid tumours[14]. As of 2025, more than 1,200 clinical trials are evaluating NK cells, including over 160 for CAR-NK cell therapy (ClinicalTrials.gov).Indeed, trials have demonstrated favourable outcomes in the treatment of haematological malignancies[15].

CAR-NK cell therapies hold promise for solid tumours[16,17]. However, key challenges remain, including limited tumour infiltration, inadequate proliferation and poor persistence in the tumour microenvironment (TME)[8,18,19]. Multiple strategies are being investigated to overcome these limitations, including cytokine engineering[20,21] and knockout of inhibitory regulators such as *CISH*[22–26], *TIM3* (ref. 27), *NKG2A*[28,29], *HIF1A*[30,31], *CALHM2* (ref. 32) or *CREM*[33]. Although gene knockout can enhance NK cell function, such an approach relies on CRISPR-mediated gene editing, which adds complexity to the manufacturing of cell-based therapies[34]. An alternative strategy is to incorporate functional 'boosters' that drive gene overexpression directly in the CAR construct, which offers a simple and scalable solution for CAR-NK cell manufacturing.

Here we performed an in vivo CRISPR activation (CRISPRa) screen followed by a targeted in vivo barcoded open reading frame (ORF) mini-screen in primary human CAR-NK cells to identify genes for which overexpression enhances antitumour activity in vivo (which we term hyperboosters or boosters). From these experiments, we identified a highly potent gene, *OR7A10*, that enhanced the functions of CAR-NK cells and displayed strong antitumour efficacy in vivo.

In vivo CRISPRa screen for CAR-NK cell boosters

To systematically identify genes that enhance the in vivo antitumour efficacy of CAR-NK cells, we performed an in vivo CRISPRa screen with a genome-scale CRISPRa single-guide RNA (sgRNA) library (SAM)[35]

[1]Department of Genetics, Yale University School of Medicine, New Haven, CT, USA. [2]System Biology Institute, Yale University, West Haven, CT, USA. [3]Center for Cancer Systems Biology, Yale University, West Haven, CT, USA. [4]Combined Program in the Biological and Biomedical Sciences, Yale University, New Haven, CT, USA. [5]Molecular Cell Biology, Genetics, and Development Program, Yale University, New Haven, CT, USA. [6]Yale MD–PhD Program, Yale University School of Medicine, New Haven, CT, USA. [7]Immunobiology Program, Yale University, New Haven, CT, USA. [8]Department of Medicine, The University of Chicago, Chicago, IL, USA. [9]Department of Neurosurgery, Yale University School of Medicine, New Haven, CT, USA. [10]Yale Comprehensive Cancer Center, Yale University School of Medicine, New Haven, CT, USA. [11]Yale Stem Cell Center, Yale University School of Medicine, New Haven, CT, USA. [12]Department of Biomedical Informatics and Data Science, Yale University School of Medicine, New Haven, CT, USA. [13]These authors contributed equally: Luojia Yang, Paul A. Renauer. [14]These authors jointly supervised this work: Lei Peng, Sidi Chen. ✉e-mail: l.peng@yale.edu; sidi.chen@yale.edu

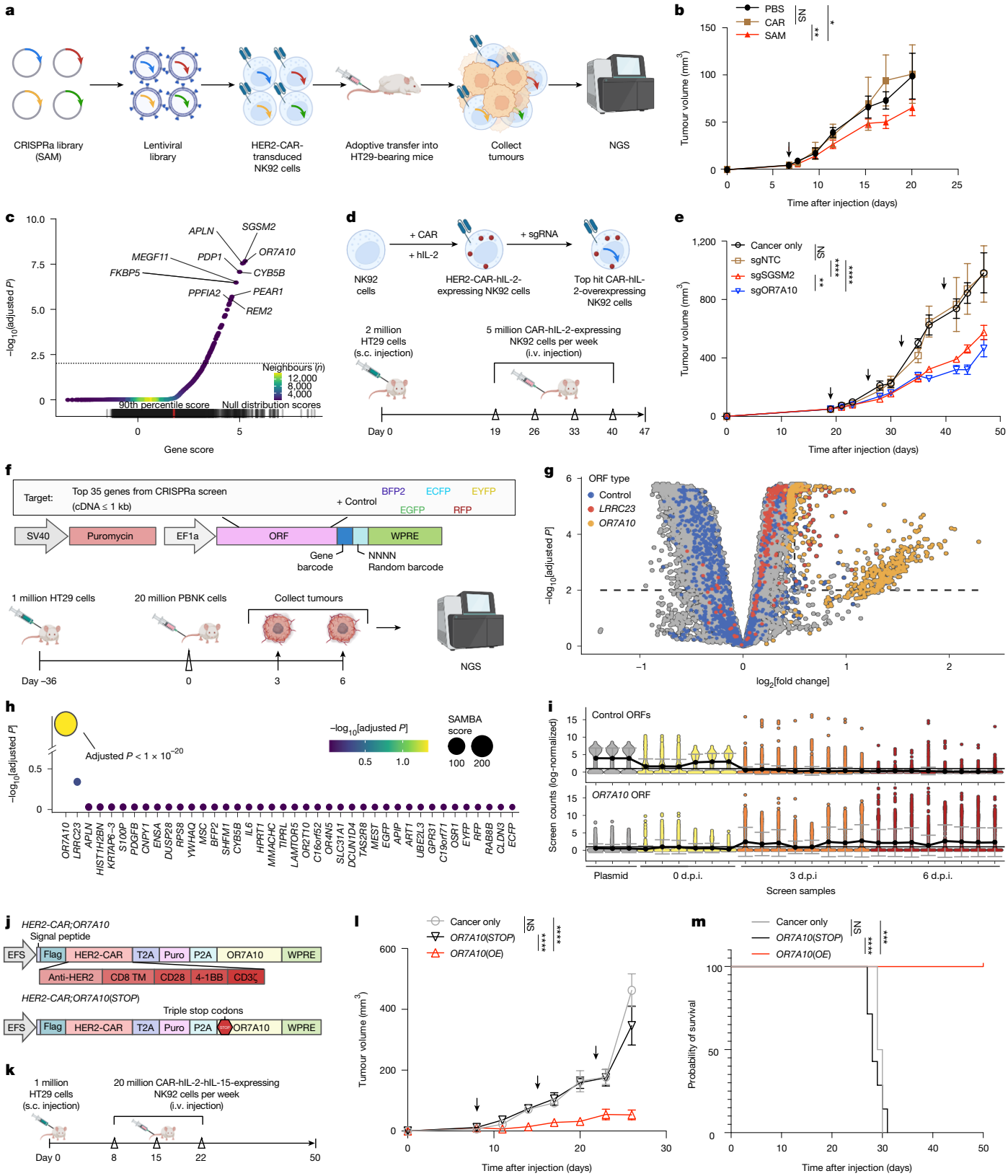

Fig. 1 | See next page for caption.

(Fig. 1a and Methods). Leveraging a HT29 xenograft colorectal cancer model, we used NK92 cells (a NK cell line) for initial screening and hit prioritization and then primary NK cells for secondary validation screening (Extended Data Fig. 1a). Note that the majority of subsequent studies were performed in human primary NK cells (see below).

Non-transduced CAR-NK92 cells did not have significant therapeutic effects compared with PBS controls, whereas SAM-transduced CAR-NK92 cells significantly suppressed tumour growth (Fig. 1b).

Next-generation sequencing (NGS) readout of the screen and analyses showed that there was a substantial difference between the tumour

Fig. 1 | In vivo CRISPRa and barcoded ORF screens identify *OR7A10* as a booster for CAR-NK cell antitumour efficacy. a, Schematic of the in vivo CRISPRa screen for CAR-transduced NK cell boosters (first screen) in the HT29 xenograft mouse model. **b**, Tumour growth curves of HT29 tumour-bearing mice after the following treatments in NK cells: PBS ($n = 4$ mice), CAR ($n = 4$ mice) or SAM-CAR ($n = 12$ mice). Arrow, timing of adoptive transfer. **c**, Scatter plot of the screen analysis results with SAMBA. Dashed line, significance threshold (adjusted $P < 0.01$). Bottom, rug plot of null distribution scores (greyscale) of the sgRNAs, with the 90th percentile (10% FDR) in red. **d**, Schematic of in vivo validation of the top hits. i.p., intraperitoneal; s.c., subcutaneous. **e**, Tumour growth curves of HT29 tumour-bearing mice treated with CAR-hIL-2-expressing NK92 cells transduced with PBS ($n = 5$ mice), sgNTC ($n = 6$ mice), sgSGSM2 ($n = 6$ mice) or sgOR7A10 ($n = 6$ mice). Arrows, timing of adoptive transfers. **f**, Schematic of the in vivo barcoded ORF mini-screen in human primary CAR-NK cells in a HT29-GL model (second screen). **g**, Volcano plot of the UMI-level results of the ORF mini-screen. ORF UMIs for control genes and *LRRC23* and *OR7A10* are indicated. Significant ORF UMIs were those with adjusted $P < 0.01$ and absolute $\log_2$[fold change] > 1. Data in **g**,**h** modeled UMI counts with respect to donor source and time (days post-injection). **h**, Bubble plot of the gene-level results of the ORF mini-screen by SAMBA. **i**, Violin plots of sequencing count distributions for control (top) and *OR7A10* (bottom) UMI ORFs across all samples. d.p.i., day post-injection. **j**, Illustration of the all-in-one constructions of *HER2-CAR*, *HER2-CAR;OR7A10* (*OR7A10*(*OE*)) and *HER2-CAR;OR7A10*(*STOP*) (*OR7A10*(*STOP*)). **k**, Schematic of in vivo validation. **l**, Tumour growth curves of HT29 tumour-bearing mice with no treatment ($n = 4$ mice) or treated with HER2-CAR-hIL-2-hIL-15-expressing NK92 cells transduced with *OR7A10*(*STOP*) ($n = 7$ mice) or *OR7A10*(*OE*) ($n = 6$ mice). Arrows, timing of adoptive transfers. **m**, Survival curves of tumour-bearing mice from **l**. Data are the mean ± s.e.m. Significance levels are indicated in the plots and were calculated using two-way analysis of variance (ANOVA) with Sidak post hoc analysis and FDR adjustment for *P* values (**b**,**e**,**l**) or Mantel–Cox test (**m**). All statistical tests are two-sided, other than the SAMBA gene-level results (**c**,**h**), which used one-sided directional tests. *n* indicates the number of biological replicates. NS, not significant, $^{*}P < 0.05$, $^{**}P < 0.01$, $^{***}P < 0.001$, $^{****}P < 0.0001$. Exact *P* values and detailed statistics are provided in the Source data. The schematics in **a**, **d**, **f** and **k** were created using BioRender (https://biorender.com).

and pre-injection CAR-NK92 cell samples (Extended Data Fig. 1b,c). To analyse the in vivo screen data more effectively, we developed a new optimized analytical method called 'screen analysis method with empirical Bayes estimates for aggregated gene scoring' (SAMBA) (Methods, Extended Data Fig. 1d and Supplementary Dataset 1). SAMBA was tailored to assess sparse data, which is common for in vivo screens of immune cells[36]. We benchmarked the performance of SAMBA against 6 popular analysis methods to detect the enrichment of tumour suppressor genes in an independent set of 71 screens for the proliferation and survival of various cell lines (Extended Data Fig. 1e,f). When we simulated data sparsity in the test dataset, SAMBA demonstrated robust performance for enrichment analysis specificity, sensitivity and overall predictive capabilities, even in datasets in which 90% of guides were undetected in each screen sample (Extended Data Figs. 1g and 2a). We also benchmarked SAMBA for the depletion of essential genes in the test datasets. Although SAMBA significantly improved overall depletion screen performance compared with five of the six methods at baseline sparseness, SAMBA performed only modestly in depletion analyses with increasing sparsity (Extended Data Fig. 2a). These combined results suggest that SAMBA is the most suitable method to analyse our in vivo screen data. Moreover, SAMBA has potential broad applications in analysing other in vivo screens. Using SAMBA, we identified 66 genes for which GOF perturbations were significantly enriched in tumour-infiltrating CAR-NK92 cells relative to pre-injection cells (false discovery rate (FDR) adjusted *P* value (q) < 0.01) (Fig. 1c and Supplementary Dataset 2). Among the top candidates (Fig. 1c), several genes, for example, *APLN*[37–39] and *PDP1* (refs. 40–43), have been previously implicated in cell proliferation, migration and metabolism. However, their roles in NK cells have not been previously reported.

Top GOF hits enhance CAR-NK92 cell function

We validated the CRISPRa-mediated overexpression of the top five hits: *SGSM2*, *OR7A10*, *APLN*, *PDP1* and *CYB5B* (Extended Data Fig. 2b). Four out of the five genes displayed low or undetectable baseline mRNA expression relative to *GAPDH* in both NK92 and human primary NK cells (Extended Data Fig. 2c). Co-culture assays showed that compared with vector alone and the non-targeting control (sgNTC), overexpression of several of these genes significantly enhanced in vitro cytotoxicity against multiple cancer cell lines to different degrees (Extended Data Fig. 2d–i). To assess the preliminary in vivo efficacy of the top hits, we generated HER2-CAR-hIL-2-expressing NK92 cells, transduced them with sgRNAs for *SGSM2* (sg*SGSM2*) or *OR7A10* (sg*OR7A10*) overexpression and adoptively transferred them into mice with HT29 tumours (Fig. 1d). sgNTC-transduced CAR-NK92 cells did not lead to a therapeutic benefit. This result highlights the resistance of HT29 tumours to unmodified CAR-NK92 cell therapy. By contrast, CAR-NK92 cells transduced with sg*SGSM2* or sg*OR7A10* significantly suppressed tumour growth compared with CAR-NK92 cells transduced with sgNTC and PBS controls (Fig. 1e).

Barcoded ORF mini-screen in primary NK cells

To further validate the top hits from the primary CRISPRa screen, we performed an independent mini-screen in primary human peripheral blood NK (PBNK) cells derived from two healthy donors. These cells were injected into the same type of HT29 subcutaneous xenograft mouse model as in the initial screen (Fig. 1f and Methods). The barcoded ORF screen data again demonstrated high quality across multiple quality-control metrics (Extended Data Fig. 2j–l and Supplementary Dataset 3). The ORF unique molecular identifier (UMI) representation and cumulative distribution function of different groups again revealed strong selective pressure of in vivo samples compared with both cell and plasmid samples (Extended Data Fig. 2m). SAMBA analysis revealed that the *OR7A10* ORF again emerged as the strongest and only significantly enriched gene. Moreover, its UMIs represented the predominant significant hits in the UMI-level analysis, dwarfing all other genes in the same pool at both time points (days 3 and 6) and in the analysis where time was modeled as a covariate (Fig. 1g,h and Extended Data Fig. 2n,o). In the gene-level analysis, the *OR7A10* ORF was also the top-ranked hit with strong enrichment (adjusted $P < 1 \times 10^{-20}$) (Fig. 1g,h and Extended Data Fig. 2n,o). The second-ranked hit, *LRRC23*, had a modest signal at the gene-level analysis that modeled time, but did not pass the statistical criteria (adjusted $P > 0.5$). Consistently, barcoded UMI-normalized counts of *OR7A10* ORF showed a strong increase in cell samples and in vivo samples, whereas the control barcoded ORFs did not (Fig. 1i). Together, these independent screens validate *OR7A10* as a consistent and robust booster of NK cell activity in vivo.

OR7A10 ORF enhances CAR-NK92 cell in vivo efficacy

OR7A10 can be harnessed to enhance NK cell therapy via cDNA overexpression, which streamlines the chemistry, manufacturing and control process. We generated a *HER2-CAR;OR7A10* construct (termed *OR7A10*(*OE*) hereafter) and a matched construct with a prematurely stopped *OR7A10* ORF containing triple-stop codons early in the ORF that terminate the ORF in all three coding frames (*HER2-CAR;OR7A10*(*STOP*), termed *OR7A10*(*STOP*) hereafter) for functional studies (Fig. 1j). We established NK92 cells that express human IL-2 and human IL-15, transduced them with the *OR7A10*(*OE*) or *OR7A10*(*STOP*) construct and adoptively transferred them into mice with HT29 tumours (Fig. 1k). *OR7A10*(*STOP*)-transduced CAR-NK92 cells showed minimal tumour

control (Fig. 1l,m), whereas *OR7A10*(*OE*)-transduced CAR-NK92 cells achieved near-complete tumour eradication, with all treated mice (6 out of 6) reaching complete remission (100% CR) and 100% survival (Fig. 1l,m). These results demonstrate that *OR7A10* ORF engineering substantially enhances NK cell antitumour efficacy in vivo and underscore its therapeutic potential and feasibility.

OR7A10 ORF enhances primary CAR-NK cell functions

To further establish the clinical potential of *OR7A10* GOF in CAR-NK cell therapy, human primary NK cells were used for subsequent experiments. PBNK cells from multiple healthy donors were isolated, expanded and transduced with *OR7A10*(*OE*) or *OR7A10*(*STOP*) lentivirus (Fig. 2a and Methods). NK cell purity, surface CAR expression and *OR7A10* overexpression were evaluated by flow cytometry and quantitative PCR with reverse transcription (RT–qPCR) (Fig. 2b and Extended Data Fig. 3a,b). Across 7 independent donors, CAR expression ranged from 22.7 to 91.1% (Fig. 2b and Extended Data Fig. 3a–m), values consistent with clinically relevant transduction efficiencies[44]. *OR7A10*(*OE*)-transduced CAR-NK cells consistently increased tumour cell killing compared with controls across all seven human donor samples (7 out of 7, 100%) (Fig. 2c). This effect was robust across tumour types, whereby *OR7A10*(*OE*)-transduced CAR-PBNK cells showed significantly enhanced cytotoxicity against HT29-GL colon cancer, H1299-PL lung carcinoma, K562-GL myelogenous leukaemia and MCF7-PL breast cancer cells (where GL and PL indicate tags for GFP–luciferase and puromycin–luciferase, respectively). Moreover, efficacy was robust across multiple effector (NK cells) to target (cancer cells) (E:T) ratios and time points (Fig. 2d and Extended Data Fig. 3c–m). *OR7A10*(*OE*)-transduced CAR-PBNK cells exhibited significantly increased degranulation after HT29 co-culture (Fig. 2e) and increased production of granzyme B (GZMB) and perforin (Fig. 2f). Moreover, *OR7A10*(*OE*)-transduced CAR-PBNK cells had significantly increased expression of the death receptors FasL and TRAIL (Fig. 2g) and significantly increased production of IFNγ and TNF compared with controls (Fig. 2h,i).

We next evaluated additional effector functions of *OR7A10*(*OE*)-transduced CAR-PBNK cells (Methods). Compared with control groups, *OR7A10*(*OE*)-transduced CAR-PBNK cells exhibited greater dye dilution (indicative of increased proliferation) and significantly higher cell counts at the end of the culture (Extended Data Fig. 3n). Because the chemokine receptor CXCR2 is essential for NK cell trafficking to tumours[45,46], we stimulated CAR-PBNK cells with HT29 cells for 24 h and observed that *OR7A10*(*OE*) transduction led to significantly upregulated surface CXCR2 expression (Extended Data Fig. 3o). We also observed multiple elevated NK cell activation markers in *OR7A10*(*OE*)-transduced CAR-PBNK cells, including CD69 (Extended Data Fig. 3p), IL-2Rα (also known as CD25) (Extended Data Fig. 3q) and the co-stimulatory receptor 4-1BB (Extended Data Fig. 3r).

To assess the exhaustion of *OR7A10*(*OE*)-transduced CAR-PBNK cells, we performed a repeated challenge assay (Methods and Extended Data Fig. 3s). *OR7A10*(*OE*)-transduced CAR-PBNK cells showed enhanced killing compared with controls at 24 h after the final stimulation (Extended Data Fig. 3s). Notably, *OR7A10*(*OE*)-transduced CAR-PBNK cells exhibited significantly reduced surface expression of exhaustion markers, including TIM-3, LAG-3, PD-1 and NKG2A (Extended Data Fig. 3t–v). Together, these data demonstrate that *OR7A10* overexpression augments the antitumour activity of CAR-PBNK cells through multiple ways, including degranulation, cytokine production, death receptor expression, proliferation, chemokine receptor expression, activation, sustained cytotoxicity and reduced exhaustion.

OR7A10 ORF enhances CAR-CBNK cell activities

To further support the clinical translatability of *OR7A10* GOF engineering in CAR-NK cells, we validated its function in NK cells derived from cord blood (CBNK cells)[44]. CBNK cells from a healthy donor were expanded and transduced with either the *OR7A10*(*OE*) or the control *OR7A10*(*STOP*) construct (Extended Data Fig. 4a). NK cell purity and CAR expression were confirmed (Extended Data Fig. 4b) before a repeated challenge assay using HT29 cancer cells to assess their persistent killing capacity (Extended Data Fig. 4c). Although all CAR-CBNK groups showed comparable and saturated killing during the first two stimulation rounds, *OR7A10*(*OE*)-transduced CAR-CBNK cells exhibited significantly enhanced cytotoxicity against HT29 cells 24 h after the third round compared with both unmodified CBNK cells and *OR7A10*(*STOP*)-transduced CAR-CBNK cells (Extended Data Fig. 4c).

Given that IL-15 expression provides cytokine support for NK cells and enhances long-term persistence and antitumour activity[47], it has been commonly incorporated into clinical CAR-NK cell constructs[44,48]. We adopted the clinically relevant co-cistronic IL-15 expression design and engineered a *HER2-CAR;hIL15;OR7A10* construct (termed *hIL15;OR7A1A* hereafter) along with a *HER2-CAR;hIL15;OR7A10*(*STOP*) control (termed *hIL15;OR7A10*(*STOP*) hereafter) (Extended Data Fig. 4d). Flow cytometry and ELISA assays validated the co-expression of CAR and hIL-15 and the secretion of hIL-15 in transduced NK cells but not in untransduced controls (Extended Data Fig. 4e,f). We confirmed NK purity and CAR expression (Extended Data Fig. 4g) and performed repeated challenge assays. Consistently, CAR-CBNK cells transduced with *hIL15;OR7A10* exhibited significantly enhanced cytotoxicity against HT29 cells 24 h after the third round of stimulation compared with controls (Extended Data Fig. 4h). These results show that *OR7A10* GOF engineering enhances the cytotoxicity and persistence of CAR-CBNK cells, which provides further support for the clinical feasibility of this platform.

OR7A10 ORF enhances CAR-CBNK cell metabolic fitness

Given the importance of metabolic fitness for sustained NK cell killing in the TME[49], we stimulated CAR-PBNK cells with HT29 cells and assessed their metabolic profiles using Seahorse real-time metabolic analyses, MitoTracker staining and transmission electron microscopy (TEM) (Fig. 3a). *OR7A10*(*OE*)-transduced CAR-PBNK cells exhibited substantially higher basal, spare and maximal oxygen consumption rates (OCRs) compared with *OR7A10*(*STOP*)-transduced cells after stimulation (Fig. 3b). Moreover, *OR7A10*(*OE*)-transduced CAR-PBNK cells had higher mitochondrial mass compared with control CAR-NK cells, as measured by MitoTracker staining (Fig. 3c). Consistently, TEM analysis revealed that *OR7A10*(*OE*)-transduced CAR-PBNK cells had a greater individual mitochondria area per cell, whereas the mitochondria length remained unchanged. Again, this result suggests that these cells have increased mitochondrial mass and enhanced metabolic capacity (Fig. 3d). These findings indicate that *OR7A10* overexpression enhances the metabolic fitness of CAR-PBNK cells after tumour stimulation.

NK cells encounter a diverse range of immunosuppressive cues in the TME that substantially limit their cytotoxic function (Fig. 3e). To determine whether *OR7A10* overexpression enables NK cells to overcome TME-induced immunosuppression, CAR-NK cells transduced with *OR7A10*(*OE*) or *OR7A10*(*STOP*) were cultured with HT29 and H1299 cancer cells under multiple suppressive conditions. Cells were treated with L-(+)-lactic acid (7.5 mM; to induce acidic conditions) (Fig. 3f), transforming growth factor-β (TGFβ, 100 ng ml^{-1}) (Fig. 3g), low IL-2 (1 ng ml^{-1}; to induce cytokine deprivation) (Fig. 3h), calcineurin inhibitors (cyclosporine A (50 nM) or tacrolimus (5 nM)) (Fig. 3i,j), an adenosine signalling agonist (CGS-21680, 20 μM) (Fig. 3k) or $CoCl_2$ (100 μM; to induce hypoxia) (Fig. 3l). *OR7A10*(*OE*) transduction significantly enhanced CAR-PBNK-cell-mediated cytotoxicity across all these conditions (Fig. 3f–l). Together, these findings indicate that *OR7A10* ORF engineering enables CAR-NK cells to resist multiple forms of immunosuppression present in the TME.

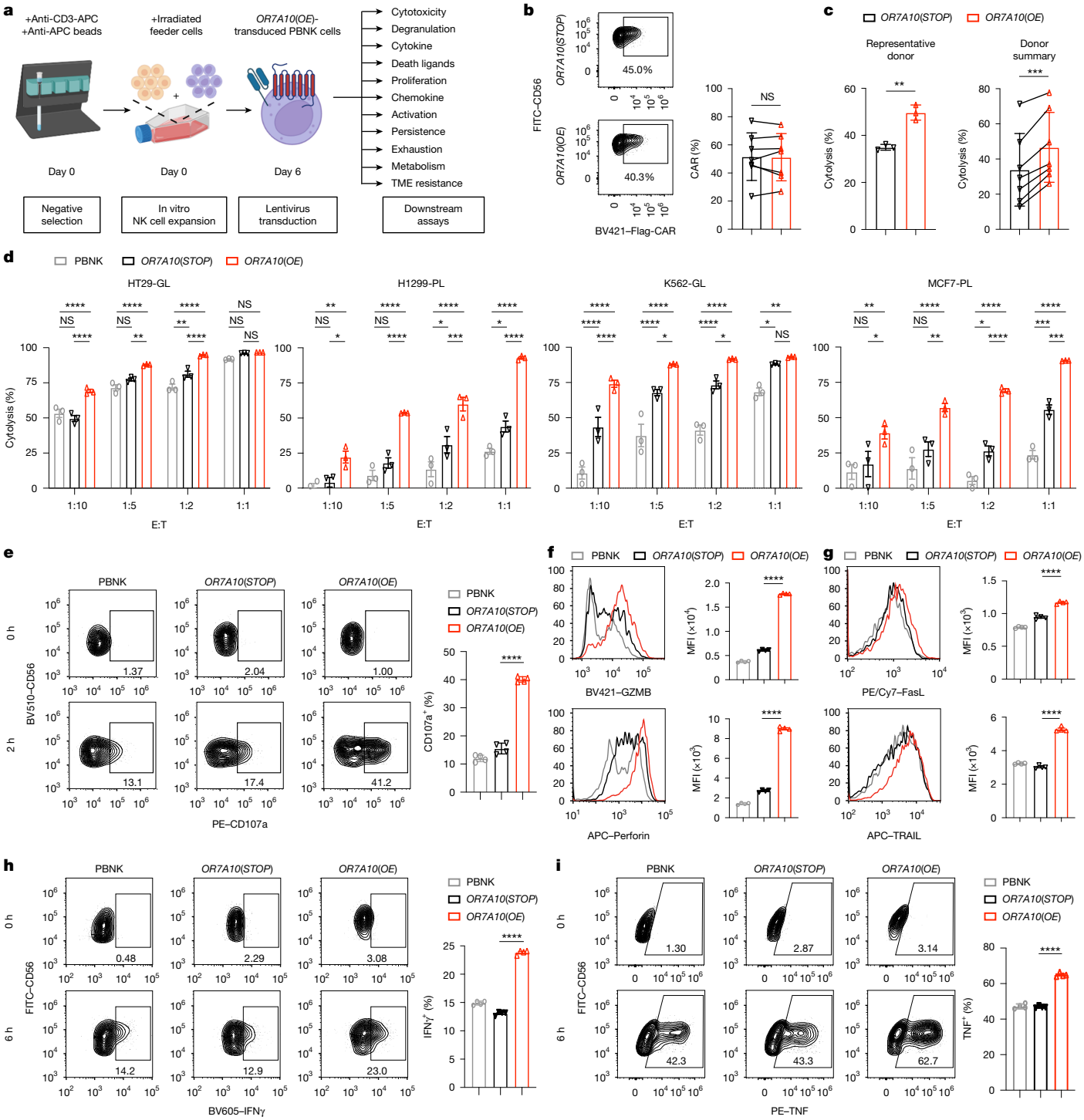

Fig. 2 | *OR7A10* ORF engineering enhances the antitumour function of CARPBNK cells. a, Schematic of the CAR-PBNK cell experiment. **b**, Flow cytometry of CAR surface expression in human primary CAR-PBNK cells of one representative donor (left) and summary of seven different human donors (right). **c**, Cytolysis of human primary CAR-PBNK cells against HT29 colon cancer cells (after 24 h, E:T = 1:10) of 1 representative donor (left), and summary of 7 different human donors (right). **d**, Cytolysis of human primary CAR-PBNK cells against 4 cancer cell lines at different E:T ratios after 6 h. Data represent triplicates from one representative donor out of two different donors. **e**–**i**, Flow cytometry of PBNK cells alone (PBNK), and PBNK cells transduced with the *OR7A10*(*STOP*) or *OR7A10*(*OE*) construct after stimulation with HT29 cells (E:T = 1:1). Data represent technical quadruplicates from one representative donor out of four different human donors. **e**, Degranulation (CD107a) levels after stimulation for 0 or 2 h. **f**, GZMB levels after stimulation for 0 or 6 h. **g**, FasL and TRAIL levels after stimulation for 0 or 24 h. MFI, mean fluorescence intensity. **h**,**i**, IFNγ (**h**) and TNF (**i**) levels after stimulation for 0 or 6 h. Data represent technical quadruplicates from one representative donor out of four different human donors. Data are the mean ± s.e.m. The significance levels are indicated in the plots and were calculated using paired *t*-test (**b**,**c**), two-way ANOVA with Sidak post hoc analysis and FDR correction of *P* values (**d**) or unpaired *t*-test (**e**–**i**). All statistical tests are two-sided unless otherwise noted. $^{*}P < 0.05$, $^{**}P < 0.01$, $^{***}P < 0.001$, $^{****}P < 0.0001$. Exact *P* values and detailed statistics are provided in the Source data. The schematic in **a** was created using BioRender (https://biorender.com).

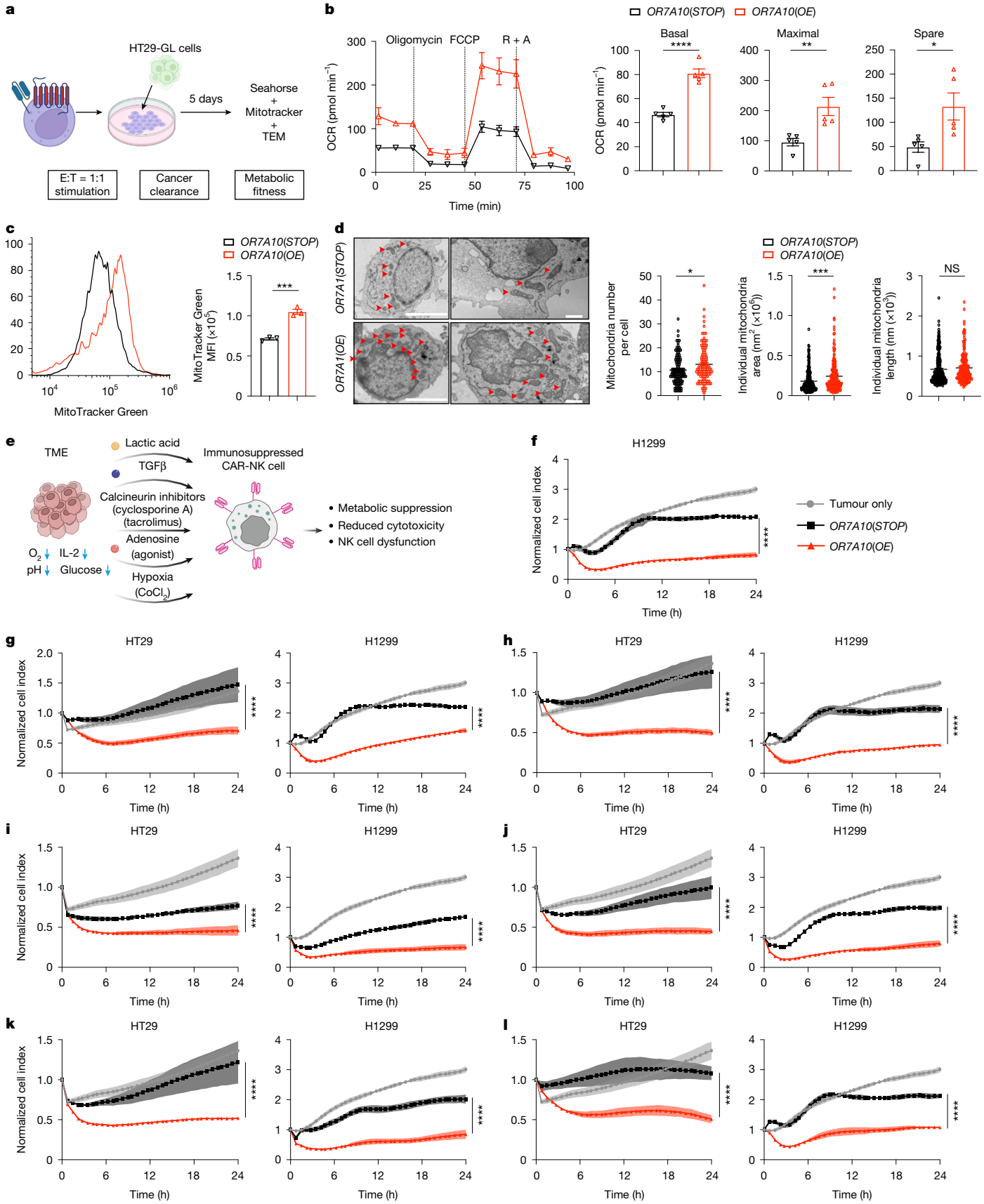

Fig. 3 | See next page for caption.

Fig. 3 | *OR7A10* ORF engineering enhances metabolic fitness and resistance to TME-relevant immunosuppression of CAR-PBNK cells. a, Schematic of metabolic profiling. NK cells were collected after 5 days of co-culture with HT29 cells at an initial E:T ratio of 1:1 to achieve complete tumour clearance, with daily replenishment of medium. **b**, Seahorse experiment and quantification of CAR-PBNK cells transduced with the *OR7A10*(*STOP*) or *OR7A10*(*OE*) construct, with a density of 1×10^6 NK cells per well. Data represent five technical replicates from one representative donor out of three different human donors. **c**, Flow cytometry of MitoTracker in CAR-PBNK cells transduced with the *OR7A10*(*STOP*) or *OR7A10*(*OE*) construct. Data represent technical quadruplicates from one out of two donors. **d**, TEM analysis and quantification of CAR-PBNK cells transduced with the *OR7A10*(*STOP*) or *OR7A10*(*OE*) construct. TEM images were examined for mitochondrial numbers (red arrowheads indicate mitochondria). Data are from one out of two donors. Numbers of mitochondria analysed: left, STOP, $n = 119$, OE, $n = 108$; middle, STOP, $n = 221$, OE, $n = 185$; right, STOP, $n = 227$, OE, $n = 203$. Scale bars, 4 µm (left column) or 10 µm (right column). **e**, Schematic of TME-relevant immunosuppression. **f**–**l**, NK cell cytotoxicity assessed by RTCA killing assays against HT29 and H1299 cells at an E:T ratio of 1:1 in the presence of the following different immunosuppressive conditions: L-(+)-lactic acid (final concentration 7.5 mM) (**f**); TGFβ1 (final concentration 100 ng ml^{-1}) (**g**); cytokine deprivation (low IL-2, final concentration 1 ng ml^{-1}) (**h**); calcineurin inhibition via cyclosporine A (final concentration 50 nM) (**i**) or tacrolimus (final concentration 5 nM) (**j**); adenosine signalling agonism via CGS-21680 (final concentration 20 µM) (**k**); and hypoxia via $CoCl_2$ (final concentration 100 µM) (**l**). Data are the mean ± s.e.m. The significance levels are indicated in the plots and were calculated using unpaired *t*-test (**b**–**d**) or two-way ANOVA (**f**–**l**). All statistical tests are two-sided unless otherwise noted. $^*P < 0.05$, $^{**}P < 0.01$, $^{***}P < 0.001$, $^{****}P < 0.0001$. Exact *P* values and detailed statistics are provided in the Source data. The schematics in **a** and **e** were created using BioRender (https://biorender.com).

Exploration of *OR7A10* GPCR signalling

Because OR7A10 is a GPCR, we next explored the GPCR signalling components in relation to the OR7A10-mediated augmentation of NK cell activities (Methods). We knocked out *GNAS* (*GNAS* KO), along with *AAVS1* (*AAVS1* KO) as a control, in primary human CAR-NK cells (Extended Data Fig. 4i). Cyclic AMP levels and PKA activity were significantly reduced in *GNAS* KO cells compared with *AAVS1* KO controls (Extended Data Fig. 4j,k). *OR7A10*(*OE*)-transduced cells showed significantly lower cAMP levels and PKA activity than *OR7A10*(STOP)-transduced controls (Extended Data Fig. 4j,k). *GNAS* KO NK cells and *AAVS1* KO NK cells were then transduced with the *OR7A10*(*OE*) or *OR7A10*(STOP) construct and cultured with HT29 cells. Notably, knocking out *GNAS* dampened the *OR7A10*(*OE*)-mediated effect of enhanced cytotoxicity in human primary CAR-PBNK cells (Extended Data Fig. 4l). Moreover, ERK1/2 phosphorylation in *OR7A10*(*OE*)-transduced CAR-PBNK cells was increased after cancer stimulation (Extended Data Fig. 4m). To assess NF-κB activation, an engineered NF-κB reporter construct (Methods) was transduced into CAR-PBNK cells. NF-κB signalling in *OR7A10*(*OE*)-transduced CAR-NK cells was significantly increased after cancer stimulation (Extended Data Fig. 4n). *GNAS* KO abolished the *OR7A10*-driven increase in ERK1/2 phosphorylation and NF-κB signalling (Extended Data Fig. 4m,n). To test whether these GPCR signalling components have a role in the *OR7A10*-mediated enhancement of cytotoxicity of in CAR-PBNK cells, we treated cells transduced with the *OR7A10*(*OE*) or *OR7A10*(*STOP*) construct with various small-molecule inhibitors. These included the pERK inhibitor ulixertinib, the NF-κB inhibitors BOT-64 and BAY 11-7082, the PKA inhibitor H89, the NFAT inhibitor INCA-6 and the Gβγ inhibitor gallein (Methods). Inhibition of all these pathways significantly dampened the *OR7A10*-driven increased cytotoxicity of CAR-PBNK cells (Extended Data Fig. 4o–t).

Differential expression of CAR-PBNK cells

We performed transcriptome profiling by bulk mRNA sequencing (mRNA-seq) and used generalized linear models (GLMs) to analyse the effects of OR7A10, CAR, immune stimulation and their interactions (Methods). Principal component analysis (PCA) revealed that the greatest variance in the data came from stimulation, followed by the effects of *OR7A10* overexpression, which separated samples by the first and second principal components, respectively (Extended Data Fig. 5a and Supplementary Dataset 4). Differential expression (DE) analyses of the effect of stimulation, independent of *OR7A10*-expression status, revealed 3,639 downregulated and 5,123 upregulated genes (Extended Data Fig. 5b). Pathway analyses revealed upregulated and downregulated pathways (Extended Data Fig. 5c). *OR7A10* overexpression resulted in 1,667 upregulated genes (such as *CISH*) and 2,316 downregulated genes (such as *PIK3IP1*) (Extended Data Fig. 5d,e). Cytotoxic effectors such as *GZMB* and inflammatory cytokines such as *CCL3* were upregulated, a result consistent with the antitumour capability of *OR7A10*-overexpressing NK cells (Extended Data Fig. 5e). The interaction between *OR7A10* and CAR was then assessed in stimulated NK cells with the interaction term of the GLM, which identified 387 upregulated genes and 78 downregulated genes (Extended Data Fig. 5f). Pathway analyses revealed that *OR7A10* overexpression induced the upregulation of multiple pathways, including immune response, immune system process, cell cycle, leukocyte activation and positive regulation of leukocyte proliferation (Extended Data Fig. 5h–j). These data further demonstrate that *OR7A10* overexpression significantly alters the gene expression landscape of human primary NK and CAR-NK cells.

OR7A10 overexpression synergizes with NKp46 signalling

To determine whether the enhanced CAR-NK cell activity conferred by *OR7A10*(*OE*) transduction is restricted to a specific co-stimulatory domain of the HER2 CAR construct (Fig. 1j), we performed cytotoxicity assays using two additional different CAR constructs with different co-stimulatory domain compositions (Methods): B7H3 CAR (which is CD28-based; Extended Data Fig. 6a–c) and CD22 CAR (which is 4-1BB-based; Extended Data Fig. 6d–f). Flow cytometry analysis confirmed comparable CAR expression levels among these cells (Extended Data Fig. 6b,e). Cytotoxicity assays demonstrated that *OR7A10* overexpression significantly augmented the antitumour activity of both B7H3 and CD22 CAR-NK cells (Extended Data Fig. 6c,f). Together with the results from HER2 CAR-NK cells, these data show that the enhancement mediated by *OR7A10* overexpression is not inherently specific to either the 4-1BB or CD28 co-stimulatory domains in second-generation CARs in NK cells.

To further evaluate how OR7A10 synergizes with other activating inputs, we assessed its interaction with signalling components from distinct NK cell receptors (Methods). CAR-NK cells transduced with the *OR7A10*(*OE*) or *OR7A10*(*STOP*) construct were subjected to mRNA electroporation to overexpress *NCR1* (which encodes NKp46), *CD16*, *NKG2D*, *2B4* or *mScarlet* (as the control). At 24 h after electroporation, flow cytometry confirmed robust receptor expression (Extended Data Fig. 6g). Then, we performed co-culture assays with HT29 tumour cells and analysed time-course cytotoxicity via real-time cell analysis (RTCA) assays. Again, *OR7A10* overexpression enhanced cytotoxicity in all the conditions, validating the above-described results (Extended Data Fig. 6h,i). Specifically, overexpression of *NCR1* further augmented the cytotoxicity of CAR-NK cells, and the effect was synergistic with *OR7A10* overexpression (Extended Data Fig. 6h,i). *CD16* overexpression itself did not augment CAR-NK cell killing; however, it showed modest synergy with *OR7A10* overexpression that was marginally significant (Extended Data Fig. 6h,i). Neither *NKG2D* nor *2B4* showed any synergy

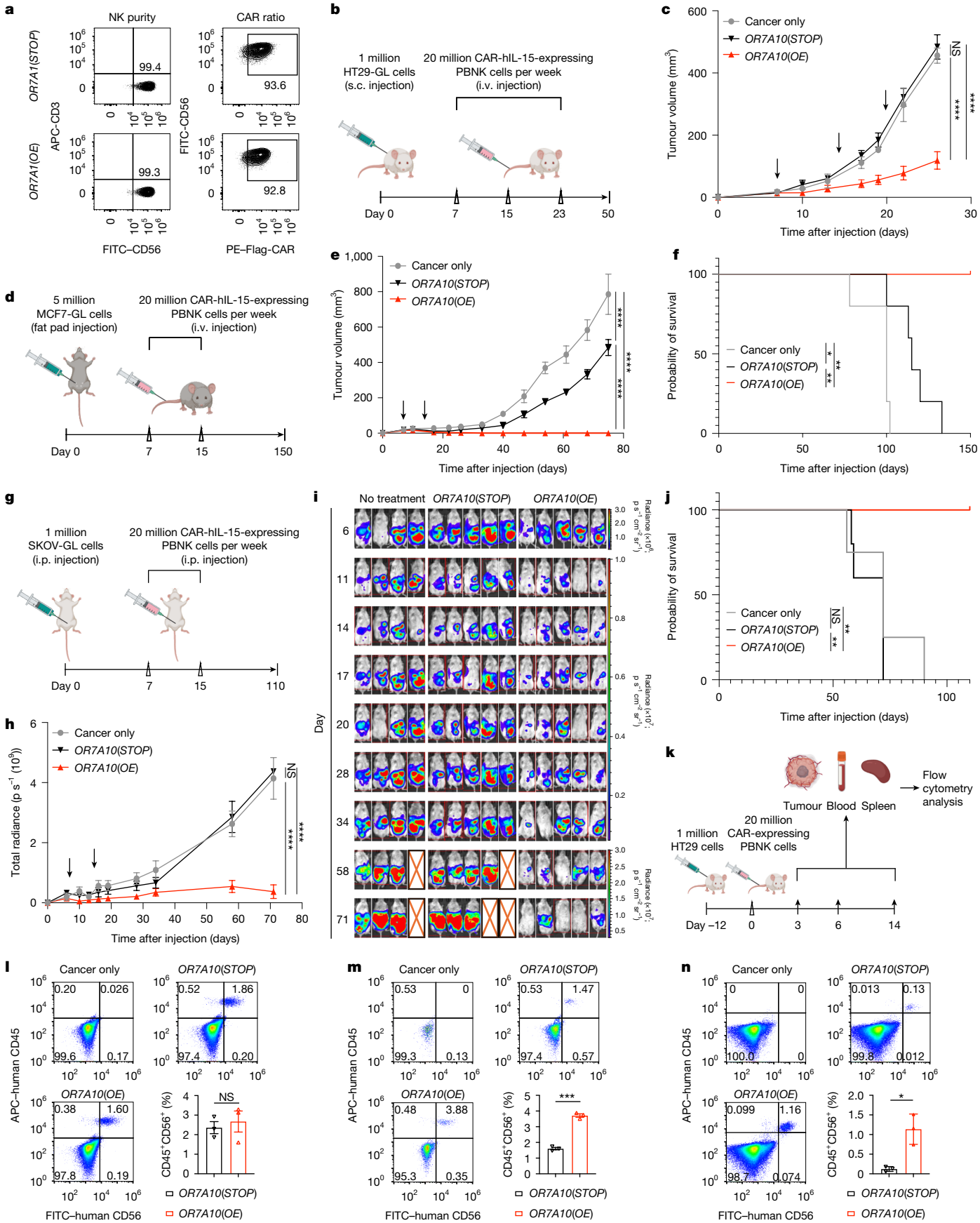

Fig. 4 | See next page for caption.

Fig. 4 | *OR7A10* ORF engineered CAR-PBNK cells show high in vivo antitumour efficacy and enhanced tumour infiltration across multiple tumour models. a, Flow cytometry of NK cell purity and CAR expression of CAR-PBNK cells transduced with the *OR7A10*(*STOP*) or *OR7A10*(*OE*) construct. **b**,**c**, Schematic (**b**) and tumour growth curve (**c**) of mice with HT29 tumours after different treatments: no treatment ($n = 3$ mice) or adoptive transfer of HER2-CAR-hIL-15-expressing PBNK cells transduced with *OR7A10*(*STOP*) ($n = 5$ mice) or *OR7A10*(*OE*) ($n = 5$ mice). Arrows indicate the time of adoptive transfer of CAR-PBNK cells. **d**–**f**, Schematic (**d**), tumour growth curves (**e**) and survival curves (**f**) of MCF7 tumour-bearing mice following different treatments: no treatment ($n = 5$ mice) or adoptive transfer of HER2-CAR-hIL-15-expressing PBNK cells transduced with *OR7A10*(*STOP*) ($n = 5$ mice) or *OR7A10*(*OE*) ($n = 5$ mice). Arrows indicate the time of adoptive transfer of CAR-PBNK cells. **g**–**j**, Schematic (**g**), quantification (**h**), bioluminescence images (**i**) and survival curves (**j**) of mice with SKOV3 tumours after different treatments: no treatment ($n = 4$ mice) or adoptive transfer of HER2-CAR-hIL-15-expressing PBNK cells transduced with *OR7A10*(*STOP*) ($n = 5$ mice) or *OR7A10*(*OE*) ($n = 5$ mice). **k**, Schematic of in vivo CAR-NK cell characterization by flow cytometry. **l**–**n**, Flow cytometry and quantification of $CD45^+CD56^+$ NK cells in the spleen (**l**), blood (**m**) and tumour samples (**n**) ($n = 3$ mice) at day 3 after NK cell transfer. Data are the mean ± s.e.m. Bioluminescence images (**i**) are shown with scaled radiance intensities (day 6: 1×10^5–3×10^6; days 11–34: 5×10^5–1×10^7; days 58–71: 3×10^6–3×10^7) and an "X" for deceased mice. The significance levels are indicated in the plots and were calculated using unpaired *t*-test (**l**–**n**), two-way ANOVA with Sidak post hoc analysis and FDR-corrected *P* values (**c**,**e**,**i**) or Mantel–Cox test (**f**,**j**). All statistical tests are two-sided unless otherwise noted. $^*P < 0.05$, $^{**}P < 0.01$, $^{***}P < 0.001$, $^{****}P < 0.0001$. Exact *P* values and detailed statistics are provided in the Source data. The schematics in **b**, **d**, **g** and **k** were created using BioRender (https://biorender.com).

with *OR7A10* overexpression under these conditions (Extended Data Fig. 6h,i). These data suggest that *OR7A10* overexpression synergizes with *NCR1*, but not *2B4* or *NKG2D*.

In vivo efficacy of CAR-PBNK cells

We next evaluated the effect of *OR7A10* overexpression on the antitumour efficacy of human primary CAR-NK cells in vivo. After NK cell purity and CAR expression were confirmed (Fig. 4a), PBNK cells transduced with the *hIL15;OR7A10* or *hIL15;OR7A10*(*STOP*) construct were evaluated for their efficacy in three solid tumour models: HT29, MCF7 and SKOV3. In the HT29 colon cancer model, tumours were established through subcutaneous injection of HT29 cells, followed by adoptive transfer of CAR-PBNK cells (Fig. 4b). *hIL15;OR7A10*-transduced CAR-PBNK cells showed significantly enhanced antitumour activity compared with both *hIL15;OR7A10*(*STOP*)-transduced CAR-PBNK cells and cancer-only control groups (Fig. 4c).

In the MCF7 breast cancer model, tumours were orthotopically induced via fat pad injection of cancer cells, followed by subsequent CAR-PBNK cell treatment (Fig. 4d). Although *hIL15;OR7A10*(*STOP*)-transduced CAR-PBNK cells retained moderate activity and partially suppressed tumour growth (Fig. 4e,f), *hIL15;OR7A10*-transduced CAR-PBNK cells exhibited substantial efficacy, with mice achieving complete tumour eradication and prolonged survival (5 out of 5 with 100% CR) (Fig. 4e,f). In the SKOV3 orthotopic ovarian cancer model with metastatic disease, NSG mice were intraperitoneally inoculated with SKOV3-GL cells and then intraperitoneally injected with CAR-PBNK cells (Fig. 4g). *hIL15;OR7A10*(*STOP*)-transduced CAR-PBNK cells did not control tumour progression (Fig. 4h–j), whereas *hIL15;OR7A10*-transduced CAR-PBNK cells led to robust antitumour activity, which in turn led to both sustained tumour control and long-term survival in all treated mice (Fig. 4h–j).

OR7A10-overexpressing CAR-CBNK cells have favourable safety

We analysed the safety profiles of *OR7A10*(*OE*)-transduced CAR-PBNK cells. Consistent with the favourable safety profile of CAR-NK cell therapy[44], no detectable differences in IFNγ or IL-6 levels were observed in mouse serum between any groups of treatment (cancer only, *OR7A10*(*OE*)-transduced CAR-PBNK cells and *OR7A10*(*STOP*)-transduced CAR-PBNK cells) (Extended Data Fig. 7a). Moreover, histological analyses using haematoxylin and eosin (H&E) staining did not reveal any pathological differences in vital organs, such as the lung, liver and kidney (Extended Data Fig. 7b), which suggests that *OR7A10* overexpression in CAR-PBNK cells did not alter the level of these cytokines in the serum and further corroborate the safety of CAR-PBNK cells. In the MCF7 orthotopic breast cancer model, in which *OR7A10*(*OE*)-transduced CAR-PBNK cells showed high efficacy, there was no obvious weight loss in mice (Extended Data Fig. 7c).

To assess the impact of *OR7A10* overexpression on genome structure integrity, we performed whole-genome sequencing (WGS) on primary human NK cells transduced with the *OR7A10*(*OE*) or *OR7A10*(*STOP*) construct. In total, 682 and 620 insertion and deletion (indel) variants were identified in *OR7A10*(*OE*)-transduced and *OR7A10*(*STOP*)-transduced NK cells, respectively, as called against the reference genome (Methods and Supplementary Dataset 5). Each NK cell group displayed comparable indel counts across chromosomes (Extended Data Fig. 7d), and there was no detectable chromosomal translocations in either *OR7A10*(*OE*)-transduced or *OR7A10*(*STOP*)-transduced groups (Extended Data Fig. 7e). These data suggest that *OR7A10* overexpression does not increase genomic aberration risk in human primary CAR-NK cells compared with the control. To study the risk of malignant transformation of *OR7A10*(*OE*)-transduced CAR-NK cells, we performed an autonomous growth assay (IL-2 withdrawal assay). In IL-2 withdrawal conditions, neither *OR7A10*(OE)-transduced nor *OR7A10*(*STOP*)-transduced human primary CAR-NK cells survived more than 21 days (Extended Data Fig. 7f). This finding indicates that *OR7A10* overexpression does not bypass IL-2 dependency and that *OR7A10*(*OE*)-transduced CAR-NK cells were not transformed.

OR7A10 expression in CAR-T and CAR-NK cells

A recent study compared CAR-T cell and CAR-NK cell therapies in animal models[50]. To directly compare the therapeutic efficacy and safety of *OR7A10* overexpression in CAR-NK and CAR-T cell therapy, we generated CAR-T cells from the same healthy donors used to generate CAR-NK cells and transduced them with the *OR7A10*(*OE*) or *OR7A10*(*STOP*) construct. We then conducted several in vitro and in vivo experiments together with the CAR-NK cell counterparts (Extended Data Fig. 7g). Purity and CAR expression of all cell types were confirmed before each of these studies (Extended Data Fig. 7h). Although *OR7A10* expression enhanced the in vitro cytotoxicity of CAR-NK cells compared with controls, it did not enhance CAR-T cell cytotoxicity (Extended Data Fig. 7i). This finding indicates that the effect of OR7A10 is specific to the NK cell type.

To evaluate the function of these cells in vivo, NSG mice were first intraperitoneally inoculated with SKOV3-GL cells and then treated with a single dose of 5 million CAR-NK or CAR-T cells (Extended Data Fig. 7j). This comparative in vivo experiment revealed that *OR7A10*(*STOP*)-transduced CAR-PBNK cells did not control tumour progression, whereas a single dose of *OR7A10*(*OE*)-transduced CAR-PBNK cells led to enhanced antitumour efficacy. Moreover, *OR7A10* expression did not provide benefit to the efficacy of CAR-T cells, and *OR7A10*(*OE*)-transduced CAR-PBNK cells had comparable efficacy to that of the two groups of CAR-T cells at the same dose level

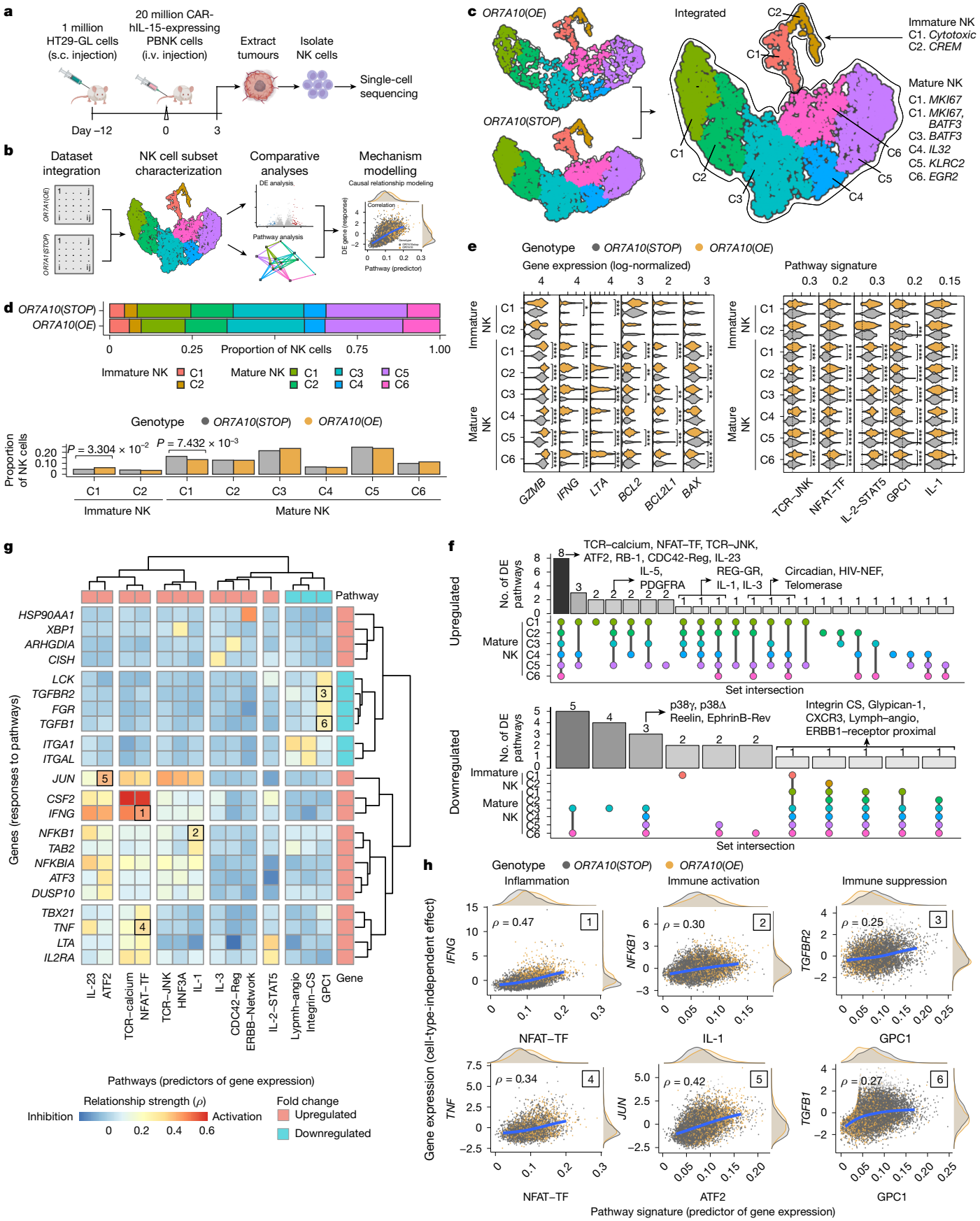

Fig. 5 | See next page for caption.

Fig. 5 | SCT reveals unbiased in vivo gene expression alterations driven by *OR7A10* overexpression in tumour-infiltrating human primary CAR-NK cells. a, Schematic of SCT of *OR7A10*(*OE*)-transduced CAR-PBNK cells from HT29-GL xenograft tumours. **b**, Schematic of the SCT analysis strategy. **c**, Uniform manifold approximation and projection (UMAP) depiction of tumour-infiltrating CAR-NK cells (separated on left; merged on right). Cells are colour-coded by clusters, which were annotated using cell-type-specific markers. **d**, Comparison of the NK cell subset distribution in stacked (top) and side-by-side (bottom) bar plots. **e**, Violin plots of DE genes (left) and pathways (right). **f**, Upset plot of DE pathways that were common between subsets of NK cells transduced with *OR7A10*(*OE*) or *OR7A10*(*STOP*). Upregulated (top) and downregulated (bottom) pathway comparisons are displayed separately. Pathways are labelled if they were significant in at least four subsets. **g**, Heatmap of the predicted cause–effect relationships between pathways (predictors; columns) and gene expression (responses; rows). DE fold change direction for pathways and genes across all NK cell subset comparisons is presented along the margins of the heatmap in red and blue (upregulation and downregulation, respectively). CS, cell surface; Lymph–angio, VEGFR3 signalling; Reg, regulation; TF, transcription factor. **h**, Scatter plots of the top predicted cause–effect relationships between DE pathways and DE genes selected from **g**. Gene expression was adjusted to be independent of cell subset effects. Trends are shown by the blue regression lines (simple generalized additive model). Pearson's correlation analysis results (rho (ρ) values and two-sided P values) are shown for correlations between pathways and the adjusted gene scores. Statistical analyses were performed using pairwise Fisher exact tests with P values adjusted using the FDR method (**d**) or two-way ANOVA tests with Tukey's post hoc analysis (**e**). All statistical tests are two-sided unless otherwise noted. *$P < 0.05$, **$P < 0.01$, ***$P < 0.001$, ****$P < 0.0001$. The schematic in **a** was created using BioRender (https://biorender.com).

(Extended Data Fig. 7k,l). Finally, *OR7A10*(*OE*)-transduced CAR-NK cells maintained a favourable safety profile, with no GVHD detected in any mice (0 out of 4, 0%) in this group during the entire course of treatment. By contrast, GVHD symptoms were detected in all mice (8 out of 8, 100%) in the two groups of CAR-T cells (Extended Data Fig. 7m).

OR7A10 overexpression enhances NK cell infiltration and survival

We next investigated tumour infiltration and in vivo survival of NK cells in mice with tumours. We examined blood, spleen and tumour samples after NK cell injection (Fig. 4k). At day 3, *OR7A10*(*OE*)-transduced CAR-PBNK cell counts were significantly increased in blood and tumours, but not spleen, compared with the control group (Fig. 4l–n). By day 6, the number of *OR7A10*(*OE*)-transduced CAR-PBNK cells in the blood was higher than that of controls, but not significant, whereas CAR-PBNK cells numbers in tumours remained significantly higher (Extended Data Fig. 7n–p). Notably, tumour weights in the *OR7A10*(*OE*)-transduced group were significantly lower than in control groups by day 6 (Extended Data Fig. 7n). This result demonstrates the efficacy of *OR7A10*(*OE*)-transduced CAR-PBNK cells; that is, gross antitumour effects were already detectable by day 6. However, few NK cells were detectable at day 14 across all tissues (Extended Data Fig. 7q–s), which revealed the limits of NK cell persistence in this model. These data show that *OR7A10* overexpression enhances CAR-PBNK cell infiltration into tumours and in vivo survival in the circulation and in tumours, as detected in the first week after adoptive transfer. These results reflect the enhanced in vivo antitumour activity of these cells compared with control CAR-PBNK cells.

Single-cell profiling of CAR-PBNK cells

To investigate how *OR7A10* overexpression enhances CAR-NK cell function in the TME in an unbiased manner, we performed single-cell transcriptomics (SCT) of tumor-infiltrating CAR-PBNK cells isolated from HT29 tumors following adoptive transfer (Fig. 5a, Methods and Supplementary Dataset 6). Integration of the *OR7A10*(*OE*)-transduced and *OR7A10*(*STOP*)-transduced CAR-PBNK cell datasets identified two clusters of immature NK ($CD56^{hi}CD16^{low}$) and six clusters of mature NK ($CD56^{low}CD16^{hi}$) cells (Fig. 5b,c and Extended Data Fig. 8a). The individual subsets were each characterized by established NK cell markers (Methods and Extended Data Fig. 8b,c) and supported by RNA-splicing dynamics and by cell cycle phasing analyses (Extended Data Fig. 8d,e).

We assessed the effect of *OR7A10* overexpression on NK cell fate in vivo and only detected a minor shift in increased cytotoxic immature NK cluster 1 (C1) at the expense of proliferating mature NK C1 (*MKI67*) (Fig. 5d), which suggests that *OR7A10* overexpression largely did not alter the cell fate of CAR-NK cells in the TME. We focused our subsequent characterizations of the effects of *OR7A10* overexpression on DE of genes in each NK subpopulation. *OR7A10* overexpression led to broad-acting effects on all eight subpopulations, which manifested across different genes, gene sets and multiple pathways (Fig. 5e and Extended Data Figs. 8f–i and 9a,b). DE analyses showed strong upregulation of the inflammatory cytokine genes *LTA* and *IFNG* in all mature NK subsets, and common downregulation of uncharacterized lincRNA species (Fig. 5e and Extended Data Fig. 8f,g). *OR7A10* overexpression led to significant changes (adjusted $P < 0.01$ and absolute $\log_2$[fold change] > 0.5) in other NK cell genes, such as increased cytotoxic *GZMB* in all six mature NK subsets (Fig. 5f). We also found increased anti-apoptotic *BCL2* and *BCL2L1* and reduced pro-apoptotic *BAX* expression across multiple mature NK subsets in the dataset of *OR7A10*-overexpressing cells compared with controls (Fig. 5e). This results is consistent with its phenotype of improved in vivo tumour survival.

Comparisons of common significant pathways across NK cell subsets revealed that *OR7A10* overexpression significantly and robustly altered immune activation signalling pathways, including increased NFAT, JNK, ATF2, RB-1 and IL-23 signatures in all six mature NK populations, but rarely in the two immature NK populations (Fig. 5e,f and Extended Data Figs. 8h,i and 9a,b). SCT data showed decreased signatures of NK cell chemotaxis and adhesion, including integrin cell signalling and CXCR3 (Fig. 5f). Investigation of the cause–effect relationships between DE pathways (Methods) showed that TCR-like calcium signalling and the downstream NFAT signalling pathway were predicted to have a strong causal relationship with several inflammatory mediator genes, including *IFNG*, *TNF* and *LTA* (Fig. 5g). Our results also revealed the following relationships: JUN expression with ATF2 and TCR-like JNK signalling; NF-κB factor genes (*NFKB1* and *NFKBIA*) with IL-23 and IL-1 signalling; and downregulated expression of immunosuppressive genes (*FGR*, *TGFB1* and *TGFBR2*) from decreased glypican-1 (GPC1) signalling (Fig. 5h and Extended Data Fig. 9c,d). Collectively, these unbiased single-cell profiling data show that *OR7A10* overexpression substantially reshapes the global transcriptomes of human primary CAR-NK cells inside tumours.

Discussion

Our in vivo GOF screens identified previously unknown NK cell hyperboosters. The top hyperbooster, the GPCR OR7A10, can be efficiently engineered via ORFs and delivered by a single vector to substantially enhance the antitumour efficacy of CAR-NK cells against solid tumours in vivo (Extended Data Fig. 10h). Additional discussions are provided in the Supplementary Discussion section in the Supplementary Information. Overall, *OR7A10*-overexpressing CAR-NK cells are manufacturable with a single vector and have the potential to be an efficacious, safe, allogeneic and off-the-shelf primary NK cell therapy. OR7A10 can also be engineered in an in vivo CAR-NK therapy.

Online content

Any methods, additional references, Nature Portfolio reporting summaries, source data, extended data, supplementary information, acknowledgements, peer review information; details of author contributions and competing interests; and statements of data and code availability are available at https://doi.org/10.1038/s41586-026-10149-8.

1. Vivier, E., Tomasello, E., Baratin, M., Walzer, T. & Ugolini, S. Functions of natural killer cells. *Nat. Immunol.* **9**, 503–510 (2008).
2. Ben-Shmuel, A., Biber, G. & Barda-Saad, M. Unleashing natural killer cells in the tumor microenvironment—the next generation of immunotherapy?. *Front. Immunol.* **11**, 275 (2020).
3. Guillerey, C., Huntington, N. D. & Smyth, M. J. Targeting natural killer cells in cancer immunotherapy. *Nat. Immunol.* **17**, 1025–1036 (2016).
4. Morvan, M. G. & Lanier, L. L. NK cells and cancer: you can teach innate cells new tricks. *Nat. Rev. Cancer* **16**, 7–19 (2016).
5. Raulet, D. H. & Guerra, N. Oncogenic stress sensed by the immune system: role of natural killer cell receptors. *Nat. Rev. Immunol.* **9**, 568–580 (2009).
6. Crinier, A., Narni-Mancinelli, E., Ugolini, S. & Vivier, E. SnapShot: natural killer cells. *Cell* **180**, 1280–1280 (2020).
7. Lanier, L. L. Up on the tightrope: natural killer cell activation and inhibition. *Nat. Immunol.* **9**, 495–502 (2008).
8. Myers, J. A. & Miller, J. S. Exploring the NK cell platform for cancer immunotherapy. *Nat. Rev. Clin. Oncol.* **18**, 85–100 (2021).
9. Huntington, N. D., Cursons, J. & Rautela, J. The cancer–natural killer cell immunity cycle. *Nat. Rev. Cancer* **20**, 437–454 (2020).
10. Bald, T., Krummel, M. F., Smyth, M. J. & Barry, K. C. The NK cell–cancer cycle: advances and new challenges in NK cell-based immunotherapies. *Nat. Immunol.* **21**, 835–847 (2020).
11. Elahi, R., Heidary, A. H., Hadiloo, K. & Esmaeilzadeh, A. Chimeric antigen receptor-engineered natural killer (CAR NK) cells in cancer treatment; recent advances and future prospects. *Stem Cell Rev. Rep.* **17**, 2081–2106 (2021).
12. Marofi, F. et al. Renaissance of armored immune effector cells, CAR-NK cells, brings the higher hope for successful cancer therapy. *Stem Cell Res. Ther.* **12**, 200 (2021).
13. Dagher, O. K. & Posey, A. D. Jr. Forks in the road for CAR T and CAR NK cell cancer therapies. *Nat. Immunol.* **24**, 1994–2007 (2023).
14. Hu, W., Wang, G., Huang, D., Sui, M. & Xu, Y. Cancer immunotherapy based on natural killer cells: current progress and new opportunities. *Front. Immunol.* **10**, 1205 (2019).
15. Albinger, N., Hartmann, J. & Ullrich, E. Current status and perspective of CAR-T and CAR-NK cell therapy trials in Germany. *Gene Ther.* **28**, 513–527 (2021).
16. Wrona, E., Borowiec, M. & Potemski, P. CAR-NK cells in the treatment of solid tumors. *Int. J. Mol. Sci.* **22**, 5899 (2021).
17. Portillo, A. L. et al. Expanded human NK cells armed with CAR uncouple potent anti-tumor activity from off-tumor toxicity against solid tumors. *iScience* **24**, 102619 (2021).
18. Shimasaki, N., Jain, A. & Campana, D. NK cells for cancer immunotherapy. *Nat. Rev. Drug Discov.* **19**, 200–218 (2020).
19. Cozar, B. et al. Tumor-infiltrating natural killer cells. *Cancer Discov.* **11**, 34–44 (2021).
20. Christodoulou, I. et al. Engineering CAR-NK cells to secrete IL-15 sustains their anti-AML functionality but is associated with systemic toxicities. *J. Immunother. Cancer* **9**, e003894 (2021).
21. Vivier, E. et al. Natural killer cell therapies. *Nature* **626**, 727–736 (2024).
22. Bernard, P. L. et al. Targeting CISH enhances natural cytotoxicity receptor signaling and reduces NK cell exhaustion to improve solid tumor immunity. *J. Immunother. Cancer* **10**, e004244 (2022).
23. Delconte, R. B. et al. CIS is a potent checkpoint in NK cell-mediated tumor immunity. *Nat. Immunol.* **17**, 816–824 (2016).
24. Zhu, H. et al. Metabolic reprograming via deletion of CISH in human iPSC-derived NK cells promotes in vivo persistence and enhances anti-tumor activity. *Cell Stem Cell* **27**, 224–237 (2020).
25. Delconte, R. B. et al. NK cell priming from endogenous homeostatic signals is modulated by CIS. *Front. Immunol.* **11**, 75 (2020).
26. Nakazawa, T. et al. CIS deletion by CRISPR/Cas9 enhances human primary natural killer cell functions against allogeneic glioblastoma. *J. Exp. Clin. Cancer Res.* **42**, 205 (2023).
27. Morimoto, T. et al. CRISPR–Cas9-Mediated *TIM3* knockout in human natural killer cells enhances growth inhibitory effects on human glioma cells. *Int. J. Mol. Sci.* **22**, 3489 (2021).
28. Mac Donald, A. et al. *KLRC1* knockout overcomes HLA-E-mediated inhibition and improves NK cell antitumor activity against solid tumors. *Front. Immunol.* **14**, 1231916 (2023).
29. Qin, Y. et al. Developing enhanced immunotherapy using *NKG2A* knockout human pluripotent stem cell-derived NK cells. *Cell Rep.* **43**, 114867 (2024).
30. Nakazawa, T. et al. Characterization of HIF-1α knockout primary human natural killer cells including populations in allogeneic glioblastoma. *Int. J. Mol. Sci.* **25**, 5896 (2024).
31. Ni, J. et al. Single-cell RNA sequencing of tumor-infiltrating NK cells reveals that inhibition of transcription factor HIF-1α unleashes NK cell activity. *Immunity* **52**, 1075–1087 (2020).
32. Peng, L. et al. In vivo AAV–SB-CRISPR screens of tumor-infiltrating primary NK cells identify genetic checkpoints of CAR-NK therapy. *Nat. Biotechnol.* **43**, 752–761 (2025).
33. Rafei, H. et al. CREM is a regulatory checkpoint of CAR and IL-15 signalling in NK cells. *Nature* **643**, 1076–1086 (2025).
34. Zhang, X. et al. Gene knockout in cellular immunotherapy: application and limitations. *Cancer Lett.* **540**, 215736 (2022).
35. Konermann, S. et al. Genome-scale transcriptional activation by an engineered CRISPR–Cas9 complex. *Nature* **517**, 583–588 (2015).
36. Zhou, X., Renauer, P. A., Zhou, L., Fang, S. Y. & Chen, S. Applications of CRISPR technology in cellular immunotherapy. *Immunol. Rev.* **320**, 199–216 (2023).
37. Chen, H. et al. APLN promotes hepatocellular carcinoma through activating PI3K/Akt pathway and is a druggable target. *Theranostics* **9**, 5246–5260 (2019).
38. Wang, Q. et al. APLN promotes the proliferation, migration, and glycolysis of cervical cancer through the PI3K/AKT/mTOR pathway. *Arch. Biochem. Biophys.* **755**, 109983 (2024).
39. Patel, S. J. et al. Identification of essential genes for cancer immunotherapy. *Nature* **548**, 537–542 (2017).
40. Karagiota, A., Kanoura, A., Paraskeva, E., Simos, G. & Chachami, G. Pyruvate dehydrogenase phosphatase 1 (PDP1) stimulates HIF activity by supporting histone acetylation under hypoxia. *FEBS J.* **290**, 2165–2179 (2023).
41. Song, Y., Zhang, J., Zhang, L., Zhang, S. & Shen, C. PDP1 promotes cell malignant behavior and is associated with worse clinical features in ovarian cancer patients: evidence from bioinformatics and in vitro level. *Comput. Math. Methods Med.* **2022**, 7397250 (2022).
42. Yuan, M. et al. PDP1 promotes KRAS mutant colorectal cancer progression by serving as a scaffold for BRAF and MEK1. *Cancer Lett.* **597**, 217007 (2024).
43. Alshamleh, I. et al. PDP1 is a key metabolic gatekeeper and modulator of drug resistance in FLT3-ITD-positive acute myeloid leukemia. *Leukemia* **37**, 2367–2382 (2023).
44. Marin, D. et al. Safety, efficacy and determinants of response of allogeneic CD19-specific CAR-NK cells in CD19$^+$ B cell tumors: a phase 1/2 trial. *Nat. Med.* **30**, 772–784 (2024).
45. Kremer, V. et al. Genetic engineering of human NK cells to express CXCR2 improves migration to renal cell carcinoma. *J. Immunother. Cancer* **5**, 73 (2017).
46. Sun, Y. et al. Adaptive NK cells exhibit tumor-specific immune memory and cytotoxicity in ovarian cancer. *Cancer Immunol. Res.* **13**, 1080–1097 (2025).
47. Liu, E. et al. Cord blood NK cells engineered to express IL-15 and a CD19-targeted CAR show long-term persistence and potent antitumor activity. *Leukemia* **32**, 520–531 (2018).
48. Liu, E. et al. Use of CAR-transduced natural killer cells in CD19-positive lymphoid tumors. *N. Engl. J. Med.* **382**, 545–553 (2020).
49. Choi, C. & Finlay, D. K. Optimising NK cell metabolism to increase the efficacy of cancer immunotherapy. *Stem Cell Res. Ther.* **12**, 320 (2021).
50. Egli, L. et al. CAR T cells outperform CAR NK cells in CAR-mediated effector functions in head-to-head comparison. *Exp. Hematol. Oncol.* **13**, 51 (2024).

Methods

Mouse models

Before all cancer-related experiments, each mouse was determined to be in good general health (bright, alert and responsive). Female mice (aged 8–12 weeks) were used for experiments in this study. *NOD-scid Il2rg-null* (NSG) mice and *NOD.Cg-KitW-41J Tyr + Prkdcscid Il2rgtm1Wjl/ThomJ* (NBSGW) mice were purchased from The Jackson Laboratory and bred in-house before their use in in vivo tumour model experiments. All animals were housed in standard individually ventilated, pathogen-free conditions, with a 12 h–12 h or 13 h–11 h light cycle, room temperature (21–23 °C) and 40–60% relative humidity.

Cell culture

NK92 cells were purchased from the American Type Culture Collection (ATCC). NK92 and CAR-NK92 cells were cultured in MEM-α (no nucleosides), supplemented with 2 mM L-glutamine, 0.2 mM myo-inositol, 0.02 mM folic acid, 0.1 mM 2-mercaptoethanol, 200 IU ml^{-1} human recombinant IL-2 (BioLegend), 10% FBS (Corning), 10% horse serum and 1% penicillin–streptomycin (Gibco). Adherent cells such as 293T human embryonic kidney (HEK) cells, HT29, MCF7, MDA-MB-231, SKOV3, A-375, NCI-H1299 and U87 cells were acquired from the ATCC or ThermoFisher. All the cell lines were authenticated by the commercial vendor using methods such as morphology and/or STR profiling. All cell line samples used in this study tested negative for mycoplasma contamination. No commonly misidentified lines were used in the study.

Cell lines were cultured in DMEM (Gibco) (D10 medium), supplemented with 10% FBS (Corning) and 1% penicillin–streptomycin (Gibco). Suspended cells such as K562 and NALM6 were bought from the ATCC and cultured in RPMI (Gibco), supplemented with 10% FBS (Corning) and 1% penicillin–streptomycin (Gibco). CAR-NK92 cells used for in vivo CRISPR screening (and in vitro and in vivo validations) were not irradiated.

HT29, SKOV3, K562, NALM6 and U87 cells were infected with lentivirus with GFP–luciferase (pXD024 plasmid, GL) for the in vitro tumour killing assays. MCF7, MDA-MB-231, SKOV3, A-375 and H1299 cells were infected with lentivirus with puromycin–luciferase (pXD023 plasmid, PL) for the in vitro tumour killing assays. MCF7-HER2-PL cells were generated by infection with HER2-blasticidin lentiviral vectors. All cells were cultured in conditions of 37 °C and 5% CO_2, with saturated humidity.

Human primary NK cell isolation and culture

Human primary NK cells were purified and expanded from peripheral blood or cord blood collected from healthy individuals. To isolate peripheral blood mononuclear cells (PBMCs) from whole blood, Human PB Leukopak (Stemcell) was diluted with sterile PBS supplemented with 2% FBS at a 1:1 v/v ratio and centrifuged at 800*g* for 20 min. The cell pellet was resuspended in 1 ml ACK lysis buffer (Lonza) for 2 min to lyse red blood cells and then neutralized with 10 ml PBS + 2% FBS. PBMCs were collected, counted and cryopreserved for subsequent experiments. To purify NK cells, PBMCs were stained with an anti-CD3 APC antibody for 20 min at 4 °C, followed by incubation with anti-APC MicroBeads (Miltenyi) for 20 min at 4 °C. NK cells were then purified using LS columns (Miltenyi) and cultured in NK cell culture medium. Antibodies were used at 1:200 dilution.

For in vitro expansion, purified NK cells were stimulated with irradiated K562 feeder cells expressing mbIL-15, mbIL-21 and 4-1BBL at an E:T ratio of 1:1 in NK cell culture medium. Human primary NK cells were cultured in IMDM (Thermo), supplemented with 10% FBS (Corning), 1% penicillin–streptomycin (Gibco), 200 IU ml^{-1} human recombinant IL-2 (BioLegend) and 5 ng ml^{-1} human recombinant IL-15 (BioLegend). Fresh medium was changed or half-changed every day or every other day. On day 6, NK cells were collected and transduced with lentivirus. CAR expression and NK cell purity were assessed by flow cytometry before proceeding with further experiments. CBNK cells were expanded by stimulating human cord blood $CD56^+$ cells (Stemcell) with irradiated K562 feeder cells at an E:T ratio of 1:1 in NK culture medium. On day 6, NK cells were collected and transduced with lentivirus. Flow cytometry was used to confirm CAR expression and NK cell purity before further experimental use.

Human primary T cell isolation and culture

Human primary T cells were isolated from PBMC samples using a Pan T cell isolation kit (Miltenyi). The purified $CD3^+$ T cells were stimulated with Dynabeads Human T-Activator CD3/CD28 (ThermoFisher) at a 1:1 bead-to-cell ratio for 24 h and cultured in cX-VIVO medium. On day 6, T cells were collected and transduced with lentivirus. Flow cytometry was used to confirm CAR expression and T cell purity before downstream experiments.

Plasmid constructs

The following lentiviral transgene plasmids were used in this study: pXD023_pLenti-EF1α-Puromycin-T2A-Luciferase-WPRE; pXD24_pLenti-EF1α-GFP-P2A-Luciferase-WPRE; pLJY22_pLenti-EFS-IL15-Puromycin-WPRE; pLJY25_pLenti-EF1α-mCherry-WPRE; pLY75c_pLenti-EFS-Leader-Flag-4D5 HER2 scFv-CD8 TM-CD28-41BB-CD3ζ-T2A-Puromycin-WPRE; pLJY77_pLenti-EFS-Leader-Flag-4D5 HER2 scFv-CD8 TM-CD28-41BB-CD3ζ-T2A-Puromycin-P2A-OR7A10-WPRE; pLJY77b_pLenti-EFS-Leader-Flag-4D5 HER2 scFv-CD8 TM-CD28-41BB-CD3ζ-T2A-Puromycin-P2A-OR7A10(triple STOP codons)-WPRE; pLJY81_pLenti-EFS-Leader-Flag-4D5 HER2 scFv-CD8 TM-CD28-41BB-CD3ζ-T2A-hIL15-P2A-OR7A10-WPRE; pLJY81b_pLenti-EFS-Leader-Flag-4D5 HER2 scFv-CD8 TM-CD28-41BB-CD3ζ-T2A-hIL15-P2A-OR7A10(triple STOP codons)-WPRE; pLJY84_ pLenti-EFS-Leader-CD22 scFv-CD8 TM-41BB-CD3ζ-T2A-hIL15-P2A-OR7A10-WPRE; pLJY84b_pLenti-EFS-Leader-CD22 scFv-CD8 TM-41BB-CD3ζ-T2A-hIL15-P2A-OR7A10(triple STOP codons)-WPRE; pLJY86_pLenti-EFS-Leader-B7H3 scFv-CD8 TM-CD28-CD3ζ-T2A-hIL15-P2A-OR7A10-WPRE; pLJY86b_pLenti-EFS-Leader-B7H3 scFv-CD8 TM-CD28-CD3ζ-T2A-hIL15-P2A-OR7A10(triple STOP codons)-WPRE; pLJY19_pLenti-EFS-4-1BBL-mCherry-WPRE; pLJY20_pLenti-EFS-mIL21-IgG1-CD28TM-CD28-41BB-CD3ζ-T2A-Puromycin-WPRE; pLJY21_pLenti-EFS-Leader-mathIL15-matIL15Ra-WPRE; pLJY91_pLenti-NF-κB GFP reporter; and EFS-puro-WPRE.

Different fragments were cloned into lentiviral vectors using Gibson assembly (NEB). The B7H3 CAR was generated as previously described[51,52].

Lentivirus production

Lentivirus was produced using low-passage HEK293T cells. One day before transfection, HEK293T cells were seeded in a 15 cm dish at 50–60% confluency. Before transfection, D10 medium was replaced with 20 ml fresh pre-warmed D10 medium. For each plate, 20 μg transfer plasmid, 15 μg psPAX2 (Addgene) and 10 μg pMD2.G (Addgene) were diluted into 700 ml DMEM (FBS free). Next, 135 μl LipoD293 (SignaGen) was diluted into 700 ml DMEM. The diluted LipoD293 was immediately added to the diluted DNA solution all at once. After pipetting up and down 3 times, the mixture was incubated for 10 min at room temperature and then added dropwise to the cells. Viral supernatant was collected 48 h after transfection, filtered using 0.45 μm filters (Fisher/VWR) to remove cell debris and then concentrated using a Lenti-X Concentrator (Takara) or ultracentrifugation. Lentiviral pellets were resuspended with NK92 or primary human NK complete culture medium, aliquoted and stored at −80 °C.

Lentiviral transduction

NK92 cells or human primary NK cells were transduced with lentivirus-encoding constructs and derivatives of HER2-CAR at 1–2 × 10^6 cells per ml in a 12-well plate, which was pre-coated with Retronectin (Takara) in PBS, overnight at 4 °C. The spin-infection was performed at 1,000*g*,

32 °C for 45 min. The CAR-positive cells were selected with 2 mg ml^{-1} puromycin for 3 days and measured at day 7 after transduction.

In vivo CAR-NK92 CRISPRa screen

HER2-CAR-NK92 cells were transduced with dCas9-VP64-Blast and MS2-P65-HSF1-Hygro (Addgene)[35] at a multiplicity of infection (MOI) of <1 and selected with hygromycin and blastcidin for 5–7 days. After complete selection, 1.8×10^8 CAR-NK92 cells were transduced with the sgRNA library (Addgene)[35] at a MOI = 0.2 (0.2 infectivity × 1.8×10^8 cells per 70,290 sgRNAs = 512× coverage). After 7 days of selection with Zeocin, >4×10^7 library-infected CAR-NK92 cells were maintained in culture (4×10^7 cells per 70,290 sgRNAs = 569×, although the coverage was limited by the previous transduction step with 512× coverage). Eight-to-12-week-old female NSG mice were inoculated with 1×10^6 HT29-GL cells through subcutaneous injection. On day 8, 5×10^6 library-infected CAR-NK92 cells were adoptively transferred into each tumour-bearing mouse via intravenous injection (5×10^6 per 70,290 sgRNAs = 71× coverage). To support CAR-NK92 cell activity, mice received daily intraperitoneal injections of 2.5 μg human IL-2 beginning on the day of NK cell transfer. On 13 day after transfer, mice were euthanized, and tumours were collected for subsequent experiments.

Primary human CAR-NK barcoded ORF UMI mini-screen

To generate the ORF library, the top 35 gene targets (cDNA length ≤ 1 kb) were chosen from the CRISPRa screen, along with five fluorescent reporter genes as null controls (*BFP2*, *ECFP*, *EYFP*, *EGFP* and *RFP*). The ORF library was synthesized as individual eBlocks (IDT), pooled at equimolar ratios and amplified with primers containing four-nucleotide random barcodes (UMIs; NNNN) to introduce molecular redundancy targeting the same gene. These UMIs enabled us to barcode each ORF construct with up to 256 distinct molecular entities that target the overexpression of the same gene. The ORF expression vector plasmid was bought from Addgene (145026). The barcoded ORF library was pool-cloned into the expression vector using Gibson assembly.

Primary human PBNK cells from two healthy donors were first transduced with HER2-CAR lentivirus and then with the ORF library lentivirus at a MOI of about 0.2. A total of 20 million library-transduced CAR-NK cells were injected into each HT29 tumour-bearing mouse ($n = 5$ mice for donor 0957 and $n = 3$ for donor 0958 for each time point). gDNA was extracted from tumours at days 3 and 6 after treatment (and from pre-injection cells), and subjected to NGS to quantify ORF and UMI barcode representations.

Tissue processing and gDNA extraction

gDNA was extracted from tumours and pre-injected cell pellets using previously described methods[53]. In brief, each sample was put in a 15 ml Falcon tube and 6 ml NK lysis buffer (50 mM Tris, 50 mM EDTA and 1% SDS, pH adjusted to 8.0) along with 30 μl 20 mg ml^{-1} proteinase K (Qiagen) were added. The samples were incubated at 55 °C overnight. After tissue digestion, 30 μl 10 mg ml^{-1} RNase A (Qiagen) was added to the lysed sample, which was then inverted 20 times and incubated at 37 °C for 30 min. Digested tissues were cooled on ice before adding 2 ml cold 7.5 M ammonium acetate (Sigma) to precipitate proteins. Samples were vortexed at high speed for 10 s and then centrifuged at 4,000*g* at 4 °C for 15 min. After the spin, the supernatant was transferred to a new 15 ml Falcon tube and 6 ml 100% isopropanol was added to each sample, which was then inverted 50 times and centrifuged at 4,000*g* at 4 °C for 10 min. gDNA pellets were visible as a small white pellet in each tube. The supernatant was discarded and 6 ml 70% ethanol was added to wash the pellet. Each sample was inverted 10 times, and then centrifuged at 4,000*g* at 4 °C for 5 min. The supernatant was discarded by pouring, and the remaining ethanol was removed using a pipette to completely remove any liquid. The precipitated gDNA was air dried for 30–60 min and then resuspended in 0.5–1 ml nuclease-free water. Samples were then left overnight at room temperature. The next day, the gDNA solution was vortexed briefly and transferred to Eppendorf tubes. The gDNA concentration was measured using a Nanodrop instrument (Thermo Scientific). For pre-injection cells, gDNA samples were extracted using a Blood and Tissue kit (Qiagen) with multiple columns and pooled together for each individual sample.

sgRNA library readout by deep sequencing

The sgRNA library readout was performed using a two-step PCR strategy, whereby the first PCR included enough gDNA to preserve full library complexity (5 μg per reaction × 20 reactions = 100 μg gDNA per sample, 100 μg gDNA per 6.6 pg gDNA per cell per 70,290 sgRNAs > 200-fold coverage), and the second PCR added appropriate sequencing adapters to the products from the first round PCR (2 μl per reaction, 6 reactions per sample).

For PCR-1, a region containing the sgRNA cassette was amplified using primers specific to the CRISPR library vector: forward: 5′-GTGCGCC AATTCTGCAGACAAATGG-3′; reverse: 5′-CAGGATCCAAAAAAAGCACC GACTC-3′.

PCR was performed using Phusion Flash High Fidelity master mix (ThermoFisher). For PCR-1, the thermocycling parameters were as follows: 98 °C for 2 min, 25 cycles of (98 °C for 1 s, 62 °C for 5 s, 72 °C for 30 s), and 72 °C for 2 min. The final PCR products for each biological sample were pooled and used for amplification with barcoded second PCR primers (Supplementary Table 1). The second PCR products were pooled and gel-purified from a 2% E-gel EX (Life Technologies) using a QiaQuick Gel Extraction kit (Qiagen). The purified library was then quantified with a gel-based method using Low-Range Quantitative Ladder (Life Technologies) and dsDNA High-Sensitivity Qubit (Life Technologies). Libraries were sequenced with PhiX using an Illumina NovaSeq sequencer at the Yale Center for Genomic Analysis (YCGA).

CRISPRa screen data analysis

sgRNA counts were quantified from all samples by trimming, aligning and quantifying sequencing reads. In brief, raw fastq files were trimmed down to the sgRNA spacer sequence with Cutadapt (v.3.4), using a 10% error rate and filtering reads <15-nucleotides long. Spacer sequences were aligned using Bowtie (v.1.3.0)[54], using the following settings: -v0, -m1 --best. The reads were quantified and analysed using the SAMBA (v.1.1) R package (https://github.com/Prenauer/SAMBA), described in the section below.

ORF UMI mini-screen data analysis

For data pre-processing, sequenced reads were demultiplexed and trimmed using Cutadapt (v.3.4) to acquire ORF library barcodes (settings: -e 0.1 -m 4 –-discard-untrimmed -g atatcttgtggaaaggacga…tgcatcgatcgagtcagctagctgat), which were subsequently aligned using Bowtie (v.1.3.0) (settings: -v 0 -m 1 --chunkmbs 2000 --best)[54]. Next, the random nucleotide UMIs were extracted from the de-multiplexed fastq files, described above, using Cutadapt to identify and trim flanking sequences (settings: -e 0.1 -m 4 --discard-untrimmed -g gatcgag tcagctagctgat…ttaagtcgacaatcaacctc). The ORF barcode reads were matched to the UMIs using the individual read IDs, and the unique barcode–UMI pairs were quantified. Finally, the mini-screen data were analysed using SAMBA, similar to the CRISPRa screen, but UMIs were used instead of sgRNAs for distinct constructs targeting the same gene.

SAMBA method details

The SAMBA R package analyses guide-level statistics and gene-level statistics using a workflow detailed in Extended Data Fig. 1. In brief, guide count data were preprocessed by adding a pseudo-count to all data instead of filtering low-count guides. This is a softer approach to distinguish low and high counts rather than using a hard threshold[55]. The data were then analysed for guide-level changes using the edgeR

package[56] with TMMwsp normalization, effective for sparse data, and by fitting a negative binomial GLM with quasi-dispersion estimates and guide-detection weights, calculated using a sigmoid function of the proportion of non-control samples that had counts above a minimum threshold (5% quantile of all counts). Guide-level changes were analysed by quasi-likelihood *F*-tests, and guide scores were defined as the posterior Bayes estimates for each guide. Gene-level scores were then calculated by adding a baseline measurement for each gene (sum of guide-score quartiles Q2–Q4) and a weighted sum of the guides for which scores were greater than the 90th percentile (representing a 10% FDR, similar to MAGeCK RRA[57]). The gene scores were then normalized to the mean scores from scrambled 'null genes'. *P* values were estimated from the normal probability distribution of normalized gene scores, and FDR-adjusted *P* values were calculated.

Comparison of CRISPR screen algorithms

To assess the performance of SAMBA to detect screen enrichment with sparse datasets, we benchmarked SAMBA against the following CRISPR screen analysis algorithms: BAGEL2 (ref. 58), CB2 (ref. 59), JACKS[55], MAGeCK[57], PBNPA[60] and Riger (RigerJ Java implementation: https://github.com/broadinstitute/rigerj). Specifically, the algorithms were used to analyse 71 CRISPR screen datasets of cancer cell proliferation and survival, generated from five large-scale publications[61–65]. Area under the curve (AUC) values were calculated with *P* values as the predictors for tumour suppressor genes (TSGs; COSMIC database: https://cancer.sanger.ac.uk/cosmic; filtered for hallmark TSGs; accessed on 20 July 2022) as a response of screen enrichment, or essential genes as a response of screen depletion[65]. We also summarized specificity and sensitivity using partial AUC analyses (range of 0.8–1) across all datasets. AUC and partial AUC values were also assessed in datasets for which sparsity was simulated by randomly assigning a specified number of zeros, using probability weights determined by the counts in the control samples. Additional comparisons were performed using relative AUC values, which were calculated as the $\log_2$[fold change] of each AUC relative to the mean AUC of that specific screen dataset. Last, statistical comparisons were made by one-way ANOVA tests with post hoc analyses using the Tukey honest-significant-differences method (TukeyHSD in R), where $^{*}P < 0.05$, $^{**}P < 0.01$, $^{***}P < 0.001$ and $^{****}P < 0.0001$.

To make the methods comparable, Riger was performed using the $\log_2$[fold changes] between the mean counts per million of screen versus control samples for each guide. BAGEL2 analyses were performed with the following training genes sets: essential genes and nonessential genes were used for depletion analyses[65]; TSGs and nonessential genes were used for enrichment analyses. Furthermore, given that BAGEL2 does not have an option for positive enrichment, we coerced the algorithm to perform enrichment analyses by multiplying the $\log_2$[fold change] values by −1. Last, PBNPA was performed using four permutations to improve parallel processing of multiple screens.

RT–qPCR

For overexpression of target genes, at least 1 week after sgRNA lentivirus transduction and Zeocin selection, CAR-NK92 cells were collected for RNA preparation. All RNA preparations were performed using a RNasy Plus Mini kit (Qiagen). Total mRNA was reverse transcribed into cDNA using SuperScript IV reverse transcriptase (ThermoFisher). Gene expression was quantified using Taqman Fast Universal PCR master mix (ThermoFisher) and Taqman probes (ThermoFisher). RNA expression levels were normalized to *GADPH* (human). Relative mRNA expression was determined via the Delta (D) C_t or DD C_t method where appropriate.

Cytotoxicity assay

To detect the cytotoxic capabilities of gene-specific overexpressing CAR-NK92 or CAR-NK cells and controls, cancer cells were seeded in a 96-well plate at 5×10^4 cells per well, then different effector (NK cells) to target (cancer cells) ratio (E:T ratio) co-cultures were set up. Cytolysis was measured by adding 150 μg ml^{-1} D-Luciferin (PerkinElmer) using a multichannel pipette. After 15 min of incubation, the luciferase bioluminescence was determined using a PerkinElmer plate reader. The luminescence units (LU) recorded were normalized to the cancer cells only group, referred to as $LU_{cancer\ only}$. The tumour killing percentage calculation formula is as follows:

$$\text{Cytotoxicity (\%)} = 100 - \frac{LU_{sample}}{LU_{cancer\ only}} \times 100$$

For xCelligence RTCA killing assays, diverse cancer cells were seeded into each well of a RTCA E-plate (Agilent). Cell index values were recorded overnight using xCelligence RTCA to monitor tumour cell growth. The next day, CAR-PBNK cells were seeded into each well of the plate. The control wells were tumour cells only. Cell index values were monitored to evaluate tumour killing. Cell index values were normalized to the time point before adding CAR-PBNK cells.

Cytotoxicity with inhibitor treatment

CAR-NK cells were pretreated for 2 h with the following pathway inhibitors before RTCA-based co-culture assays: the pERK inhibitor ulixertinib[66] (MCE HY-15816; 5 μM); the NF-κB inhibitor BOT-64 (MCE HY-136741; 100 μM) or BAY 11-7082 (MCE HY-13453, 5 μM); the PKA inhibitor H89 (Cell Signaling 9844; 30 μM); the NFAT inhibitor INCA-6 (MCE HY-108544; 25 μM); or the Gβ/γ inhibitor gallein (MCE HY-D0254, 10 μM). HT29 cancer cells were seeded at an E:T ratio of 1:2 or 1:5 before NK cell addition. Tumour cells receiving the corresponding inhibitor treatment served as tumour-only controls.

In vivo antitumour efficacy testing

NSG mice and NBSGW mice were purchased from The Jackson Laboratory and bred in-house. Eight-to-12-week-old mice of both sex were used for cancer modelling and efficacy testing. On the basis of previous literature that reported the safety of CAR-NK cells[44,67], and the use of multiple doses in animal models[68–70], we chose to use a dose of 20 million CAR-NK cells per injection, with weekly injections for 2–3 doses.

For the colon cancer model, HT29 cancer cells were inoculated via subcutaneous injection, and CAR-NK92 (5×10^6 cells per dose per week for 4 weeks) or CAR-PBNK (2×10^7 cells per dose per week for 3 weeks) cells were intravenously injected into the tumour-bearing mice at the indicated time points. For the breast cancer orthotopic model, MCF7-GL cancer cells were inoculated via fat pad injection, followed by intravenous administration of CAR-PBNK cells (2×10^7 cells per dose per week for 2 weeks) at the indicated time points. For the ovarian cancer orthotopic model, SKOV3-GL cancer cells were inoculated via intraperitoneal injection, and CAR-PBNK cells (2×10^7 cells per dose per week for 2 weeks) were intraperitoneally delivered at the indicated time points. Treatment doses and time points are indicated in the corresponding figure panels. Ovarian cancer progression was measured by bioluminescence imaging using an IVIS system. Solid tumour volumes were measured using calipers and calculated with the following formula: volume = π/6 × length × width × height. All mice were euthanized once they reached the end point based on protocols approved by the Institutional Animal Care and Use Committee (IACUC). The maximal tumour volume that was permitted by the approved IACUC protocol is 3,000 mm^3, and this limit was not exceeded in any of the experiments.

Histology and H&E staining

Mouse tissues (tumours, livers, kidneys and lungs) were collected and submerged to 10% formalin for 24 h then transferred to 70% ethanol. H&E staining were performed by the Yale Department of Pathology.

Bulk mRNA-seq library preparation

To evaluate the interaction between CAR and OR7A10-mediated signalling, we generated six distinct lentiviral constructs: *OR7A10*, *OR7A10(STOP)*, *HER2-CAR;OR7A10*, truncated *HER2-CAR* (*tHER2-CAR;OR7A10*(*STOP*)), full-length *HER2-CAR;OR7A10* and full-length *HER2-CAR;OR7A10*(*STOP*). Thus, this RNA-seq experiment has three main biological factors: genotype (OR7A10 versus control); CAR (functional CAR versus truncated CAR or no CAR); and stimulation (24 h versus 0 h).

Human primary NK cells were infected with one of the above-described lentiviral constructs and stimulated with HT29 cancer cells at an E:T ratio of 1:1 for 0 or 24 h. CAR-NK cells were stained with APC–CD56 antibody and isolated with anti-APC magnetic beads. NK cell purity was confirmed by flow cytometry, after which RNA was extracted for mRNA-seq library preparation. The mRNA library preparations were performed using a NEBNext Ultra RNA Library Prep kit, and samples were multiplexed using barcoded primers provided by NEBNext Multiplex Oligos for Illumina (index primers set 2). Libraries were sequenced using a Novaseq platform (Illumina). Antibodies were used at 1:200 dilution.

RNA-seq data analysis

Raw FASTQ files were first assessed for quality using FastQC (v.0.12.1). Reads were then aligned to the GRCh38 reference genome using STAR aligner, and gene-level quantification was performed using Gencode annotations (GRCh38_v45). Gene count tables were merged using a custom R script, and genes with fewer than 20 total counts across all samples and conditions were considered universally not expressed and subsequently filtered out. Transcripts were quantified using kallisto (v.0.48.0). The resulting raw count matrix was normalized and subjected to DE analysis using DESeq2 (v.1.42.1). DESeq2 fits a complete GLM based on negative binomial distribution. The design matrix of the complete model (design = overexpression × CAR) for the stimulated population includes the main effect of *OR7A10* overexpression, the main effect from CAR construct and the interaction terms between the two variables. PCA and heatmaps were generated for quality control and to evaluate sources of variance across samples. Differentially expressed genes were identified using thresholds of $|\log_2[\text{fold change}]| > 0.5$ and adjusted $P < 0.05$. Gene set enrichment analysis (GSEA) and the ClusterProfiler (v.4.10.1) R package were used to perform pathway enrichment analysis.

Ki-67 and cleaved caspase-3 assay

CAR-NK cells were stained with live/dead staining dye (Thermo, 1:1,000 dilution) and anti-CD56 antibody (1:200 dilution). After fixation with the FOXP3/transcription factor staining buffer set (eBioscience), cells were permeabilized and stained with anti-Ki-67 and anti-cleaved caspase-3 antibodies (1:200 dilution). Cells were analysed using a BD FACSAria cytometer.

CD107a degranulation assay

MCF-7-HER2-PL or HT29 cells were seeded in a 96-well plate at 1×10^5 cells per well. CAR-NK92 or CAR-PBNK cells were added at an E:T ratio of 1:2 and stimulated for 0, 2, 4 or 6 h. One hour before collection, the medium was supplemented with 2 nM monensin and anti-CD107a antibody (1:200 dilution). At the end of each co-culture, CAR-NK92 were washed with PBS and stained with live/dead staining dye (1:1,000 dilution) and anti-CD56 antibody (1:200 dilution) for 30 min on ice. Cells were analysed using a BD FACSAria cytometer.

Flow cytometry for surface activation markers

After co-culture with HT29 cancer cells at an E:T ratio of 1:1 for 0, 6 or 24 h, CAR-NK92 or CAR-PBNK cells were collected and washed once using MACS buffer (0.5% BSA and 2 mM EDTA in PBS) before staining. CAR-NK92 cells were stained on ice for 30 min after adding live/dead staining dye (1:1,000 dilution) and antibodies (1:200 dilution), and then washed twice with 1 ml cold MACS buffer. All samples were run on a BD FACSAria cytometer, and analysis was performed using FlowJo software (Threestar).

Flow cytometry for NK cell exhaustion

To assess the exhaustion of *OR7A10*(OE)-transduced CAR-PBNK cells, a repeated challenge assay was performed. CAR-PBNK cells were co-cultured with HT29 cells at an E:T ratio of 1:1 across three sequential stimulation rounds. Cytolysis was measured and exhaustion markers were analysed at the end point by flow cytometry of the surface expression of exhaustion markers, including TIM-3, LAG-3, PD-1 and NKG2A, using the following antibodies at 1:200 dilution: Brilliant Violet 510 anti-human CD366 (TIM-3) (BioLegend, 345029); Brilliant Violet 605 anti-human CD223 (LAG-3) (BioLegend, 369323); APC anti-human CD279 (PD-1) (BioLegend, 329908); and PerCP/Cyanine5.5 anti-human CD159a (NKG2A) (BioLegend, 375126).

Flow cytometry for intracellular cytokines

For effective cytokine measurement, CAR-NK cells were co-cultured with HT29 cancer cells at an E:T of 1: 1 for 0, 6 or 24 h. Brefeldin A (5 mg ml^{-1}) was added to the co-culture medium 6 h before collection. For hIL-15 measurement, CAR-NK cells expressing hIL-15 cells were treated with brefeldin A (5 mg ml^{-1}) and monensin (2 nM) for 4 h. At the end of each co-culture, cells were collected, washed and stained for live/dead staining dye (1:1,000 dilution) and membrane protein (1:200 dilution). Cells were fixed and permeabilized using a BD Cytofix/Cytoperm Fixation/Permeabilization kit (Thermo Fisher), followed by intracellular staining with anti-IFNγ, anti-TNF, anti-GZMB, anti-perforin or anti-hIL-15 antibodies (1:200 dilution). All sample data were acquired on a BD FACSAria cytometer, and data were analysed using FlowJo software (Threestar).

cAMP and PKA activity assays

A total of 1×10^7 CAR-PBNK expressing CD22 cells were incubated with 10 μg ml^{-1} soluble CD22-biotin protein (SinoBiological 11958-H08H-B) on ice for 30 min. Following binding, cells were washed twice with MACS buffer. Streptavidin was added to a final concentration of 10 μg ml^{-1}, and cells were lysed with RIPA buffer 5 min later. Protein concentrations were determined using a BCA assay, and after normalization, lysates were used for cAMP (R&D KGE002B) or PKA kinase activity (Abcam ab139435) measurements according to the manufacturers' protocols.

pERK1/2 assay

In brief, 1×10^7 per ml CAR-PBNK cells underwent serum starvation overnight to minimize background phosphorylation. Next, 1×10^7 per ml HT29 cells were added to the wells to stimulate CAR-PBNK cells at the indicated E:T ratios for different time points. After stimulation, cells were rapidly fixed using prewarmed Fix Buffer I (BD Biosciences) for 10 min at 37 °C. Fixed cells were permeabilized with cold Phosflow Perm Buffer III (BD Biosciences) for 30 min on ice. Then cells were stained with PE pERK1/2 (pT202/pY204) (BioLegend, 1:200 dilution) and subjected to flow cytometery analysis.

Calcium flux assay

In brief, 1×10^7 CAR-NK92 cells were stained with 5 μM Cal520, AM (AAT Bioquest) in complete RPMI medium with 0.04% Pluronic F-127 (Thermo) at 37 °C for 30 min. The cells were then washed once with Hank's balanced salt solution (HBSS) and incubated with 10 μg ml^{-1} soluble HER2-biotin protein (Acro Biosystems) on ice for 30 min. After binding with HER2 protein, the cells were washed twice with HBSS and resuspended in 1 ml HBSS. The cells were then incubated at 37 °C for 10 min and flow recorded for baseline FITC fluorescence at 37 °C. Streptavidin was added to a final concentration of 10 μg ml^{-1},

and the cells were continuously recorded for FITC signal changes for 10 min.

TEM sample processing and imaging

CAR-NK cells were washed with PBS and fixed in 2.5% glutaraldehyde in 0.1 M sodium cacodylate buffer (pH 7.4) for 1 h. After buffer rinsing, cells were pelleted in 2% agar, and chilled agar blocks were trimmed and post-fixed in 1% osmium tetroxide for 1 h. Following additional buffer rinses, samples were then stained with aqueous 2% uranyl acetate for 1 h, rinsed in distilled water, dehydrated through a graded ethanol series and infiltrated with Embed 812 resin (Electron Microscopy Sciences). Resin polymerization steps were performed overnight at 60 °C in silicone moulds. Hardened blocks were sectioned at 60 nm using a Leica UltraCut UC7 ultramicrotome. Sections were collected on nickel grids coated with Formvar and carbon, then sequentially stained with 2% uranyl acetate and lead citrate for contrast enhancement. Grids were imaged at 80 kV using a FEI Tecnai Biotwin transmission electron microscope. Digital images for quantification were acquired randomly with an AMT NanoSprint 15 Mk II camera. All quantifications were conducted on double-blinded, randomized and anonymized image fields. Image acquisition was performed by staff of the Yale Center for Cellular and Molecular Imaging, Electron Microscopy Facility.

Seahorse assay

OCRs and extracellular acidification rates were measured in XF medium (Agilent) supplemented with 25 mM glucose, 2 mM L-glutamine and 1 mM sodium pyruvate. Next, 1 mM oligomycin, 1.5 mM fluoro-carbonyl cyanide phenylhydrazone (FCCP) and 50 nM rotenone and 0.5 mM antimycin A were used for testing extra mitochondrial capacity, spare respiratory capacity, under stress and measuring extracellular acidification rates. CAR-PBNK cells were seeded at 1×10^6 per well into a XF cell culture microplate (Agilent) that was pre-coated with poly-D-lysine (Sigma), which can facilitate cell adhesion to the plate surface for spare respiratory capacity detection. The microplate was incubated for 30–60 min at 37 °C in a non-CO_2 incubator before running in a Seahorse XF24 Analyzer (Agilent). A standard Seahorse program setup was used: calibration; equilibration; base line reading (loop 3 times), mix 3 min, measurement 3 min, end loop; injection port A (loop 3 times), mix 3 min, measurement 3 min, end loop; injection port B (loop 5 times), mix 3 min, measurement 3 min, end loop; injection port C (loop 3 times), mix 3 min, measurement 3 min, end loop; end program.

SCT analyses

Tumour model and NK cell source for SCT. In vivo xenograft models were generated using HT29-GL cells and NSG mice, and mice were treated with CAR-PBNK cells expressing hIL-15 and transduced with *OR7A10*(OE) or *OR7A10*(*STOP*). Tumour-infiltrating CAR-PBNK cells were extracted and profiled by SCT in an unbiased manner.

Data processing and population characterization. Single-cell datasets for *OR7A10*(*OE*) and *OR7A10*(*STOP*) samples were preprocessed and aligned to the human transcriptome reference (GRCh38 Gencode V37)[71] using CellRanger (v.4.3.0 default settings) (10x Genomics). The filtered data matrices were aggregated into a Seurat object (Seurat package v.4.4.0)[72] and filtered for gene detection (>3 cells) and high-quality cells (mtDNA <20% of UMIs, >200 genes detected, and low-quality marker genes (*MALAT1* and *KCNQ1OT1*) < 5% of UMI). The two datasets were then integrated using rliger integrated non-negative-matrix-factorization (iNMF) using default normalization, gene selection, scaling, iNMF (lambda = 10) and factor alignment[73]. The normalized iNMF matrix was dimensionally reduced by UMAP (min.dist = 0.01), a shared nearest neighbour graph was constructed from UMAP embeddings, and cells were clustered using the Leiden method with an optimal resolution of 0.116, determined by within-cluster sum-of-squares and average-silhouette width metrics. For NK cell subset classification, cell populations were first classified into immature NK and mature NK cell groups on the basis of the expression of *NCAM1* (CD56) and *FCGR3A* (CD16) genes. The individual subsets were each characterized by established NK cell markers from molecular and SCT studies of tumour-infiltrating NK cells, including those for proliferation (*MKI67*), NK differentiation (*BATF3*), *IL32*, memory-like NK phenotype (*KLRC2*), stress (*CREM*) and NK cell dysfunction (*EGR2*)[74].

Next, NK cell subsets were distinguished by performing DE analyses between subsets (Seurat Wilcox test with one-versus-all approach) and matching top overexpressed genes to known markers of different NK cell subsets[74]. The classification of immature and mature NK cell clusters was further supported by scVelo analysis of RNA-splicing dynamics and by cell cycle phasing analyses. Last, the NK subset percentages were compared between for *OR7A10*(*OE*) and *OR7A10*(*STOP*) groups using a pairwise Fisher exact test, with the *P* values adjusted for multiple testing.

RNA-velocity and cell cycle analyses. RNA-velocity analysis was performed using the scVelo package (v.0.2.5) for Python[75]. In brief, CellRanger BAM files were processed into splice-distinguished loom files by velocyto tools (v.0.17). scVelo was then used to combine the loom files, and data were filtered and annotated to match the corresponding Seurat dataset. Data were then normalized, genes were filtered (≥100 shared cells) and subsequently, velocity pseudotime and latent time were estimated using the default scVelo pipeline with the following adjustments: n_neighbors = 30 and velocity mode = "dynamical". Cell cycle analysis was performed by Seurat using the CellCycleScoring function with default parameters[75].

DE analyses. Transcriptional differences between *OR7A10*(*OE*) and *OR7A10*(*STOP*) groups were assessed by DE analyses in each NK cell subset (Seurat Wilcox tests). For pathway analyses, we used AUcell package (v.1.26.0)[76] to compute single-cell signatures from the Protein Interaction Database using MSigDb gene sets[77,78]. The single-cell pathway signatures were then compared between *OR7A10*(*OE*) and *OR7A10*(*STOP*) samples by DE analyses for each NK cell subset (Seurat Wilcox tests).

To further understand how *OR7A10* overexpression affects CAR-NK cell states in vivo at the level of gene sets or pathways in an unbiased manner, single-cell pathway analyses were performed with AUCell signature predictions[76] and pathways from the Protein Interaction database[77]. Pathway networks were constructed using cell subsets, genotypes and pathways as nodes, connected by edges derived from DE $\log_2$[fold changes]. The network layout was then determined using the Fruchterman–Reingold algorithm using the igraph package (v.2.1.4).

Dynamic signature relationships were modelled between single-cell pathway scores and gene expression data using the bam function of the mgcv package (v.1.9-3) with the following formula: y ~ geno + ct + $s(x, \text{bs} = \text{"ps"}, k = 10)$ + offset(umi), where gene-level UMI counts (y) were modeled with a negative binomial distribution as a function of genotype (geno), NK cell subset (ct), and a smooth function of the pathway signature score ($s(x)$), applied with a P-spline basis ($k = 10$)), and a log-UMI offset to account for sequencing depth. Next, partial residuals were calculated from the smoothed pathway term and fitted residuals with or without the genotype term. These partial residuals, which we referred to as 'adjusted effects', were compared with pathway signatures by Pearson's correlation tests as a metric for dynamic relationships between a pathway and gene expression.

Cause–effect analysis. To understand the cause–effect relationships between DE pathways and genes, the SCT data were used to model how well the pathway signature levels can predict the expression of

DE genes using generalized additive models with dynamic signature relationships (DSRs). Heatmap values were the correlation coefficient (ρ) between the pathway predictor and gene expression, adjusted to be independent of the effects of cell subset and genotype (adjusted gene effect). SCT data were also used to model pathway–gene relationships independent from the effects of NK cell subset type and *OR7A10* overexpression to determine whether a pathway that was upregulated by *OR7A10* can independently explain the downstream changes in gene expression. Pairwise pathway–gene relationships were filtered by the quality of DSR model fitting and the correlation between pathways and the unbiased adjusted effect on gene expression (DSR score = correlation ρ).

NF-κB reporter line and activation assay

A NF-κB reporter construct from a previous report[79], pSIRV-NF-κB-eCFP (plasmid 118094), was acquired from Addgene. pLJY91_pLenti-NF-kB GFP reporter;EFS-puro-WPRE was generated using PCR and Gibson methods. Lentivirus was packaged and used to transduce primary NK cells. Reporter-positive cells were sorted after puromycin treatment. The reporter cells were then transduced with either the *OR7A10*(*OE*) or *OR7A10*(*STOP*) vector. Transduced reporter NK cells were co-cultured with HT29 cells at an E:T ratio of 1:1 for 24 h. GFP expression was recorded by flow cytometry.

GNAS or *AAVS1* KO NK cell generation

Before electroporation, crRNA and tracrRNA were mixed in 1:1 ratio (final concentration 50 mM), heated at 95 °C for 5 min in a thermal cycler, then gradually cooled to room temperature. Next, 3 µl Cas9 protein (61 mM) was mixed with 2 µl buffer R for each reaction (Neon Transfection System kit, Thermo Fisher), then mixed with 5 µl annealed crRNA–tracrRNA duplex, and incubated the mixture at room temperature for 15 min. During incubation, CAR-PBNK cells were collected and washed with PBS to completely remove the medium, and 3×10^6 NK cells per reaction were resuspended in 100 µl buffer R, which included 10 µl RNP complex, then carefully loaded into the Neon Pipette without any bubbles. The electroporation parameter was set at 1,600 V, 10 ms for 3 pluses.

Secreted cytokine levels

Human NK cell-secreted IL-6 and IFNγ were detected using an ELISA MAX Deluxe set (BioLegend) per the manufacturer's instructions. hIL-15 levels from CAR-NK cells expressing hIL-15 were detected using a Human IL-15 ELISA kit–Quantikine (R&D) per the manufacturer's instructions.

WGS preparation

Primary human NK cells were transduced with lentiviral vectors carrying *OR7A10*(*OE*) and *OR7A10*(*STOP*) constructs. gDNA was isolated using a Monarch Spin gDNA Extraction kit (NEB). DNA from *OR7A10*(*OE*)-transduced or *OR7A10*(*STOP*)-transduced NK cells, along with non-transduced (NT) controls, were submitted to the YCGA for WGS library preparation and sequencing on the NovaSeq platform (Illumina).

WGS data analysis

Raw sequencing data quality was initially assessed using FastQC (v.0.12.1). Adapter trimming was performed with Cutadapt (v.5.0), and reads were aligned to the GRCh38 reference genome (Gencode v.47) in paired-end mode using BWA-mem (v.0.7.17-r1188). The resulting BAM files were sorted with SAMtools (v.1.21), and duplicate reads were marked using Picard (v.2.25.6). To minimize technical artefacts, genomic regions listed in the ENCODE blacklist for GRCh38 were excluded using BEDtools (v.2.30.0). Variant calling was conducted with GATK HaplotypeCaller (v.4.6.0.0), followed by joint genotyping and filtering across related samples. Indels were filtered using the following criteria: QD > 2.0, QUAL > 30.0, FS < 200.0 and ReadPosRankSum > −20.0. A secondary filtering step was applied using a custom Python script, requiring ≥8 variant-supporting reads and a variant allele frequency of >35%. Variants detected in all four samples were classified as germline and excluded from further analysis. GRIDDS (v.2.13.2-3) was used to identify structural variants, which were similarly filtered if present across all samples or located within 50 bp proximity, which was probably due to repetitive genomic regions. Final data visualization was performed using GraphPad Prism (v.9 or after, for example, v.10.2.0) or R (v.4.2 or after) and the RCircos package (v.1.2.2).

TME-related immunosuppressive drug treatment

OR7A10(*OE*)-transduced or *OR7A10*(*STOP*)-transduced NK cells were co-cultured with HT29 or H1299 cancer cells at an E:T ratio of 1:1 in the presence of the following immunosuppressive treatments: an adenosine signalling agonist (CGS-21680 (Tocris 1063), final concentration 20 µM); the calcineurin inhibitor tacrolimus (Tocris 3631, final concentration 5 nM) or cyclosporine A (Tocris 1101, final concentration 50 nM); cytokine deprivation (low IL-2); TGFβ (100 ng ml^{-1}); $CoCl_2$ (100 µM); or l-(+)-lactic acid (7.5 mM). Cytolytic activity was measured in real time using a RTCA assay.

mRNA overexpression of co-receptors on CAR-NK cells

G-blocks of cDNA encoding NKp46, CD16, NKG2D and 2B4 with T7 promoter were synthesized (IDT). The DNA fragments were amplified by PCR and then be purified. mRNA in vitro transcription was performed using a HiScribe T7 ARCA mRNA kit (with tailing) (Biolabs, E2060S) per the manufacturer's instructions. Next, 1×10^6 NK cells per reaction were resuspended in 100 µl buffer R, which included 3 µg mRNA, then carefully loaded into a Neon Pipette without any bubbles. The electroporation parameter was set at 1,600 V, 10 ms for 3 pluses. Surface protein expression was analysed by flow cytometry using the following antibodies: BV605 anti-human CD335 (NKp46; clone 9E2, BioLegend, 331925); BV421 anti-human CD16 (clone 3G8, BioLegend, 302037); BV421 anti-human cd314 (NKG2D; clone 1D11, BioLegend, 320821); and BV421 anti-human CD244 (2B4; clone 2-69, BioLegend, 393503). Antibodies were used at 1:200 dilution.

OR7A10 overexpression synergy with co-receptors

Co-receptor-overexpressed *OR7A10*(*OE*)-transduced or *OR7A10*(*STOP*)-transduced CAR-NK cells were co-cultured with HT29 cancer cells at an E:T ratio of 1:1 and analysed by RTCA. Synergistic analyses of RTCA data were performed using univariate three-way ANOVA tests with repeated measures, assuming sphericity (afex R package v.1.5-0), followed by a post hoc analysis of the estimated marginal means for the combinatorial effect of model variables (emmeans R package v.2.0.0). *P* values were adjusted for multiple testing using the Sidak method, and the sign of the estimated marginal means (synergy scores) were flipped to reflect the synergistic effect of the variables on cancer cell killing.

Flow gating

Flow cytometry gating was performed according to the field's standard in the literature or the laboratory's previous work. Representative flow gating plots are shown in Extended Data Fig. 10a–g.

Sample size determination

Sample sizes were determined according to the laboratory's previous work or from published studies of similar scope in the appropriate fields.

Replication

The number of biological replicates (typically $n \geq 3$) are indicated in the figure legends. Key findings (non-NGS) were replicated in at least

two independent experiments. NGS experiments were performed with biological replications, as indicated in the paper.

Randomization and blinding statements

Regular in vitro experiments were not randomized or blinded. Mouse experiments were randomized by using littermates and blinded using generic cage barcodes and ear tags where applicable. High-throughput experiments and analyses were blinded by barcoded metadata.

Standard statistical analysis

Standard statistical analyses were performed using common statistical methods with GraphPad Prism, Excel and R. Different levels of significance were assessed based on specific *P* values and type I error cut-off values (0.05, 0.01, 0.001 and 0.0001). Further details of statistical tests are provided in the figure legends and/or Supplementary information.

Data collection summary

Flow cytometry data were collected using a Cytek Aurora. All deep-sequencing data were collected using Illumina sequencers at the YCGA. Co-culture killing assay data were collected using a PE Envision plate reader.

Data analysis summary

Flow cytometry data were analysed using FlowJo (v.10.7 or higher). All simple statistical analyses were done with Prism (v.8 or higher). All NGS analyses were performed using custom codes.

Ethics statement

This study received institutional regulatory approval. All recombinant DNA and biosafety work was performed under the guidelines of the Yale Environment, Health and Safety Committee with an approved protocol (Chen-rDNA 15-45; 18-45; 21-45). All human sample work was performed under the guidelines of the Yale University Institutional Review Board with an approved protocol (HIC#2000020784), with only de-identified samples (exemption 4). All animal work was performed under the guidelines of Yale University IACUC with approved protocols (Chen 20068).

Material availability

Relevant biological materials and resources are generally available for academic or non-for-profit entities from the lead corresponding author (S.C.) upon reasonable request, typically via a material transfer agreement.

Reporting summary

Further information on research design is available in the Nature Portfolio Reporting Summary linked to this article.

Data availability

All generated data and analyses, information and results for this study are included in this Article's figures, extended data figures and supplementary datasets. Data are available at GitHub (https://github.com/Prenauer/OR7A10_NK_GOF_2025). Raw sequencing data are available for download from the Gene Expression Omnibus with the super-series accession number GSE309802 (https://www.ncbi.nlm.nih.gov/geo/query/acc.cgi?acc=GSE309802). Original cell lines are available at the commercial sources listed in the Methods and/or the Reporting Summary. Source data are provided with this paper.

Code availability

The code used for data analyses and the generation of figures related to this study is available from GitHub (https://github.com/Prenauer/OR7A10_NK_GOF_2025).

51. Modak, S., Kramer, K., Gultekin, S. H., Guo, H. F. & Cheung, N. K. Monoclonal antibody 8H9 targets a novel cell surface antigen expressed by a wide spectrum of human solid tumors. *Cancer Res.* **61**, 4048–4054 (2001).
52. Ahmed, M. et al. Humanized affinity-matured monoclonal antibody 8H9 has potent antitumor activity and binds to FG loop of tumor antigen B7-H3. *J. Biol. Chem.* **290**, 30018–30029 (2015).
53. Ye, L. et al. In vivo CRISPR screening in CD8 T cells with AAV-Sleeping Beauty hybrid vectors identifies membrane targets for improving immunotherapy for glioblastoma. *Nat. Biotechnol.* **37**, 1302–1313 (2019).
54. Langmead, B., Trapnell, C., Pop, M. & Salzberg, S. L. Ultrafast and memory-efficient alignment of short DNA sequences to the human genome. *Genome Biol.* **10**, R25 (2009).
55. Allen, F. et al. JACKS: joint analysis of CRISPR/Cas9 knockout screens. *Genome Res.* **29**, 464–471 (2019).
56. Lun, A. T., Chen, Y. & Smyth, G. K. It's DE-licious: a recipe for differential expression analyses of RNA-seq experiments using quasi-likelihood methods in edgeR. *Methods Mol. Biol.* **1418**, 391–416 (2016).
57. Li, W. et al. MAGeCK enables robust identification of essential genes from genome-scale CRISPR/Cas9 knockout screens. *Genome Biol.* **15**, 554 (2014).
58. Kim, E. & Hart, T. Improved analysis of CRISPR fitness screens and reduced off-target effects with the BAGEL2 gene essentiality classifier. *Genome Med.* **13**, 2 (2021).
59. Jeong, H. H., Kim, S. Y., Rousseaux, M. W. C., Zoghbi, H. Y. & Liu, Z. Beta-binomial modeling of CRISPR pooled screen data identifies target genes with greater sensitivity and fewer false negatives. *Genome Res.* **29**, 999–1008 (2019).
60. Jia, G., Wang, X. & Xiao, G. A permutation-based non-parametric analysis of CRISPR screen data. *BMC Genomics* **18**, 545 (2017).
61. Wang, T. et al. Identification and characterization of essential genes in the human genome. *Science* **350**, 1096–1101 (2015).
62. Wang, T. et al. Gene essentiality profiling reveals gene networks and synthetic lethal interactions with oncogenic Ras. *Cell* **168**, 890–903 (2017).
63. Aguirre, A. J. et al. Genomic copy number dictates a gene-independent cell response to CRISPR/Cas9 targeting. *Cancer Discov.* **6**, 914–929 (2016).
64. Meyers, R. M. et al. Computational correction of copy number effect improves specificity of CRISPR–Cas9 essentiality screens in cancer cells. *Nat. Genet.* **49**, 1779–1784 (2017).
65. Hart, T. et al. High-resolution CRISPR screens reveal fitness genes and genotype-specific cancer liabilities. *Cell* **163**, 1515–1526 (2015).
66. Sullivan, R. J. et al. First-in-class ERK1/2 inhibitor ulixertinib (BVD-523) in patients with MAPK mutant advanced solid tumors: results of a Phase I dose-escalation and expansion study. *Cancer Discov.* **8**, 184–195 (2018).
67. Lei, W. et al. Safety and feasibility of 4-1BB co-stimulated CD19-specific CAR-NK cell therapy in refractory/relapsed large B cell lymphoma: a phase 1 trial. *Nat. Cancer* **6**, 786–800 (2025).
68. Albinger, N. et al. Primary CD33-targeting CAR-NK cells for the treatment of acute myeloid leukemia. *Blood Cancer J.* **12**, 61 (2022).
69. Guo, S. et al. CD70-specific CAR NK cells expressing IL-15 for the treatment of CD19-negative B-cell malignancy. *Blood Adv.* **8**, 2635–2645 (2024).
70. Bexte, T. et al. CRISPR/Cas9 editing of *NKG2A* improves the efficacy of primary CD33-directed chimeric antigen receptor natural killer cells. *Nat. Commun.* **15**, 8439 (2024).
71. Frankish, A. et al. Gencode 2021. *Nucleic Acids Res.* **49**, D916–D923 (2021).
72. Hao, Y. et al. Dictionary learning for integrative, multimodal and scalable single-cell analysis. *Nat. Biotechnol.* **42**, 293–304 (2024).
73. Welch, J. D. et al. Single-cell multi-omic integration compares and contrasts features of brain cell identity. *Cell* **177**, 1873–1887 (2019).
74. Tang, F. et al. A pan-cancer single-cell panorama of human natural killer cells. *Cell* **186**, 4235–4251 (2023).
75. Bergen, V., Lange, M., Peidli, S., Wolf, F. A. & Theis, F. J. Generalizing RNA velocity to transient cell states through dynamical modeling. *Nat. Biotechnol.* **38**, 1408–1414 (2020).
76. Aibar, S. et al. SCENIC: single-cell regulatory network inference and clustering. *Nat. Methods* **14**, 1083–1086 (2017).
77. Schaefer, C. F. et al. PID: the Pathway Interaction Database. *Nucleic Acids Res.* **37**, D674–D679 (2009).
78. Liberzon, A. et al. The Molecular Signatures Database (MSigDB) hallmark gene set collection. *Cell Syst.* **1**, 417–425 (2015).
79. Rosskopf, S. et al. A Jurkat 76 based triple parameter reporter system to evaluate TCR functions and adoptive T cell strategies. *Oncotarget* **9**, 17608–17619 (2018).

Acknowledgements We thank H. Zhao, J. Burdekin and various other laboratory members for assistance; all members of the Chen Laboratory and various colleagues at Yale for assistance and/or discussion; and staff at the YCGA, the Cancer Center, the High Performance Computing Center, the West Campus Analytical Chemistry Core, the Center for Cellular and Molecular Imaging, the Electron Microscopy Facility and the Keck Biotechnology Resource Laboratory for technical support. We thank X. Su and Y. Xiong (Yale University) for providing the B7H3 CAR constructs. S.C. is supported by a Cancer Research Institute Lloyd J. Old STAR Award and CLIP Award (CRI4964, CRI13945), the NIH/NCI (DP2CA238295, R01CA231112, R33CA281702 and R33CA281702), the DoD (W81XWH-20-1-0072, W81XWH-21-1-0514, HT9425-23-1-0472 and HT9425-23-1-0860), the Alliance for Cancer Gene Therapy (ACGT), the Pershing Square Sohn Cancer Research Alliance, the Sontag Foundation, Dexter Lu and Bill Sperry. P.A.R. is supported by a Yale PhD training grant from the NIH (T32GM007499), a Lo Fellowship of Excellence of Stem Cell Research and a YCC T32 fellowship program (T32CA193200). L.P. is supported by DoD (OC240337P1) and Yale Neurosurgery. L.Z. is supported by a Gruber Science Fellowship and a Lo Fellowship of Excellence of Stem Cell Research. K.T. is supported by a Gruber Science Fellowship. J.S. and S.D. are supported by a Yale MSTP training grant from the NIH (T32GM136651). C.Z. is supported by a Yale PhD training grant from the NIH (T32HD007149). S.-H.L. is supported by a Korean fellowship and a Leslie Warner fellowship. S.F. is supported by the American Heart Association.

Author contributions L.P. and S.C. conceived the study. L.P., L.Y. and P.A.R. designed the screens. L.Y. and L.P. performed the screens and most experiments with assistance from various co-authors. P.A.R. developed SAMBA and performed screen and single-cell analyses. K.T. performed RNA-seq and WGS analyses. J.S., L.Z., C.Z., S.-H.L., M.F., S.J.-N., B.W., S.D., P.F., B.C., G.S., S.F., K.Z., D.P., F.Z. and J.T. assisted with various experiments and analyses. J.C., J.M. and M.G. supervised various trainees and provided support. L.Y., P.A.R., L.P., K.T., J.S., L.Z. and S.C. prepared the manuscript with input from all authors. S.C. secured funding and provided overall supervision of the project.

Competing interests A patent application has been filed by Yale University and Cellinfinity Bio related to the data in this study (US patent application no. 63/624,561; PCT WO2025158400A1). S.C. is a (co)founder of EvolveImmune Tx, Cellinfinity Bio, MagicTime Med and Chen Consulting. The other authors declare no competing interest.

Additional information

Supplementary information The online version contains supplementary material available at https://doi.org/10.1038/s41586-026-10149-8.

Correspondence and requests for materials should be addressed to Lei Peng or Sidi Chen.

Peer review information *Nature* thanks May Daher, Katayoun Rezvani, Rizwan Romee and the other, anonymous, reviewer(s) for their contribution to the peer review of this work. Peer reviewer reports are available.

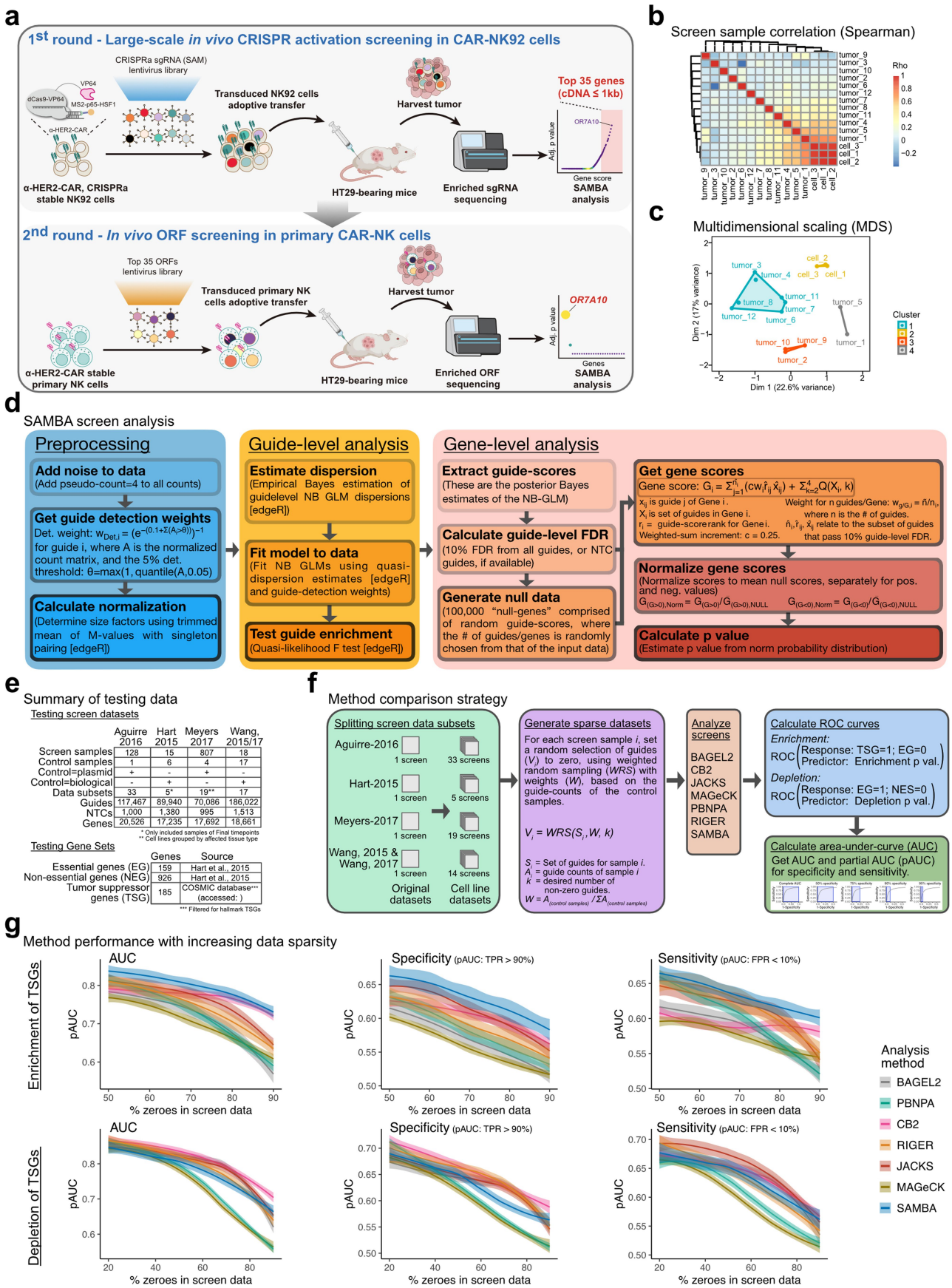

Extended Data Fig. 1 | See next page for caption.

Extended Data Fig. 1 | In vivo GOF CRISPRa screens identified boosters that enhance CAR-NK anti-tumor function. a, Schematics of the two in vivo GOF screens that identified functional boosters that enhance CAR-NK anti-tumor function. **Top**, Schematics of the primary screen (1st screen) - a CRISPRa screen using SAM sgRNA library with CAR-NK92 cells in HT29 tumor model. **Bottom**, Schematics of the secondary screen (2nd screen) - a barcoded UMI ORF mini-screen using top hits from the primary screen with human primary CAR-NK cells in HT29 tumor model. **b**, Heatmap of the correlation between CRISPRa screen samples. Sample correlation is presented as the Spearman rho values. **c**, Plot of the multidimensional scaling of data from CRISPRa screen samples. The samples were clustered by k-means, and a convex hull was drawn around the clustered samples. **d**, Schematic for a Screen Analysis Method with empirical Bayes estimates for Aggregated gene scoring (SAMBA). **e**, Summary information of the datasets and gene sets used to benchmark CRISPR screen analysis methods. **f**, Schematic describing the strategy for benchmarking CRISPR screen analysis methods against six other algorithms for enrichment and depletion analyses of datasets with simulated sparsity levels. **g**, Line plots showing the performance characteristics of different analysis methods, when guide detection is decreased among screen samples. Overall detection performance was measured by area-under-curve (AUC) values, specificity by the partial-AUC (pAUC) with a true-positive rate > 90%, and sensitivity by the pAUC with a false-positive rate <10%. Trendlines are the loess curves (opaque line) of AUC/pAUC values at each data sparsity level, shown with the standard error +/− the mean (shaded line) (see Methods for more details). The trendline of the area-under-curve (AUC) and partial-AUC (pAUC) values for 71 screens at different levels of data sparsity (see Methods for details). Each method is presented with a loess curve (opaque line), shown with the standard error +/− the mean (shaded line). The schematic in **a** was created using BioRender (https://biorender.com).

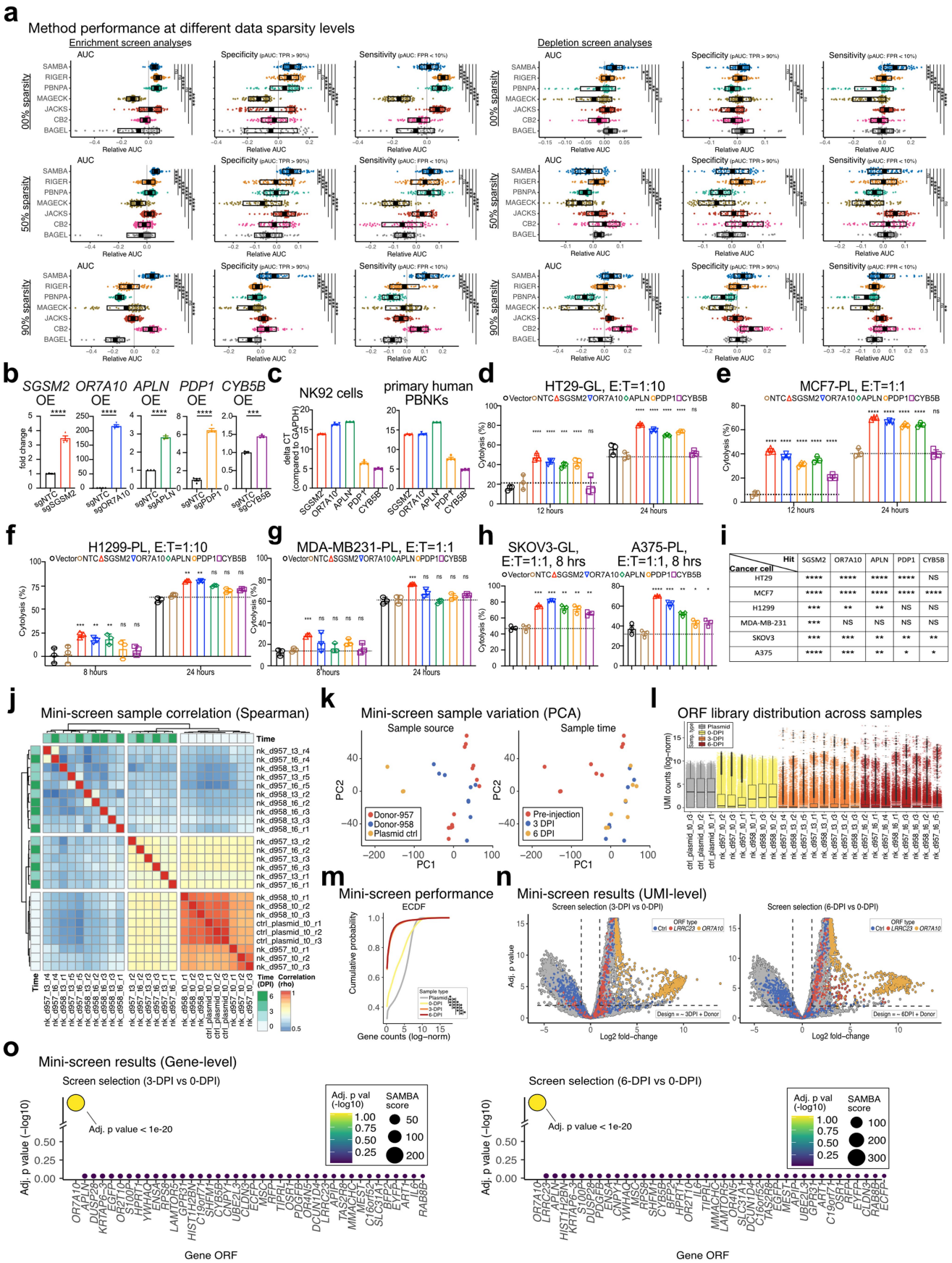

Extended Data Fig. 2 | See next page for caption.

Extended Data Fig. 2 | Additional in vitro assays of hit validation for lead selection, and barcoded ORF mini-screen analysis in primary human CAR-NK cells. a, Box plots showing the performance characteristics of different analysis methods at different levels of data sparsity. Performance is presented with relative AUC (rAUC) values, representing the AUC log2 fold-change to the mean AUC for each screen. Each screen analysis result is shown by a dot, the mean +/− standard error is depicted by the boxes, and error bars are shown for the ANOVA analysis of rAUCs with post-hoc analysis using the Tukey method. Error bars are only shown for comparisons with SAMBA, and significance is based on FDR-adjusted p values. **b**, RT-qPCR for overexpression of *SGSM2*, *OR7A10*, *APLN*, *PDP1*, and *CYB5B* after lentiviral transduction (n = 4 for *SGSM2*, *OR7A10*, and *PDP1*; n = 3 for *APLN* and *CYB5B*). **c**, Delta CT values for *SGSM2*, *OR7A10*, *APLN*, *PDP1*, and *CYB5B* compared to GAPDH in NK92 cells and primary human PBNKs (n = 4 for *SGSM2*, *OR7A10*, and *PDP1*; n = 3 for *APLN* and *CYB5B*). **d**-**h**, Co-culture assays of *SGSM2/OR7A10/APLN/PDP1/CYB5B*-OE CAR-NK92 cells and Vector/NTC controls with indicated cancer cells, with indicated E: T ratios at indicated time points. Individual replicate data points were shown (n = 3). The statistical significance levels are compared to the NTC control groups. **i**, Summary of statistical results from co-culture assays for the top five CAR-NK hyperbooster candidates tested. Statistical significance was assessed using Two-way ANOVA (**d**-**g**) or two-sided unpaired t test (**h**). ns, not significant; *, $p < 0.05$; **, $p < 0.01$; ***, $p < 0.001$; ****, $p < 0.0001$. Exact p-values and detailed statistics are provided in the Source Data Excel file. **j**, Heat map of the between-sample correlation (Spearman rho) for the ORF mini-screen data. Sample IDs are presented with cell/plasmid type, donor ID, time of cell extraction from tumors, and replicate number. Cell extraction times are also shown in the plot margins. **k**, Plots of between-sample variation, based on the first two principal components of PCA. Each sample is presented as a dot, color-coded by plasmid/donor (left) and the time of NK cell extraction from tumors (right). **l**, Box-whisker plots of the ORF-UMI count distributions across screen samples. Boxes are drawn for the 25th, 50th, and 75th percentile, color-coded by sample type and tumor-extraction time. Counts were presented as the log2 counts-per-million reads (log-norm). **m**, Plots of screen performance via empirical cumulative distribution function lines, color-coded by sample type and tumor-extraction time. Sample distributions were compared using two-sample Wasserstein tests, and p values were adjusted for FDR. **n**, Volcano plots of the UMI-level results of the ORF mini-screen, highlighting ORF-UMIs for the control genes (blue dots) and the top two significant hits: *LRRC23* and *OR7A10* (red and yellow dots, respectively). The data were analyzed by SAMBA to compare 3-DPI vs 0-DPI and 6-DPI vs 0-DPI (left and right plots, respectively). Significant ORF-UMIs were those with an adjusted (adj.) $p < 0.01$ and an absolute log2-fold-change > 1. **o**, Bubble plot of the gene-level results of the ORF mini-screen with genes ordered by decreasing significance. The data were analyzed by SAMBA to compare 3-DPI vs 0-DPI and 6-DPI vs 0-DPI (left and right plots, respectively), and results for each gene were presented with adj. p value and screen-enrichment score by dot color and size, respectively. Note: in all bar blots, data are shown as mean ± SEM. The statistical significance levels are indicated in the plots by Two-way ANOVA with Sidak post-hoc analysis and FDR-correction to p values (**d**-**g**) or unpaired t test (**b, h**). Statistical tests are two-sided other than SAMBA gene-level results (**o**), which use one-sided directional tests. ns, not significant; *, $p < 0.05$; **, $p < 0.01$; ***, $p < 0.001$; ****, $p < 0.0001$. Exact p-values and detailed statistics are provided in the Source Data Excel file.

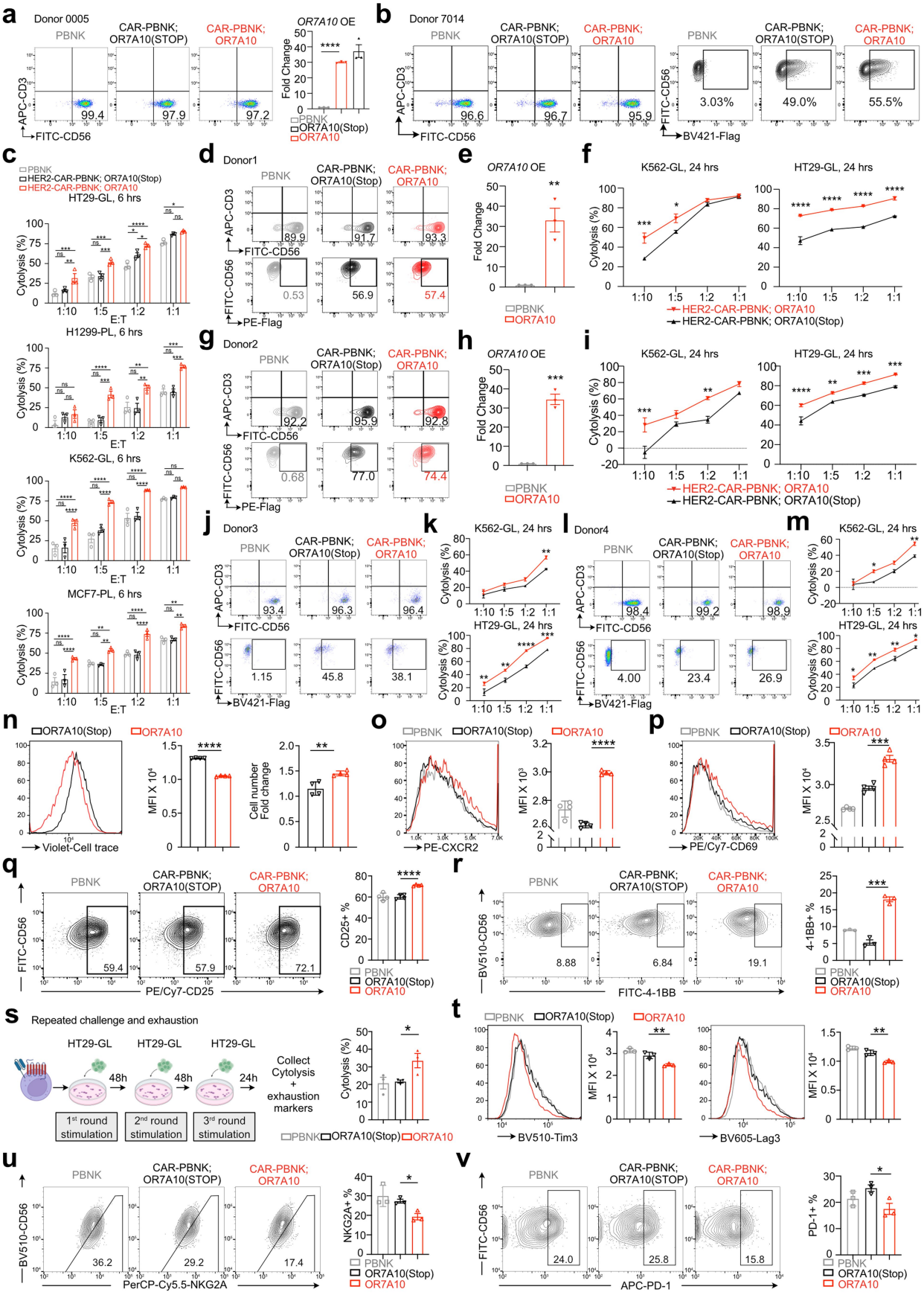

Extended Data Fig. 3 | See next page for caption.

Extended Data Fig. 3 | *OR7A10* ORF engineering enhances multiple effector functions of human primary CAR-PBNK cells, validated with multiple independent donors. a, **Left**, Flow cytometry of population in CAR-PBNK cells derived from Donor 0005 (same representative donor in Fig. 2). **Right**, RT-qPCR for overexpression of OR7A10 in CAR-PBNK cells from Donor 0005 (same representative donor in Fig. 2). **b**, Flow cytometry of population (**left**) and surface flag-CAR expression (**right**) in CAR-PBNK cells derived from Donor 7014. **c**, Co-culture assays of PBNK, CAR-PBNK;OR7A10(STOP) and CAR-PBNK;OR7A10 cells with HT29-GL, H1299-PL, K562-GL and MCF-PL cancer cells with indicated E: T ratios at 6 h (n = 3). **d**, Flow cytometry of population and surface flag-CAR expression in CAR-PBNK cells derived from Donor 1. **e**, RT-qPCR for overexpression of OR7A10 in CAR-PBNK cells (n = 3). **f**, Co-culture assays of CAR-PBNK;OR7A10(STOP) and CAR-PBNK;OR7A10 cells with K562-GL and HT29-GL cells with indicated E: T ratios at different time points (n = 3). **g**, Flow cytometry of population and surface flag-CAR expression in CAR-PBNK cells derived from Donor 2. **h**, RT-qPCR for overexpression of OR7A10 in CAR-PBNK cells (n = 3). **i**, Co-culture assays of CAR-PBNK;OR7A10(STOP) and CAR-PBNK;OR7A10 cells with K562-GL and HT29-GL cells with indicated E: T ratios at different time points (n = 3). **j**, Flow cytometry of population and surface flag-CAR expression in CAR-PBNK cells derived from Donor 3. **k**, Co-culture assays of CAR-PBNK;OR7A10(STOP) and CAR-PBNK;OR7A10 cells with K562-GL and HT29-GL cells with indicated E: T ratios at different time points (n = 3). **l**, Flow cytometry of population and surface flag-CAR expression in CAR-PBNK cells derived from Donor 4. **m**, Co-culture assays of CAR-PBNK;OR7A10(STOP) and CAR-PBNK;OR7A10 cells with K562-GL and HT29-GL cells with indicated E: T ratios at different time points (n = 3). **n**, Flow cytometry of cell trace dye dilution and cell count of PBNK, CAR-PBNK;OR7A10(STOP) and CAR-PBNK;OR7A10 cells after 3 days of culture, starting from 1 million cells per group. **o**, Flow cytometry of chemokine receptor CXCR2 surface expression of PBNK, CAR-PBNK;OR7A10(STOP) and CAR-PBNK;OR7A10 cells upon HT29 stimulation at E: T = 1: 1 for 24 h. **p**-**r**, Flow cytometry of activation marker CD69 and CD25 and costimulatory receptor 4-1BB surface expression of PBNK, CAR-PBNK;OR7A10(STOP) and CAR-PBNK;OR7A10 cells upon HT29 stimulation at E: T = 1: 1 for 6 h. Data represent technical quadruplicates from one representative donor out of 2 different human donors. **s**, Schematic representation of repeated challenge and cytolysis after the third round of stimulation. The E: T ratio was maintained at 1: 1 across three rounds of stimulation. Data represent technical triplicates from one representative donor out of 3 different human donors. **t**-**v**, Flow cytometry of exhaustion markers Tim-3, Lag-3, NKG2A, and PD-1 expression in PBNK, CAR-PBNK;OR7A10(STOP) and CAR-PBNK;OR7A10 cells at 24 h following the third round of stimulation with HT29 cells. Data represent technical triplicates from one representative donor out of 3 different human donors. Note: in all bar blots, data are shown as mean ± SEM. The statistical significance levels are indicated in the plots by Two-way ANOVA with Sidak post-hoc analysis and FDR-correction to p values (**c**, **f**, **i**, **k**, and **m**) or unpaired t test (**a**, **e**, **h**, **n**, **o**, **p**, **q**, **r**, **s**, **t**, **u**, and **v**). Statistical tests are two-sided unless otherwise noted. ns, not significant; *, $p < 0.05$; **, $p < 0.01$; ***, $p < 0.001$; ****, $p < 0.0001$. Exact p-values and detailed statistics are provided in the Source Data Excel file. The schematic in **s** was created using BioRender (https://biorender.com).

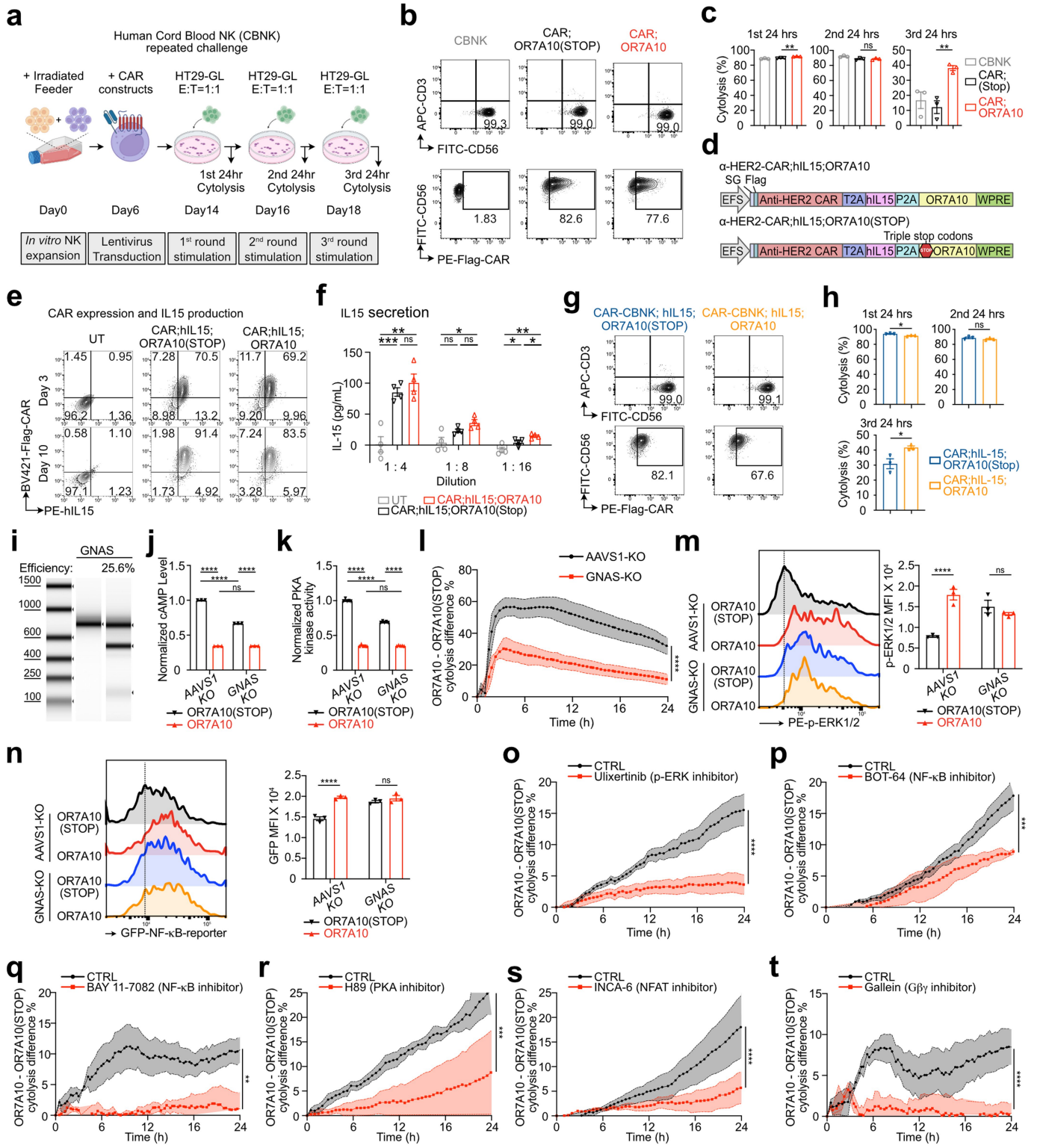

Extended Data Fig. 4 | See next page for caption.

Extended Data Fig. 4 | *OR7A10* ORF engineering enhances effector functions of human primary CAR-CBNK cells and exploration of GPCR signaling components in relation to OR7A10-driven effects in human primary CAR-NK cells. a, Schematic representation of production process for human Cord blood-derived CAR-NK;OR7A10 cells and experimental design for repeated challenge. E: T ratio was maintained at 1: 1 across 3 rounds of stimulation, with each round lasting 48 h. **b**, Flow cytometry of NK purity and CAR expression of CBNK, CAR-CBNK;OR7A10(STOP) and CAR-CBNK;OR7A10 cells. **c**, Cytolysis of CBNK, CAR-CBNK;OR7A10(STOP) and CAR-CBNK;OR7A10 cells with HT29-GL cells at 24 h post each round stimulation with HT29 cells (n = 3). **d**, Schematic illustration of the "all-in-one" constructs α-HER2-CAR; hIL-15;OR7A10 and α-HER2-CAR;hIL-15;OR7A10(STOP). **e**, Flow cytometry analysis of CAR expression and hIL-15 production in untransduced NK cells, CAR-NK;hIL15;OR7A10(STOP), and CAR-NK;hIL15;OR7A10 cells. Cells were collected on day 3 and 10 after lentivirus transduction. **f**, ELISA analysis of human IL-15 levels in the supernatant of untransduced NK cells, CAR-NK;hIL15; OR7A10(STOP), and CAR-NK;hIL15;OR7A10 cells. A total of 0.05 M cells were cultured per well in a 96-well plate, and supernatants were collected after 3 days. **g**, Flow cytometry analysis of NK cell purity and CAR expression in CAR-CBNK; hIL15;OR7A10(STOP) and CAR-CBNK;hIL15;OR7A10 cells. **h**, Cytotoxicity of CAR-CBNK;hIL15;OR7A10(STOP) and CAR-CBNK;hIL15;OR7A10 cells against HT29-GL target cells 24 h after each round stimulation (n = 3). **i**, T7E1 assay on *AAVS1*/*GNAS* KO human primary NK cells. **j-k**, Effects of knockout of *GNAS* on cAMP level (**b**, n = 3) and PKA activity (**c**, n = 5) of CAR-NK;OR7A10 or Stop control cells. **l**, Effects of knockout of *GNAS* on the cytotoxicity of OR7A10 or OR7A10(STOP)-OE HER2-CAR-NK cells against HT29-GL cells with E: T = 1: 2 (n = 4). **m**, Effects of knockout of *GNAS* on ERK1/2 phosphorylation (pT202/pY204) of CAR-NK;OR7A10(STOP) or CAR-NK;OR7A10 cells upon HT29 stimulation with E: T = 1: 1 at 5 min (n = 4). **n**, Effects of knockout of *GNAS* on NF-kB activity of CAR-NK;OR7A10(STOP) and CAR-NK;OR7A10 cells upon HT29 stimulation with E: T = 1: 1 at 6 h (n = 3). **o**, Effects of p-ERK inhibitor Ulixertinib (5 μM) on cytotoxicity of CAR-NK;OR7A10(STOP) and CAR-NK;OR7A10 cells upon HT29 stimulation with E: T = 1: 2 (n = 4). **p**, Effects of NF-kB inhibitor BOT-64 (100 μM) on cytotoxicity of CAR-NK;OR7A10(STOP) and CAR-NK;OR7A10 cells upon HT29 stimulation with E: T = 1: 2 (n = 4). **q**, Effects of NF-kB inhibitor BOY 11-7082 (5 μM) on cytotoxicity of CAR-NK;OR7A10(STOP) and CAR-NK;OR7A10 cells upon HT29 stimulation with E: T = 1: 5 (n = 3). **r**, Effects of PKA inhibitor H89 (30 μM) on cytotoxicity of CAR-NK;OR7A10(STOP) and CAR-NK;OR7A10 cells upon HT29 stimulation with E: T = 1: 2 (n = 4). **s**, Effects of NFAT inhibitor INCA-6 (25 μM) on cytotoxicity of CAR-NK;OR7A10(STOP) and CAR-NK;OR7A10 cells upon HT29 stimulation with E: T = 1: 2 (n = 4). **t**, Effects of Gβγ inhibitor Gallein (10 μM) on cytotoxicity of CAR-NK;OR7A10(STOP) and CAR-NK;OR7A10 cells upon HT29 stimulation with E: T = 1: 5 (n = 3). Note: data are shown as mean ± SEM. The statistical significance levels are indicated in the plots by unpaired t test (**c**, **f**, **h**, **j**, **k**, **m**, and **n**) or Two-way ANOVA with Sidak post-hoc analysis and FDR-correction to p values (**l**, **o-t**). Statistical tests are two-sided unless otherwise noted. ns, not significant; *, $p < 0.05$; **, $p < 0.01$; ***, $p < 0.001$; ****, $p < 0.0001$. Exact p-values and detailed statistics are provided in the Source Data Excel file. The schematic in **a** was created using BioRender (https://biorender.com).

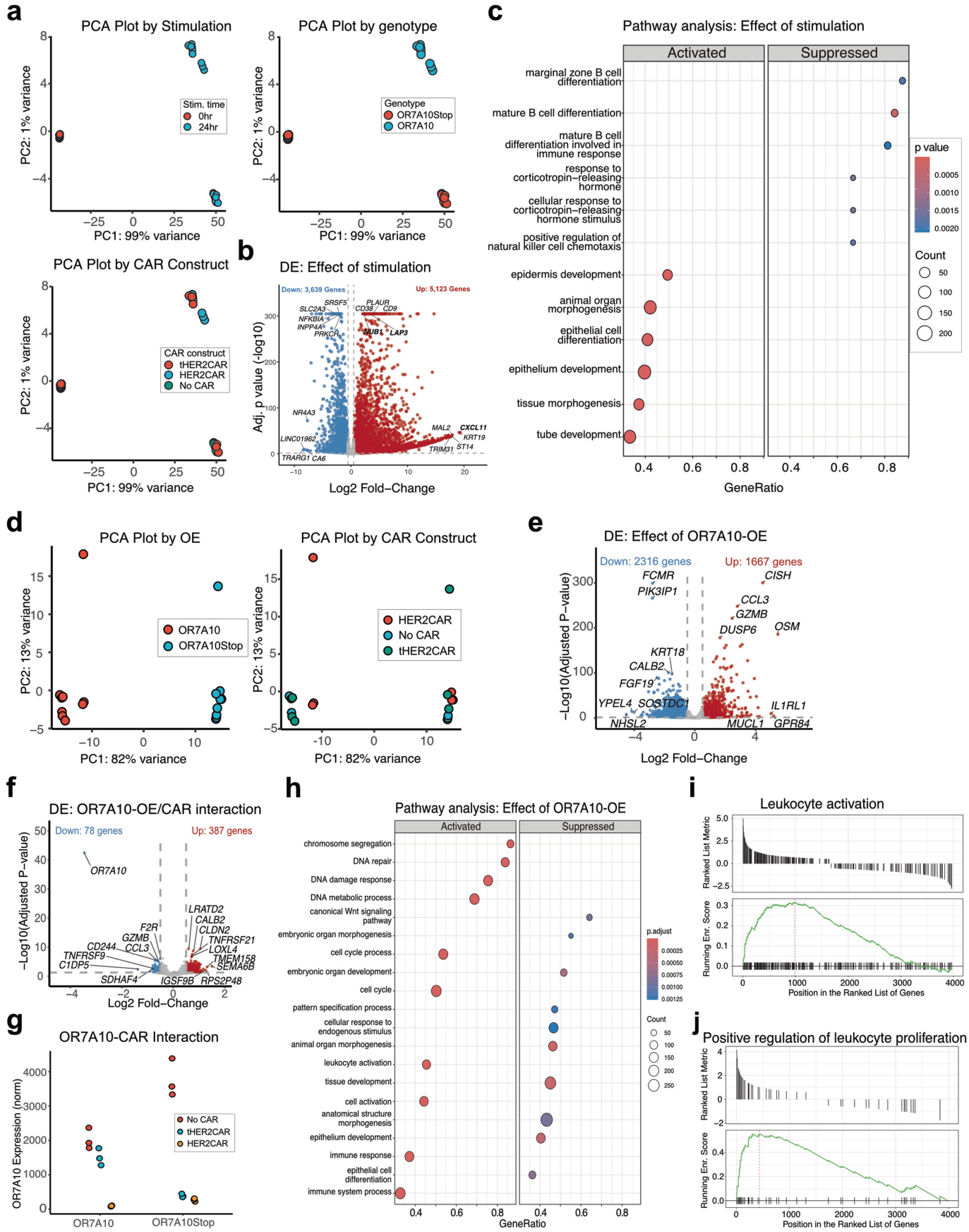

Extended Data Fig. 5 | See next page for caption.

Extended Data Fig. 5 | Bulk mRNA-Seq revealed OR7A10-driven gene expression changes and interaction between OR7A10 and CAR signaling. **a**, Principal Component Analysis (PCA) plot for RNA-Seq samples, label by stimulation condition (left: Stimulation for 24hrs vs Unstimulated), overexpression construct (middle: OR7A10 vs OR7A10Stop), or CAR construct (right: truncated CAR (tHER2CAR), complete CAR, No CAR). **b**, Volcano plot showing the differential expressed genes caused by stimulation main effect. Upregulated genes were labeled with red, downregulated genes were labeled with blue, and not significant differential expressed genes were label with grey. |Log2FoldChange| > 0.5 and adjusted p-value < 0.05 were used as threshold for significant expressed genes. **c**, Bubble plot showing Gene Set Enrichment Analysis (GSEA) result (GO-BP pathways) of the differentially expressed genes caused by stimulation main effect. Color scale represents the adjusted p-value. Size of the bubble represent the number of differentially expressed gene in the pathway. **d**, PCA plot for stimulated samples only. label overexpression construct (top: OR7A10 vs OR7A10Stop) or CAR construct (bottom: truncated CAR, complete CAR, No CAR). **e**, Volcano plot showing the differential expressed genes of OR7A10 vs OR7A10Stop overexpression main effect. Upregulated genes were labeled with red, downregulated genes were labeled with blue, and not significant differential expressed genes were label with grey. |Log2FoldChange| > 0.5 and adjusted p-value < 0.05 were used as threshold for significant expressed genes. **f**, Volcano plot showing the differential expressed genes of interaction between OR7A10 and HER2CAR. Upregulated genes were labeled with red, downregulated genes were labeled with blue, and not significant differential expressed genes were label with grey. |Log2FoldChange| > 0.5 and adjusted p-value < 0.05 were used as threshold for significant expressed genes. **g**, Interaction plot showing the change in normalized expression of OR7A10 between OR7A10 and OR7A10Stop overexpression is different for groups: No CAR, truncated HER2 CAR (tHER2CAR), and complete HER2 CAR. **h**, Bubble plot showing the pathway analysis (GO-BP) result of the differentially expressed genes caused by OR7A10 vs OR7A10Stop overexpression main effect. Color scale represent the adjusted p-value. Size of the bubble represent the number of differentially expressed gene in the pathway. **i**, GSEA plot showing the differentially expressed genes of OR7A10 vs OR7A10Stop overexpression main effect in pathway "leukocytes activation". **j**, GSEA plot showing the differentially expressed genes of OR7A10 vs OR7A10Stop overexpression main effect in pathway "positive regulation of leukocyte proliferation". DE analyses were performed by DESeq2 Wald tests. Statistical tests are two-sided unless other than GSEA results (**c** and **g**), which use one-sided directional tests.

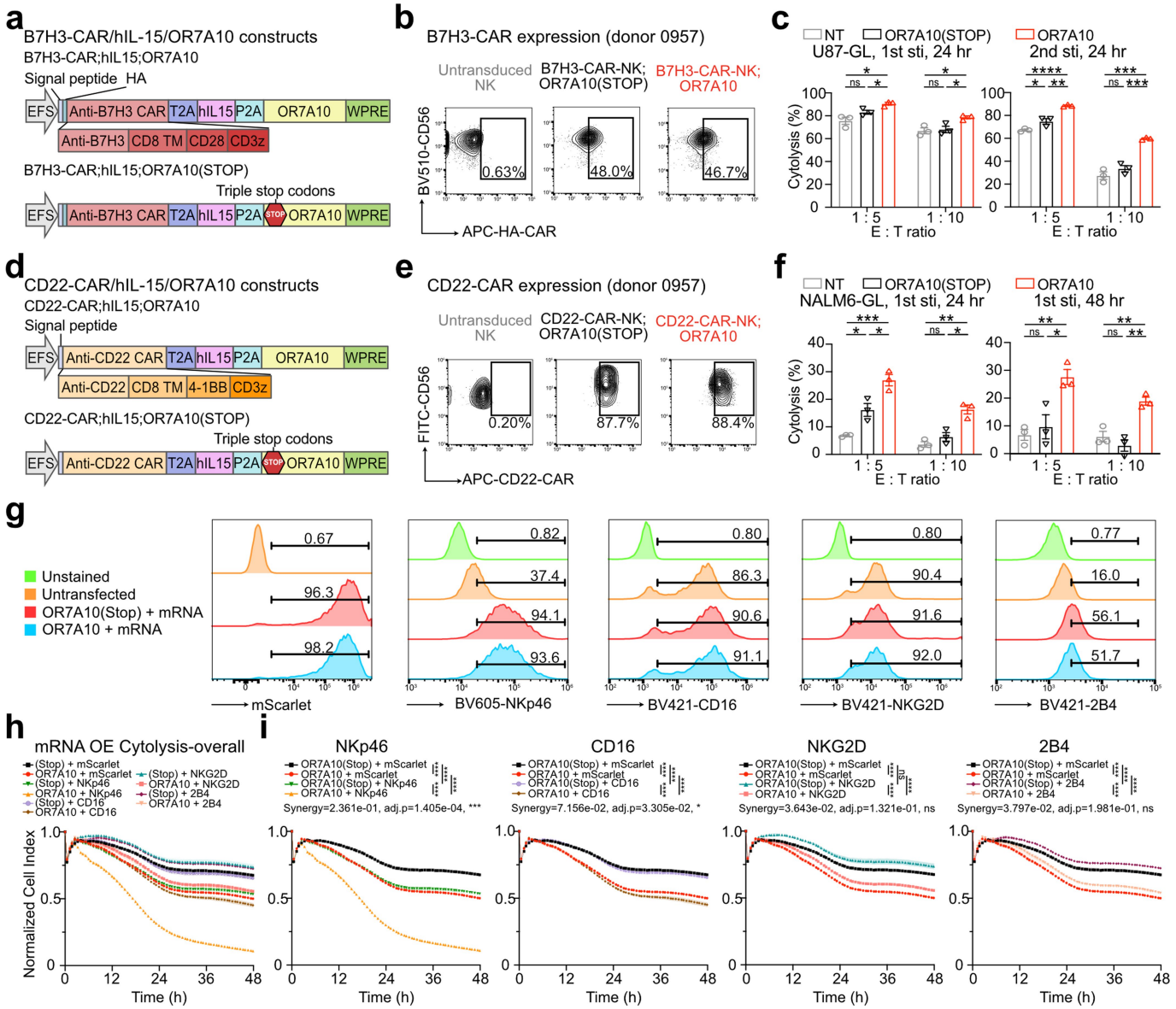

Extended Data Fig. 6 | OR7A10-OE enhances cytotoxicity of 2nd generation CAR constructs and synergizes NKp46 signaling. a, Schematic illustration of the "all-in-one" constructs B7H3-CAR;hIL-15;OR7A10 and B7H3-CAR;hIL-15;OR7A10(STOP). **b**, Flow cytometry analysis of B7H3-CAR expression in untransduced NK cells, B7H3-CAR-NK;hIL15;OR7A10(STOP), and B7H3-CAR-NK;hIL15;OR7A10 cells. **c**, Cytotoxicity of untransduced NK cells, B7H3-CAR-NK;hIL15;OR7A10(STOP) and B7H3-CAR-NK;hIL15;OR7A10 cells against U87-GL target cells 24 h after each round stimulation (n = 3). Statistical significance was assessed using two-sided unpaired t test. **d**, Schematic illustration of the "all-in-one" constructs CD22-CAR;hIL-15;OR7A10 and CD22-CAR;hIL-15;OR7A10 (STOP). **e**, Flow cytometry analysis of CD22-CAR expression in untransduced NK cells, CD22-CAR-NK;hIL15;OR7A10(STOP), and CD22-CAR-NK;hIL15; OR7A10 cells. **f**, Cytotoxicity of untransduced NK cells, CD22-CAR-NK;hIL15; OR7A10(STOP), and CD22-CAR-CBNK;hIL15;OR7A10 cells against NALM6-GL target cells at 24 and 48 h post stimulation (n = 3). Statistical significance was assessed using two-sided unpaired t test. **g**, Flow cytometry analysis confirming overexpression of activating receptors NKp46, CD16, NKG2D, 2B4, and mScarlet control, 24 h after mRNA electroporation. **h-i**, NK Cytotoxicity assessed by RTCA killing assays against HT29 targets at an E: T ratio of 1:1, using NK cells overexpressing mScarlet, NKp46, CD16, NKG2D, or 2B4 to assess synergistic effects with OR7A10. Note: in all bar blots, data are shown as mean ± SEM. The statistical significance levels are indicated in the plots by univariate three-way ANOVA tests with Sidak post-hoc analysis and FDR-correction to p values (**i**) or two-sided unpaired t test (**c** and **f**). Statistical tests are two-sided, where appropriate. ns, not significant; *, $p < 0.05$; **, $p < 0.01$; ***, $p < 0.001$; ****, $p < 0.0001$. Exact p-values and detailed statistics are provided in the Source Data Excel file.

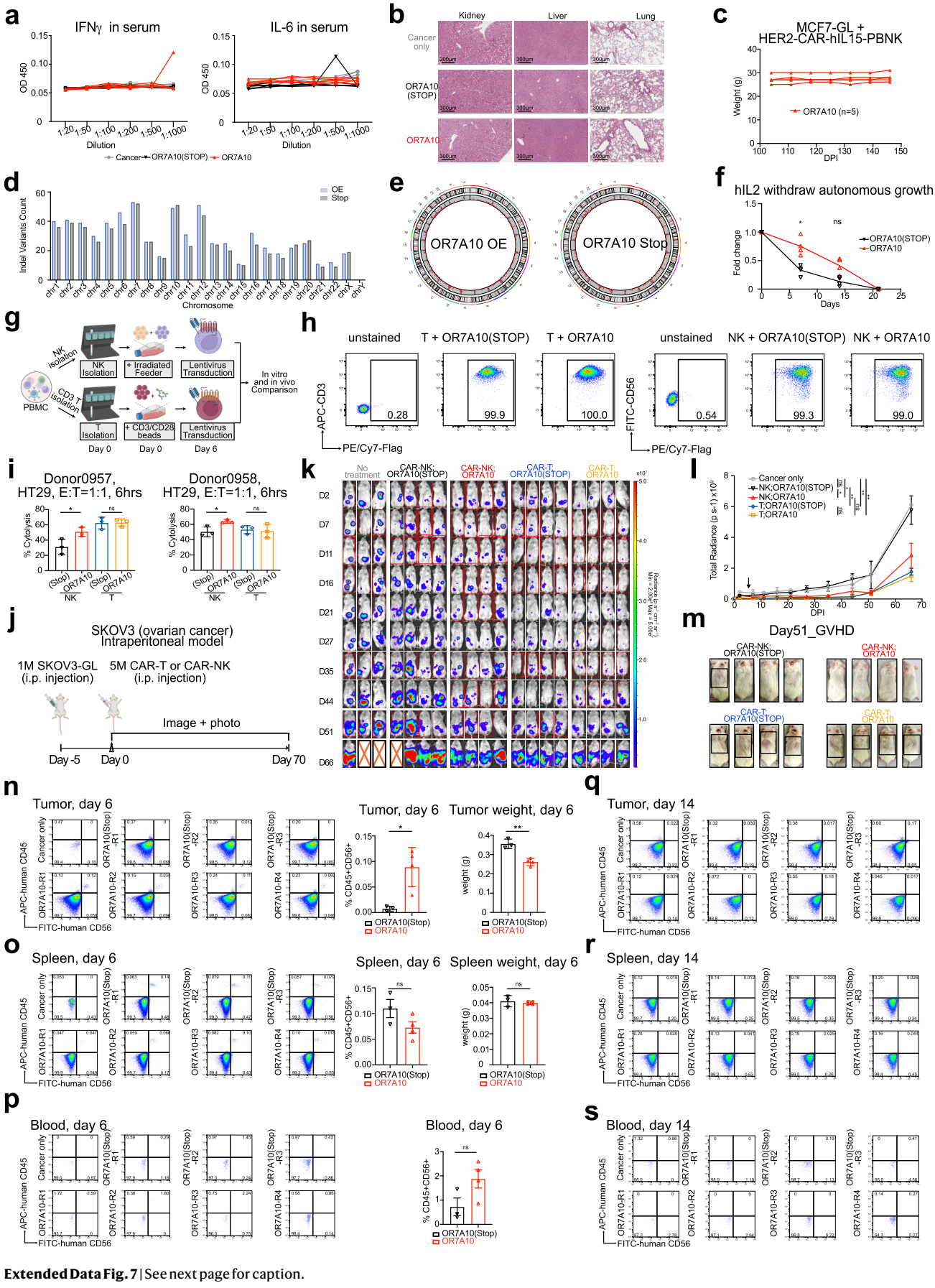

Extended Data Fig. 7 | See next page for caption.

Extended Data Fig. 7 | Safety, effect, and immune profile of OR7A10-OE on human primary CAR-NK cells. a, Elisa assay of IFNg and IL-6 level in mouse serum received different treatment in Fig. 5b,c. **b**, Histology sections stained by hematoxylin and eosin of tumors derived from Fig. 5b,c. High magnification image scale bar: 300 μm. **c**, Weight of mice which received CAR-PBNK;hIL15; OR7A10 cells in Fig. 5d–f. **d**, Bar plot showing the distribution of indel variants identified by whole genome sequencing (WGS) on different chromosomes. **e**, RCircos plot showing the distribution of indel and structural variants across the whole genome for OR7A10 overexpression (OR7A10 OE, **left**) sample and OR7A10 stop (OR7A10 Stop, **right**) control. No chromosome translocation was detected. **f**, proliferation of CAR-PBNK;hIL15;OR7A10 cells or CAR-PBNK;hIL15; OR7A10(STOP) cells under hIL2-withdrawal condition. **g**, Schematic of the production process for CAR-NK;OR7A10(STOP), CAR-NK;OR7A10, CAR-T; OR7A10(STOP), and CAR-T;OR7A10 cells derived from the same healthy PBMC donor. **h**, Flow cytometry of population and CAR surface expression in CAR-T and CAR-NK cells. **i**, Cytolysis of CAR-NK;OR7A10(STOP), CAR-NK;OR7A10, CAR-T;OR7A10(STOP), and CAR-T;OR7A10 cells (n = 3) derived from two healthy PBMC donors against HT29 colon cancer cells. Statistical significance was assessed using two-sided unpaired t test. **j**-**l**, Schematic (**j**), bioluminescence imaging (**k**), and tumor burden quantification (**l**), and SKOV3 tumor-bearing mice following different treatments: no treatment (n = 3 mice), adoptive cell transfer of CAR-NK;OR7A10(STOP) (n = 4 mice), CAR-NK;OR7A10 (n = 4 mice), CAR-T;OR7A10(STOP) (n = 4 mice) or CAR-T;OR7A10 (n = 4 mice). **m**, Brightfield photos of mice as in (**d**-**f**) at day 51 post treatment. Areas with symptoms of GvHD were shown in black boxes. **n**, Flow cytometry (**left**) and quantification (**middle**) of CD45 + CD56 + NK cells in the Tumor samples at Day 6 after NK transfer and tumor weights (**right**) at Day 6 after NK transfer. Statistical significance was assessed using two-sided unpaired t test. **o**, Flow cytometry (**left**) and quantification (**middle**) of CD45 + CD56 + NK cells in the Spleen samples at Day 6 after NK transfer and spleen weights (**right**) at Day 6 after NK transfer. Statistical significance was assessed using two-sided unpaired t test. **p**, Flow cytometry (**left**) and quantification (**right**) of CD45 + CD56 + NK cells in the Blood samples at Day 6 after NK transfer. Statistical significance was assessed using two-sided unpaired t test. **q**-**s**, Flow cytometry of CD45 + CD56 + NK cells in the Spleen, Blood, and Tumor samples at Day 14 after NK transfer. Note: data are shown as mean ± SEM. The statistical significance levels are indicated in the plots by Two-way ANOVA with Sidak post-hoc analysis (**f**), mixed-effects model with Tukey's post-hoc analysis (**l**) or unpaired t test (**i** and **n**-**p**). Statistical tests are two-sided, and FDR-corrected p values are depicted in **f**-**l**, where appropriate. ns, not significant; *, $p < 0.05$; **, $p < 0.01$; ***, $p < 0.001$; ****, $p < 0.0001$. Exact p-values and detailed statistics are provided in the Source Data Excel file. The schematics in **g** and **j** were created using BioRender (https://biorender.com).

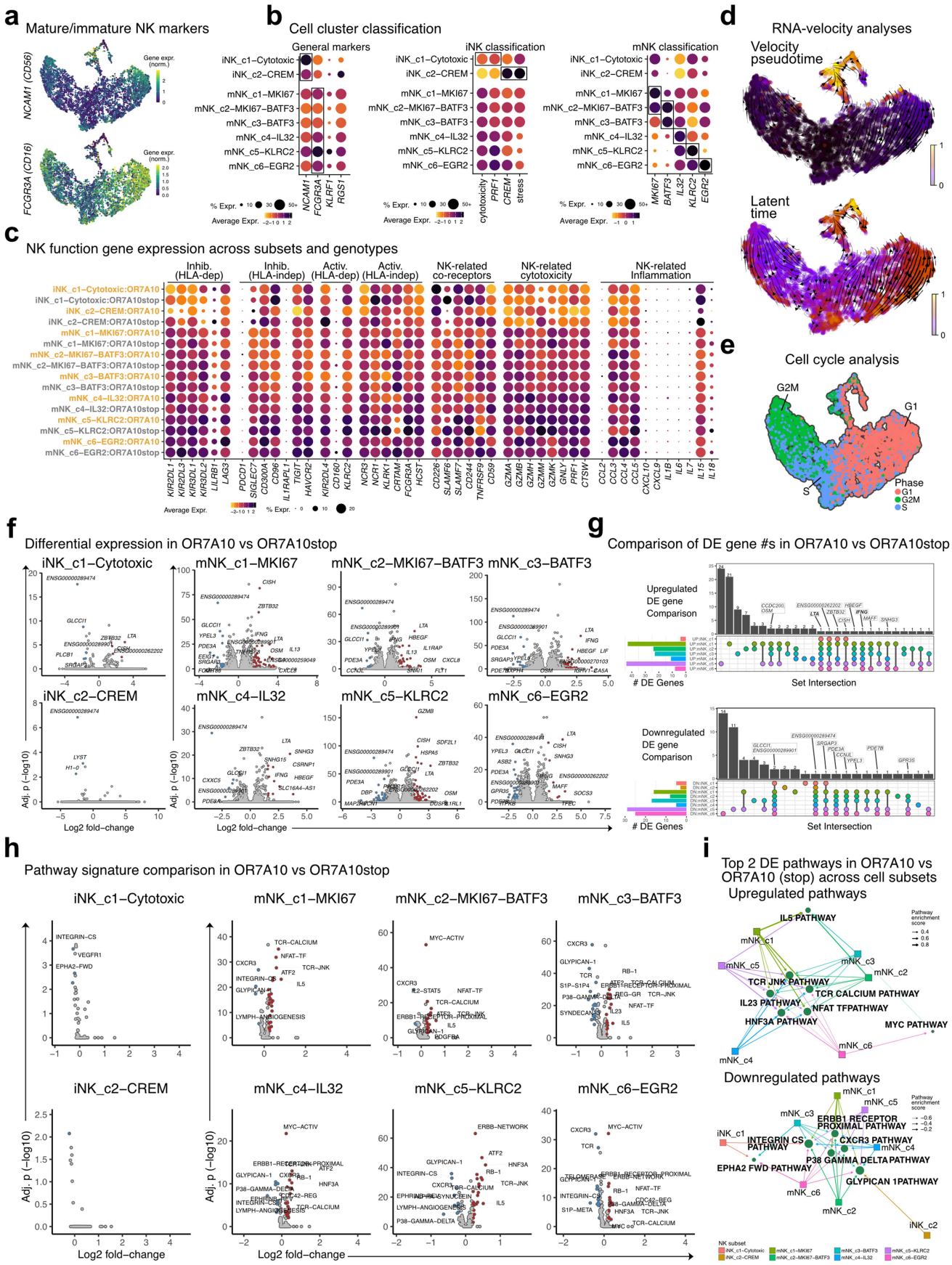

Extended Data Fig. 8 | See next page for caption.

Extended Data Fig. 8 | Single-cell transcriptomic analysis of tumor-infiltrating human primary CAR-NK cell subsets. a, UMAP embedding with heatmap depiction of gene expression markers used to distinguish immature NK (CD56-hi CD16-lo) and mature NK (CD56-lo CD16-hi) cells. **b**, Heatmap dot plots of gene expression and signature markers used to distinguish NK subsets across single-cell transcriptomic (SCT) cell clusters. Dot color and size were used to represent the mean gene/signature expression, and the % of clustered cells with detected expression. Labels are italicized and capitalized for gene names, while signatures were presented with normal fonts. **c**, Heatmap dot plots of the expression of NK function genes. **d**, UMAP presented with RNA splicing kinetics analysis results (scVelo) estimating population-level trajectories in differentiation. Velocity pseudotime and latent time estimates predicted trajectories of transcriptional profile changes and putative cellular ages, respectively. **e**, UMAP depiction of cell cycle predictions (Seurat method), based on the expression of characteristic marker genes. **f**, Volcano plots of the differential expression (DE) analyses between OR7A10-OE vs OR7A10-(stop) NK subsets. Significant DE genes were those with an adj. $p < 0.01$ and a log2 foldchange > 1.5 (upregulation = red dot) or < −1.5 (downregulation = blue dot). **g**, Upset plot of DE genes that were common between different NK subset. The upregulated and downregulated DE gene comparisons are displayed separately in the top and bottom panels, respectively. Genes were labeled when significant in at least four subsets. **h**, Volcano plots of the differential expression (DE) pathway analyses between OR7A10-OE vs OR7A10-(stop) NK subsets. Pathway signatures were assessed at a single-cell level by AUCell method, and signatures were compared by Wilcox test (Seurat method). Significant DE pathways were those with an adj. $p < 0.01$ and a log2 foldchange > 0.2 (upregulation = red dot) or < −0.2 (downregulation = blue dot). **i**, Network plots of the top two DE pathways that were identified in each NK subset. Plots are shown with square nodes color-coded for the NK subsets, and pathways are depicted by green circle nodes, sized by number subsets for which each pathway was found significant. The width of the network edges (lines) represents the log2 fold change from the DE analysis. The upregulated and downregulated DE gene comparisons are displayed separately in the left and right panels, respectively. DE analyses (**f** and **h**) were performed by pseudo-replicate Wilcox tests, and all statistical tests are two-sided.

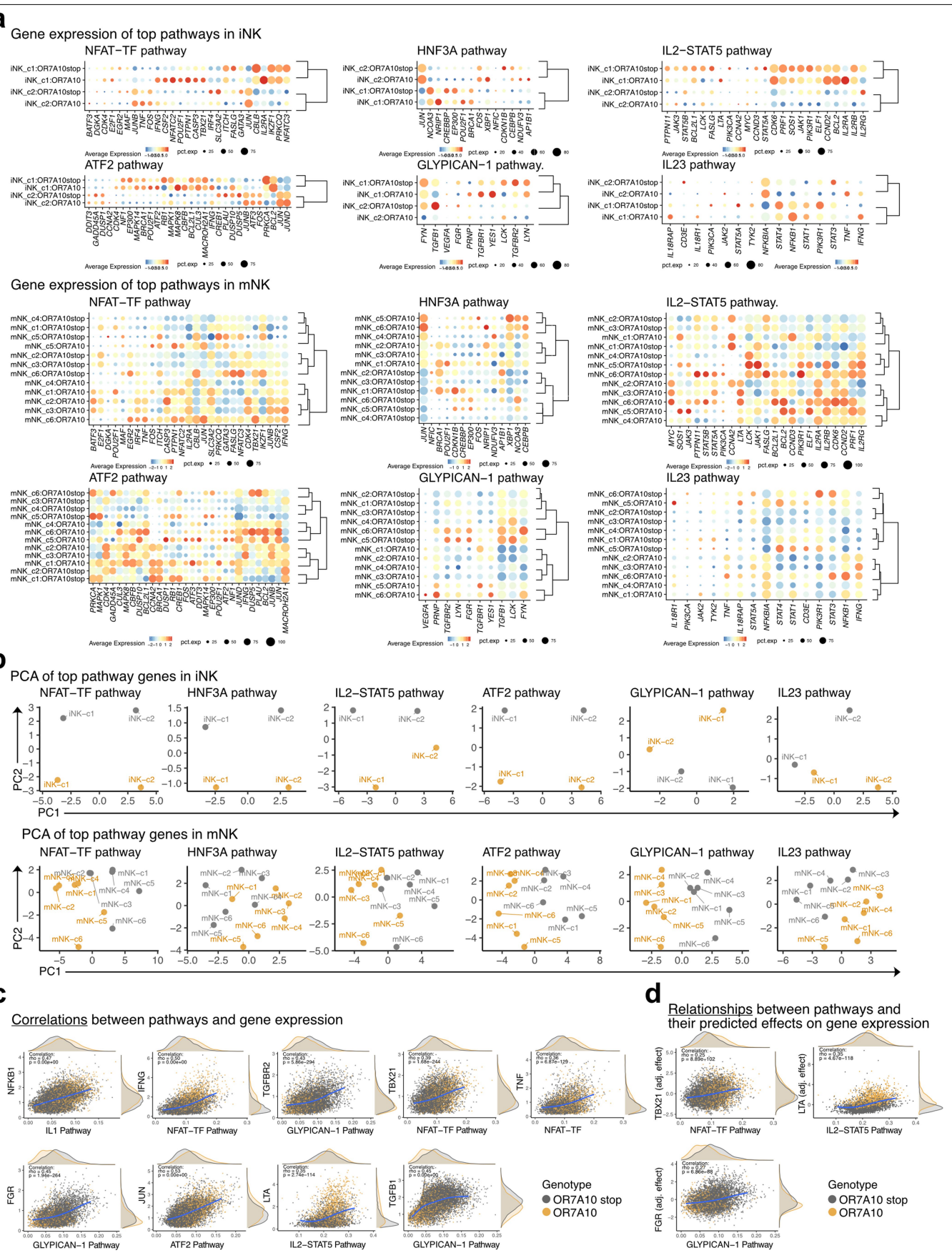

Extended Data Fig. 9 | See next page for caption.

Extended Data Fig. 9 | Gene expression patterns for select significant pathways affected by OR7A10-OE in tumor-infiltrating human primary CAR-NK cells across different subsets. a, Heatmap dot plots of gene expression for six significant pathways across immature and mature NK (iNK and mNK, respectively) subsets. The genes presented were filtered to include those that were expressed in at least 20% of cells. Dot color and size were used to represent the mean gene expression, and the % of clustered cells with detected expression. **b**, Principal components analysis (PCA) plots of comparing NK cell subsets, separated by genotype, based on the expression of genes related to six significant pathways. The genotype of each NK cell subset was presented by color-coded dots. **c**, Scatter plots of the correlations between top DE pathways and DE genes. For each plot, normalized gene expression was compared to pathway signatures. **d**, Scatter plots of the top predicted cause-effect relationships between DE pathways and DE genes. Gene expression values were adjusted to be independent of cell subset effects. For **c** and **d**, trends were shown by blue regression lines (simple generalized additive model); and Pearson correlation analysis results (rho values and two-sided p values) are shown for correlations between pathways and genes.

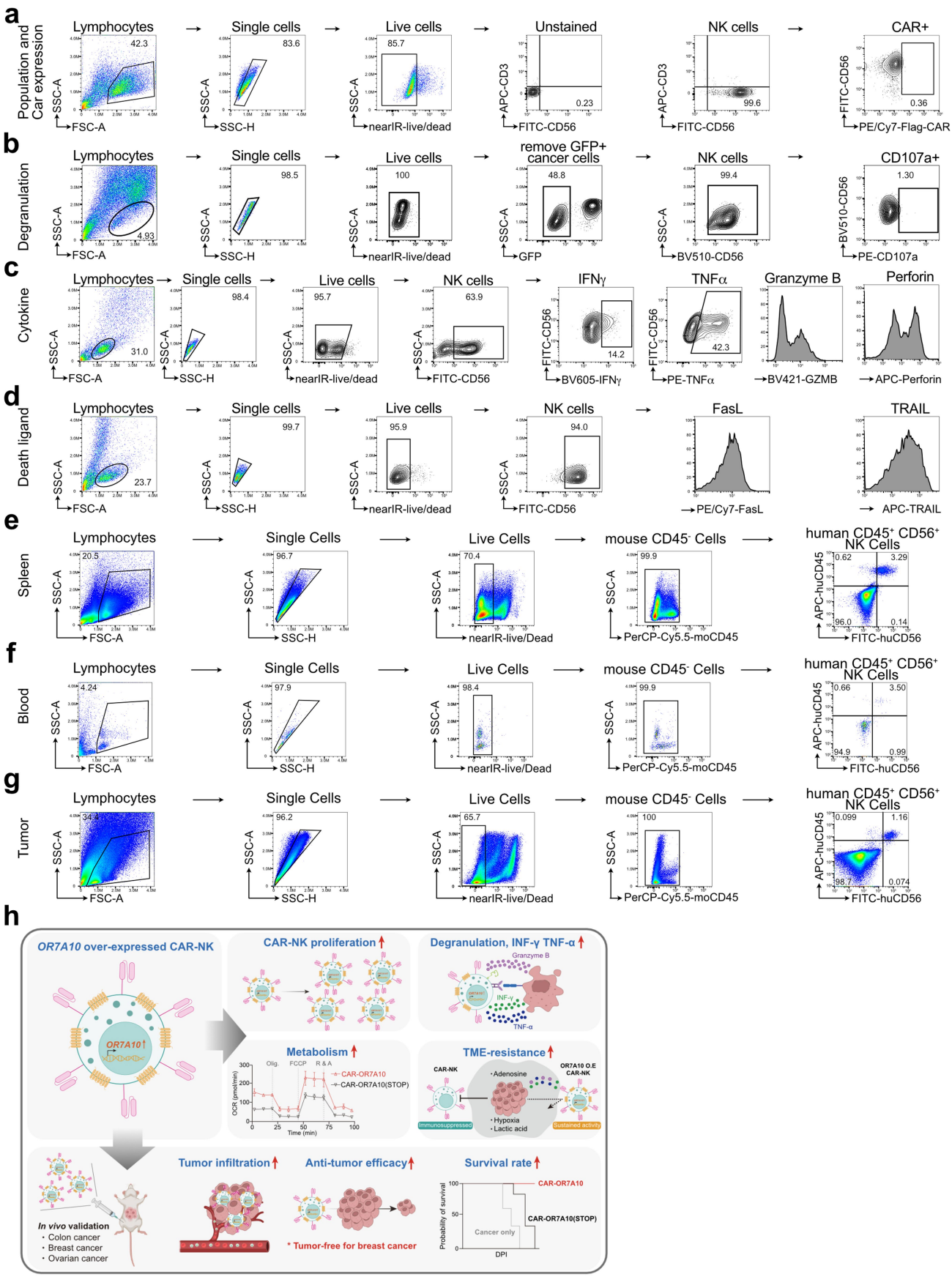

Extended Data Fig. 10 | See next page for caption.

Extended Data Fig. 10 | Flow gating strategy of anti-tumor functions of CAR-NK cells and graphical summary. a, Gating strategy of Flow cytometry of NK population and CAR expression in Fig. 2b and Extended Data Fig. 7. **b**, Gating strategy of Flow cytometry of degranulation in Fig. 2e. **c**, Gating strategy of Flow cytometry of production of effector cytokines in Fig. 2f and Fig. 2h,i. **d**, Gating strategy of Flow cytometry of surface FasL and TRAIL in Fig. 2g. **e-g**, Gating strategy of Flow cytometry of NK presentation in the Spleen, Blood, and Tumor samples in Fig. 5l–n and Extended Data Fig. 7. **h**, Graphical summary of OR7A10 engineering boosts CAR-NK anti-tumor functions. The schematic in **h** was created using BioRender (https://biorender.com).

nature portfolio

Corresponding author(s): Sidi Chen, Lei Peng

Last updated by author(s): 12/26/2025

Reporting Summary

Nature Portfolio wishes to improve the reproducibility of the work that we publish. This form provides structure for consistency and transparency in reporting. For further information on Nature Portfolio policies, see our Editorial Policies and the Editorial Policy Checklist.

Statistics

For all statistical analyses, confirm that the following items are present in the figure legend, table legend, main text, or Methods section.

n/a	Confirmed
☐	☒ The exact sample size (*n*) for each experimental group/condition, given as a discrete number and unit of measurement
☐	☒ A statement on whether measurements were taken from distinct samples or whether the same sample was measured repeatedly
☐	☒ The statistical test(s) used AND whether they are one- or two-sided *Only common tests should be described solely by name; describe more complex techniques in the Methods section.*
☐	☒ A description of all covariates tested
☐	☒ A description of any assumptions or corrections, such as tests of normality and adjustment for multiple comparisons
☐	☒ A full description of the statistical parameters including central tendency (e.g. means) or other basic estimates (e.g. regression coefficient) AND variation (e.g. standard deviation) or associated estimates of uncertainty (e.g. confidence intervals)
☐	☒ For null hypothesis testing, the test statistic (e.g. *F*, *t*, *r*) with confidence intervals, effect sizes, degrees of freedom and *P* value noted *Give P values as exact values whenever suitable.*
☒	☐ For Bayesian analysis, information on the choice of priors and Markov chain Monte Carlo settings
☐	☒ For hierarchical and complex designs, identification of the appropriate level for tests and full reporting of outcomes
☐	☒ Estimates of effect sizes (e.g. Cohen's *d*, Pearson's *r*), indicating how they were calculated

Our web collection on statistics for biologists contains articles on many of the points above.

Software and code

Policy information about availability of computer code

Data collection	Flow cytometry data was collected by Four-laser Aria II (BD), Five-laser Symphony S6 (BD), Cytek Aurora (Cytek Biosciences); All deep sequencing data were collected using Illumina Sequencers at Yale Center for Genome Analysis (YCGA). Co-culture killing assay data were collected with PE Envision Plate Reader.

Data analysis	All statistical methods are described in figure legends and/or supplementary Excel tables. The p values and statistical significance were estimated for most analyses. Different levels of statistical significance were accessed based on specific p values and type I error cutoffs (0.05, 0.01, 0.001, 0.0001). Data analysis was performed using GraphPad Prism v.10. and RStudio. Source data and statistics were provided in supplemental excel files. Data analysis was performed using the following software / packages: FlowJo ≥ v.10.9.0; Prism ≥ 9 (e.g. 10.2.0); BEDtools v2.30.0; Bowtie 1.3.0; BWA v0.7.17; Cutadapt v3.4.0; FlowJo ≥ v.10.9.0; GATK v4.6.0.0; GRIDDS v2.13.2-3; Picard v2.25.6; Prism ≥ 9; SAMtools v1.21; STAR v2.7.4a Python ≥ v3.9; scVelo v0.2.5; velocyto v0.17 R ≥ v4.2; afex R package v1.5-0; AUCell R package v1.26.0; clusterProfiler R package v4.12.6; DESeq2 R package v1.44.0; edgeR R package v4.2.2; emmeans R package v2.0.1; igraph R package v2.2.1; mgcv R package v1.9.4; RCircos R package v1.2.2; rliger R package v2.2.1; SAMBA R package v1.2.5; Seurat R package v5.4.0; SeuratWrappers R package v0.4.0

For manuscripts utilizing custom algorithms or software that are central to the research but not yet described in published literature, software must be made available to editors and reviewers. We strongly encourage code deposition in a community repository (e.g. GitHub). See the Nature Portfolio guidelines for submitting code & software for further information.

Data

Policy information about availability of data

All manuscripts must include a data availability statement. This statement should provide the following information, where applicable:

- Accession codes, unique identifiers, or web links for publicly available datasets
- A description of any restrictions on data availability
- For clinical datasets or third party data, please ensure that the statement adheres to our policy

All generated data and analysis information/results for this this study are included in this article's figures, extended data figures, supplementary datasets and source data files. Analysis code and data are available at GitHub at the following repository: https://github.com/Prenauer/OR7A10_NK_GOF_2025. Raw sequencing data are available for download from the Gene Expression Omnibus (GEO) with super-series accession number: GSE309802. To review GEO accession GSE309802: Go to https://www.ncbi.nlm.nih.gov/geo/query/acc.cgi?acc=GSE309802. Original cell lines are available at the commercial sources listed in methods and/or reporting summary.

Field-specific reporting

Please select the one below that is the best fit for your research. If you are not sure, read the appropriate sections before making your selection.

☒ Life sciences ☐ Behavioural & social sciences ☐ Ecological, evolutionary & environmental sciences

For a reference copy of the document with all sections, see nature.com/documents/nr-reporting-summary-flat.pdf

Life sciences study design

All studies must disclose on these points even when the disclosure is negative.

Sample size	Sample size was determined according to the lab's prior work or similar approaches in the field. For examples: P eng et al. Nat Biotechnol. 2025 May;43(5):752-761. doi: 10.1038/s41587-024-02282-4. Epub 2024 Jun 25. PMID: 38918616. Ye et al. Cell Metab. 2022 Apr 5;34(4):595-614.e14. doi: 10.1016/j.cmet.2022.02.009. Epub 2022 Mar 10. PMID: 35276062
Data exclusions	No data was excluded.
Replication	Number of biological replicates (usually n >= 3) are indicated in the figure legends. Key findings (non-NGS) were replicated in at least two independent experiments. NGS experiments were performed with biological replications as indicated in the manuscript.
Randomization	Regular in vitro experiments were not randomized or blinded due to small sample size and clear groups. Mouse experiments were randomized by using littermates, and blinded using generic cage barcodes and eartags where applicable. High-throughput experiments and analyses were blinded by barcoded metadata.
Blinding	Regular in vitro experiments were not randomized or blinded due to small sample size and clear groups. Mouse experiments were randomized by using littermates, and blinded using generic cage barcodes and eartags where applicable. High-throughput experiments and analyses were blinded by barcoded metadata.

Reporting for specific materials, systems and methods

We require information from authors about some types of materials, experimental systems and methods used in many studies. Here, indicate whether each material, system or method listed is relevant to your study. If you are not sure if a list item applies to your research, read the appropriate section before selecting a response.

Materials & experimental systems

n/a	Involved in the study
☐	☒ Antibodies
☐	☒ Eukaryotic cell lines
☒	☐ Palaeontology and archaeology
☐	☒ Animals and other organisms
☐	☒ Human research participants
☒	☐ Clinical data
☒	☐ Dual use research of concern

Methods

n/a	Involved in the study
☒	☐ ChIP-seq
☐	☒ Flow cytometry
☒	☐ MRI-based neuroimaging

Antibodies

Antibodies used

PE anti-DYKDDDDK Tag Antibody (L5), Biolegend, Cat#637310;
BV421 anti-DYKDDDDK Tag Antibody, Biolegend, Cat#637322;
PE/Cyanine7 anti-DYKDDDDK Tag Antibody, Biolegend, Cat#637323;
APC anti-human CD3 Antibody, Biolegend, Cat#300312;
FITC anti-human CD56 (NCAM) Antibody, Biolegend, Cat#Cat#362546;
APC anti-human CD56 (NCAM) Antibody, Biolegend, Cat#318310;
Brilliant Violet 510™ anti-human CD56 (NCAM) Antibody, Biolegend, Cat# 362533;
PE anti-human CD107a (LAMP-1) Antibody, Biolegend, Cat#328608;
BV605 anti-human IFN-γ Antibody, Biolegend, Cat#502536;
PE anti-human TNF-α Antibody, Biolegend, Cat#502909;
Brilliant Violet 421™ anti-human/mouse Granzyme B Recombinant Antibody, Biolegend, Cat#396414;
APC anti-human Perforin Antibody, Biolegend, Cat#308111;
PE/Cyanine7 anti-human CD178 (Fas-L) Antibody, Biolegend, Cat#306417;
APC anti-human CD253 (TRAIL) Antibody, Biolegend, Cat#308209;
PE anti-human CD182 (CXCR2) Antibody, Biolegend, Cat#320705;
FITC CD137 (4-1BB) Monoclonal Antibody (4B4 (4B4-1)), eBioscience, Cat#11-1379-42;
PE/Cyanine7 anti-human CD69 Antibody, Biolegend, Cat#310912;
PE/Cyanine7 anti-human CD25 Antibody, Biolegend, Cat#985808;
Brilliant Violet 510™ anti-human CD366 (Tim-3) Antibody, Biolegend, Cat#345029;
Brilliant Violet 605™ anti-human CD223 (LAG-3) Antibody, Biolegend, Cat#369323;
APC anti-human CD279 (PD-1) Antibody, Biolegend, Cat#329908;
PerCP/Cyanine5.5 anti-human CD159a (NKG2A) Antibody, Biolegend, Cat#375126;
PE anti-ERK1/2 Phospho (Thr202/Tyr204) Antibody, Biolegend, Cat# 369505;
BV605 anti-human cd335 (NKp46), Clone 9E2, Biolegend # 331925;
BV421 anti-human CD16, Clone 3G8, Biolegend # 302037;
BV421 anti-human cd314 (NKG2D), Clone 1D11, Biolegend # 320821;
BV421 anti-human CD244 (2B4), Clone 2-69, Biolegend # 393503;
All antibodies were used in 1:200 dilution.

Validation

Concentration of antibodies were validated by the manufacturers based on manufacturing instructions. Certain antibodies were further validated for their specificity using proper controls.

Eukaryotic cell lines

Policy information about cell lines

Cell line source(s)

HEK293T ATCC Catalog Number: CRL-3216™
NK92 ATCC Catalog Number: CRL-2407™
K-562 ATCC Catalog Number: CCL-243™
NALM6 ATCC Catalog Number: CRL-3273 ™
HT29 ATCC Catalog Number : HTB-38™
MCF7 ATCC Catalog Number: HTB-22™
MDA-MB-231 ATCC Catalog Number: HTB-26™
SKOV3 ATCC Catalog Number: HTB-77™
A-375 ATCC Catalog Number: CRL-1619™
NCI-H1299 Catalog Number: CRL-5803™

Authentication

Cell lines were authenticated by the commercial vendor, using methods such as morphology and/or STR profiling.

Mycoplasma contamination

All cell line samples used in this study tested negative for mycoplasma contamination.

Commonly misidentified lines (See ICLAC register)	No commonly misidentified lines were used in the study.

Animals and other organisms

Policy information about studies involving animals; ARRIVE guidelines recommended for reporting animal research

Laboratory animals	NOD-scid IL2Rgammanull (NSG) mice and NOD.Cg-KitW-41J Tyr + Prkdcscid Il2rgtm1Wjl/ThomJ (NBSGW) were purchased from JAX and bred in-house for all experiments. Mice, both female and male, aged 8-12 weeks were used for experiments. All animals were housed in standard individually ventilated, pathogen-free conditions, with 12h:12h or 13h:11h light cycle, room temperature (21-23 C) and 40-60% relative humidity.
Wild animals	No wild animals involved in this study.
Field-collected samples	No field-collected samples involved in this study.
Ethics oversight	All recombinant DNA and biosafety work were performed under the guidelines of Yale Environment, Health and Safety (EHS) Committee with an approved protocol (Chen-rDNA 15-45; 18-45; 21-45). All animal work was performed under the guidelines of Yale University Institutional Animal Care and Use Committee (IACUC) with approved protocols (Chen 20068).

Note that full information on the approval of the study protocol must also be provided in the manuscript.

Human research participants

Policy information about studies involving human research participants

Population characteristics	Human primary CD8 T cells, CD4 T cells or PBMC were taken from healthy human donors. Certificates are available from STEMCELL TECHNOLOGIES.
Recruitment	Human primary CD8 T cells, CD4 T cells or PBMC were taken from healthy human donors by STEMCELL TECHNOLOGIES.
Ethics oversight	All human sample work was performed under the guidelines of Yale University Institutional Review Board (IRB) with an approved protocol (HIC#2000020784).

Note that full information on the approval of the study protocol must also be provided in the manuscript.

Flow Cytometry

Plots

Confirm that:

☒ The axis labels state the marker and fluorochrome used (e.g. CD4-FITC).

☒ The axis scales are clearly visible. Include numbers along axes only for bottom left plot of group (a 'group' is an analysis of identical markers).

☒ All plots are contour plots with outliers or pseudocolor plots.

☒ A numerical value for number of cells or percentage (with statistics) is provided.

Methodology

Sample preparation	Surface staining for flow cytometry and cell sorting was performed by pelleting cells and resuspending in 100 µL of MACS Buffer (5% BSA in PBS, and 2mM EDTA) with antibodies (1:200 dilution) for 30 minutes at 4C in the dark. Cells were washed once in MACS buffer before resuspension. For intracellular staining, cells were fixed and permeabilized by fixation/permeabilization solution (BD) for 20 min. and resuspending in 100 µL of permeabilization/wash Buffer with antibodies (1:1000 dilution) for 30 minutes at 4C in the dark. Cells were washed three times in MACS buffer before resuspension.
Instrument	Flow cytometric analysis was performed on an BD FACSAria II or thermo Attune™ NxT.
Software	FlowJo v.10.7.1 was used for flow ctyometry data analysis.
Cell population abundance	CAR-NK92 cells were selected with puromycin. The survived cells were re-measured by FACS to confirm the purity (>90%).
Gating strategy	A lymphocyte gate was defined first from FSC-A v SSC-A. Singlet gates were then defined on SSC-H v SSC-A. Additional gating was performed as described in figure and extended data legends for individual experiments.

☒ Tick this box to confirm that a figure exemplifying the gating strategy is provided in the Supplementary Information.